DEPARTMENT OF AEROSPACE ENGINEERING
COLLEGE OF ENGINEERING & TECHNOLOGY
OLD DOMINION UNIVERSITY
NORFOLK, VIRGINIA 2359-0247

MODELING OF STRUCTURAL-ACOUSTIC INTERACTION USING COUPLED FE/BE METHOD AND CONTROL OF INTERIOR ACOUSTIC PRESSURE USING PIEZOELECTRIC ACTUATORS

By

Chuh Mei, Principal Investigator
Yacheng Shi, Graduate Research Assistant

Final Report
For the period ending August, 1997

Prepared for
National Aeronautics and Space Administration
Langley Research Center
Hampton, Virginia, 26665

Under
Research Grant NAG1-1684
Travis L. Turner, Technical Monitor
Structural Acoustics Branch
ODURF #151651

August 1997

DEPARTMENT OF AEROSPACE ENGINEERING
COLLEGE OF ENGINEERING & TECHNOLOGY
OLD DOMINION UNIVERSITY
NORFOLK, VIRGINIA 2359-0247

MODELING OF STRUCTURAL-ACOUSTIC INTERACTION USING COUPLED FE/BE METHOD AND CONTROL OF INTERIOR ACOUSTIC PRESSURE USING PIEZOELECTRIC ACTUATORS

By

Chuh Mei, Principal Investigator
Yacheng Shi, Graduate Research Assistant

Final Report
For the period ending August, 1997

Prepared for
National Aeronautics and Space Administration
Langley Research Center
Attn: Joseph Murray, Mail Stop 126
Hampton, Virginia, 26665

Under
Research Grant NAG1-1684
Travis L. Turner, Technical Monitor
Structural Acoustics Branch
ODURF #151651

Submitted by the
Old Dominion University Research Foundation
P.O. Box 6396
Norfolk, VA 23508-0369

August 1997

ABSTRACT

MODELING OF STRUCTURAL-ACOUSTIC INTERACTION USING COUPLED FE/BE METHOD AND CONTROL OF INTERIOR ACOUSTIC PRESSURE USING PIEZOELECTRIC ACTUATORS

Yucheng Shi

Department of Aerospace Engineering, Old Dominion University

Advisor: Dr. Chuh Mei

A coupled finite element (FE) and boundary element (BE) approach is presented to model full coupled structural/acoustic/piezoelectric systems. The dual reciprocity boundary element method is used so that the natural frequencies and mode shapes of the coupled system can be obtained, and to extend this approach to time dependent problems. The boundary element method is applied to interior acoustic domains, and the results are very accurate when compared with limited exact solutions. Structural—acoustic problems are then analyzed with the coupled finite element/boundary element method, where the finite element method models the structural domain and the boundary element method models the acoustic domain. Results for a system consisting of an isotropic panel and a cubic cavity are in good agreement with exact solutions and experiment data. The response of a composite panel backed cavity is then obtained. The results show that the mass and stiffness of piezoelectric layers have to be considered.

The coupled finite element and boundary element equations are transformed into modal coordinates, which is more convenient for transient excitation. Several transient problems are solved based on this formulation.

Two control designs, a linear quadratic regulator (LQR) and a feedforward controller, are applied to reduce the acoustic pressure inside the cavity based on the equations in modal coordinates. The results indicate that both controllers can reduce the interior acoustic pressure and the plate deflection.

FOREWORD

The research results contained in this technical report were performed under a NASA Langley Research Center Grant NAGI-1684 entitled, "Experimental and Numerical Analysis of Structural Acoustic Control for Interior Noise Reduction." The report is based essentially on a Ph.D. dissertation prepared by Yucheng Shi under the supervision of Dr. Chuh Mei. The document presents a coupled finite element and boundary element formulation for the modeling of fully coupled structural/acoustic/piezoelectric systems and the active control of interior acoustic pressure using piezoelectric actuators. The work was conducted at the Department of Aerospace Engineering, Old Dominion University. Mr. Travis L. Turner of Structural Acoustic Branch, NASA Langley Research Center, was the technical monitor.

ACKNOWLEDGMENTS

I would like to take this opportunity to express my deepest appreciation to my advisor, Dr. Chuh Mei, for his encouragement, motivations, and helpful guidance throughout this investigation. Specifically, his invaluable efforts in directing me to finish this interesting topic are greatly appreciated.

I would also like to thank my dissertation committee members, Drs. Jen-Kuang Huang, Brett Newman, and Hideaki Kaneko, for their support and suggestions. The efforts from all my committee members have made this multi-disciplinary research successful.

I would also like to thank everyone in the Department of Aerospace Engineering and the Department of Mechanical Engineering for their input and backing. The author is indebted to the Aerospace Engineering Department and the National Aeronautics and Space Administration Langley Research Center for their financial support through the course of research.

Most importantly, the deepest appreciation would extend to my family members for their patience, sacrifice, encouragement and supports during the course of this research.

TABLE OF CONTENTS

LIST OF TABLES

LIST OF FIGURES

Chapter 1
INTRODUCTION

1.1 Preliminary Remarks

The physical manifestation of sound is a time-dependent pressure fluctuation around the static pressure in a compressible fluid, such as air or water. One such source for these pressure fluctuation is a vibrating elastic structure. The fluctuating pressure on the surface of the structure constitutes the radiation loading. Generally, because of the low density of air compared to structural materials, radiation loading exerted by the atmosphere is usually small enough to have a negligible effect on the structural vibrations. Consequently, the two theoretically coupled systems, the elastic structure and its dynamic response within the atmosphere under prescribed driving forces and the acoustical pressure field generated by the velocity distribution over the structure-atmosphere interface, can be analyzed independently.

However, this is not always the case. For example, when a volume of air in contact with the structure is confined in a small enclosure, or when the structure is exceptionally light, the influence upon the structural motion due to radiation loading has to be considered. In those circumstances, the structure vibrating in air is more like a structure vibrating in contact with a fluid of comparable density, where radiation loading is comparable to the inertial and elastic forces of the structure. Hence, the elastic and acoustical dynamics, and their interactions, must be modeled simultaneously.

True structural-acoustic systems can be found in numerous industrial applications such as interior noise, or noise transmitted into a cavity. For example, the sound inside a fuselage of an aircraft with engines or fluid flow as outside sound sources, or the noise inside the automobile passenger compartment with the engine or driveline vibration or body vibration as the outside sources are important engineering problems. Shown in Figure 1.1 is a general sketch of these types of problems. The sound sources and the cavity are separated by an elastic structure. The vibration of the elastic structure, here a flexible plate, is excited by radiation loading on the exterior surface of the plate due to

the sound source. This induces a sound pressure fluctuation field inside the cavity due to the velocity distribution on the inner surface of the plate. The coupling between the acoustic field and structure vibration on the outer surface is negligible because of the low density of air compared to the structural material. Radiation loading on the outer surface of the flexible plate acts like an external force only and the plate has no effect on the outside acoustic field except reflection and absorbing. On the other hand, the coupling between the plate vibration and the acoustic field inside the cavity has to be considered.

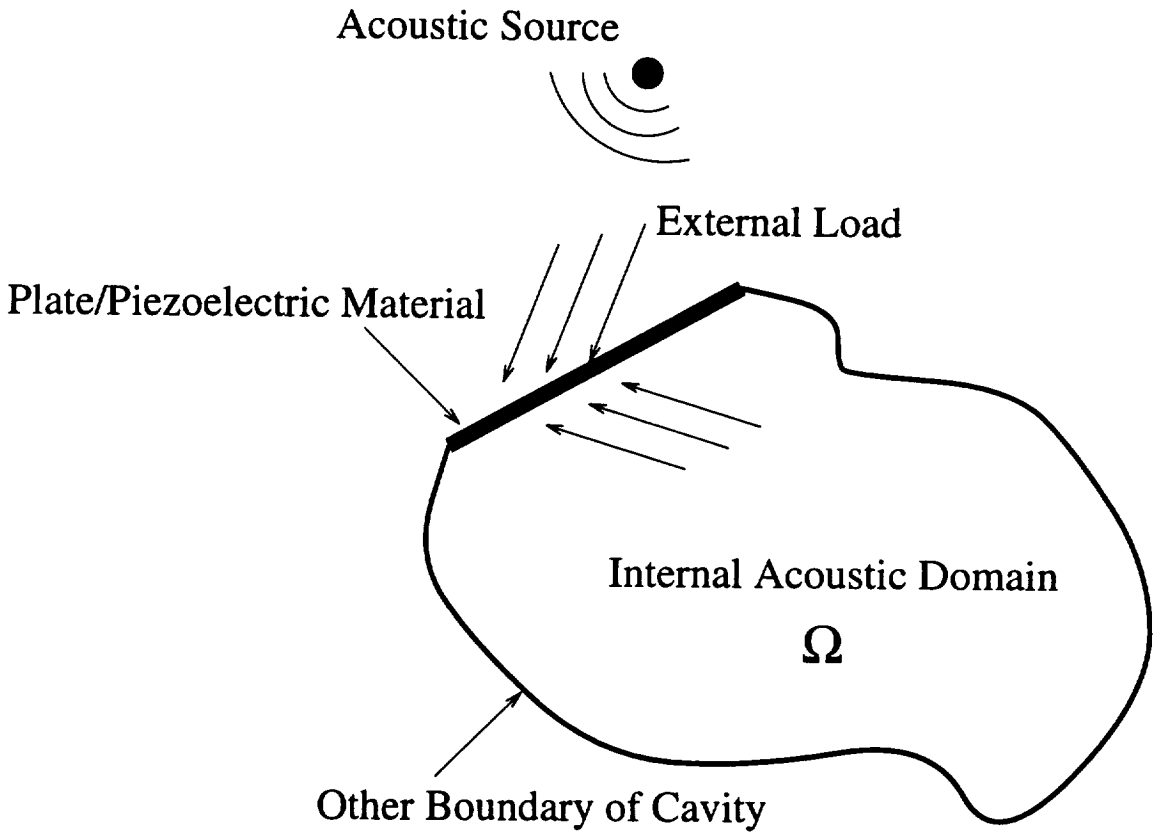

Figure 1.1 The structural-acoustic interaction problem

Over the past several decades, aerospace and automotive industries have given more attention to acoustic excitation, because this is not only a passenger comfort issue but also a safety concern. The acoustic pressure level outside an aircraft fuselage can reach

164 dB[1], and may go as high as 190 dB[2] for some new supersonic aircraft, indicating radiation loading on the fuselage is an important design parameter. Under such conditions, the interaction between the internal acoustic field and the structure vibration becomes extremely important. Mathematical models which can predict the response of the coupled structural—acoustic system under prescribed external forces becomes a necessary tool for designers.

The prediction of the sound pressure field inside the cavity and the dynamic response of the plate is not the final goal of analysts. Other objectives are to reduce the inside pressure level and the structure vibration. These objectives are not independent of the modeling of the structural-acoustic interaction. In addition to the requirement for a control system, more features are required in the coupled structural—acoustic mathematical model to represent the control design based on piezoelectric materials.

1.2 Review of Previous Work

Research in both the modeling of the structural-acoustic interaction problem and the active control of structurally transmitted noise has been performed. In this section, a brief review of both topics is given.

Modeling of Structural-Acoustic Interaction

It is not until recent years that the structural-acoustic interaction problem has captured interest in the aerospace and automotive industries. However, the basic problem is an old one. The oldest studies can be traced back to World War I, when Rayleigh published the first modern text on acoustics, the Theory of Sound[3]. He formulated the equation of motion of a rigid spring piston radiating into an acoustic fluid, and considered the effect of the acoustic fluid by increasing the damping and mass of the single-degree-of-freedom system.[4]

Even the study of radiation of sound by a vibrating structure into an acoustic cavity has a history of more than 30 years. The first investigation was performed by Lyon[5] in 1963. In his work, a rectangular plate backed by a rectangular cavity was studied in a straightforward but approximate manner. This problem was then investigated by many

researchers such as Dowell and Voss[6], Bhattacharya and Crocker[7], Guy[8, 9], McDonald et al.[10]. In 1977, Dowell, Gorman, and Smith[11] derived the general governing equation for the coupled structural-acoustic system, so-called "acoustoelasticity". In this classic paper, a comprehensive theoretical model was developed for interior acoustic fields which were created by flexible wall motion resulting from exterior sound fields, and accurate coupling between the wall and interior acoustic cavity was considered. A modal interaction approach, which assumed that the coupled modes of the cavity wall system can be expressed as a linear combination of the rigid wall cavity acoustic modes and invacuo plate modes, was also proposed for multiply connected cavities. The comparison of the numerical results and experiment data was shown to be in good agreement[11]. Based on Dowell's formulation, extensive works by others in the field followed[12–16]. Bokil[17] obtained a closed-form solution for the acoustic pressure transmitted through a rectangular cavity backed flexible plate.

On the other hand, in 1966, Gladwell and Zimmermann[18] developed an energy formulation of the acoustic-structure interaction problem, this paper set the stage for the application of finite element methods to cavity-structure analysis. This numerical method makes the consideration of complex cavity and structure geometry, structure boundary condition, and acoustic boundary condition conceptually no more difficult than simpler problems. Three different formulations were derived using the pressure[19–23], fluid particle displacement[24–27], or velocity potential[28] as the fundamental unknowns in the fluid region. The finite element approach for the structural-acoustic interaction problem seems well developed. In 1970's, even the computer tool NASTRAN had the capability of cavity-structure analysis[29,30]. Neffske et al.[31] analyzed the acoustic pressure field of complex automobile passenger compartments using NASTRAN in 1980 and found good agreement with experiment data.

As a powerful alternative to the finite element method, the boundary element method (BEM) or the boundary integral element method (BIEM) had its beginnings in the early 1960s based on the boundary integral equation theory developed in 1800s and 1900s[32]. This method was first applied to the acoustic area to solve an acoustic radiation problems

by Chen and Schweikert in 1963[33], followed by extensive research work from 1960s to 1990s[34–42]. Most of the boundary element method applications in acoustics focused on the acoustic radiation and scattering problems, where boundary element methods have an incompatible advantage for dealing with infinite domain. Not until 1982 did Koopmann and Benner present the application of this method to internal domains[43]. Suzuki et al.[44], Tanaka and Masuda[45,46], Mariem and Hamdi[47], and Pates[48] applied this method to structural-acoustic interaction problems assuming a sinusoidal time dependence. A common feature of those investigations is the joining of the boundary element method with the finite element method. The finite element method was used to model the structures, while fluid domain was handled by a boundary element method.

The most important issue for boundary element methods is the selection of the fundamental solutions. For an internal acoustic problem, the general governing equation is the well-known three dimensional wave equation. Based on various different assumptions, different choices of the fundamental solution lead to different approaches[49]. If the fundamental solution of the wave equation is selected[50], the boundary element equations need no domain integral, but it becomes impossible to form an eigenvalue problem to obtain eigenvectors. If the fundamental solution of the Laplace operator is used, the time-dependent term will inevitably lead to domain integrations[51].

Active Control of Acoustic Pressure Level Inside the Cavity

There are two different concepts in active noise control, one is the use of secondary sound sources, such as microphones, to reduce the undesired noise[52–63], the other is to reduce the original noise source[64–68]. For transmitted acoustic pressure through elastic structure, using piezoelectric materials embedded in the structure to reduce the pressure level belongs to the later case. The piezoelectric actuators will control the vibration of the elastic structure so that the acoustic pressure level transmitted inside the cavity can be reduced. Note the objectives of active control may involve more than just reduction of structure deflection.

Early attempts at reducing radiated sound from a vibrating structure by active control utilized point forces in a feedforward control loop[57,58]. This approach was then extended to applying bending moments and in-plane forces using piezoelectric actuators[64, 66]. Analytical and experimental work supported the feasibility of using active vibration control through force inputs in structures to reduce interior cavity noise level[65, 68]. However, most all studies have been based on modal analysis or frequency response input/output analysis, which does not include direct coupling of the structure and the acoustic cavity[68]. Banks et al.[66, 67] proposed a time-domain state space formulation based on the finite element model of a two-dimensional rectangular cavity backed by an isotropic beam. The structural-acoustic interaction was considered, but the coupling between the structure and the piezoelectric actuators was not complete. Only the control force from the actuators was included, the mass and stiffness of the actuator, or the piezoceramic patches, were ignored.

On the other hand, the control system design based on the coupled structural-acoustic model was performed using secondary sound sources[52,54]. Snyder et al.[56] presented a theoretical framework suitable for control system design. They proposed various control objectives such as minimization of acoustic potential energy in the cavity, minimization of acoustic pressure amplitude at a discrete location, or minimization of structure kinetic energy. Thomas et al.[60, 61] presented a numerical control simulation of sound transmission through a cylindrical shell using secondary sources. Results indicated the possibility of reducing the acoustic potential energy in the cylinder and the acoustic pressure amplitude at a discrete location using various weighting matrices in a linear quadratic regulator controller.

1.3 Objective and Outline

The overall objective of the present study is to apply available control techniques to reduce the transmitted acoustic pressure level inside the cavity. To perform this task, three steps are required. The first objective is to develop a coupled finite element and boundary element method to model the structural-acoustic system. The second step is

to transform the coupled equations into the time-domain modal formulation. The third step is to apply the linear quadratic regulator and least-mean-square (LMS) controllers to reduce the sound pressure level inside the cavity based on the modal formulation.

Since the control design is based on the numerical model, some restriction must be considered in the structural-acoustic model. The finite element method used to model the flexible plate has to be able to deal with non-homogeneous materials, that is, a composite laminate with embedded piezoelectric material layers. This involves not only the mechanical and electric coupling properties of piezoelectric materials, but also the mass and stiffness of the piezoelectric layers which have never been considered in studies reported in the literature. This feature can be easily accommodated with the versatility of the finite element method, but the requirement of transient response predictions on the combined finite element and boundary element method for the coupled structural-acoustic system does need some additional effort, specially for the boundary element model of the acoustic cavity. The boundary element method used has to be able to handle the time-dependent loads and also be able to calculate the eigenmodes of the coupled system. The dual reciprocity boundary element method[69, 70] is used in present study, this new coupled finite element and boundary element method introduces an innovative and powerful approach. The formulation of the finite element method for a composite plate with embedded piezoelectric material layers, the dual reciprocity boundary element method for the time-dependent acoustic problem, and the coupled finite element and boundary element method for the structural-acoustic interaction problem are all developed in Chapter 2. The numerical results and their comparison with exact solutions, experimental data, and other numerical approaches are given in Chapter 3.

The modal formulation is also given in Chapter 2 with numerical results for various loading cases presented in Chapter 3. To transform the coupled equation into modal formulation, the modal coordinates, or the basis of the solution space, has to be determined first. The modal shapes of the coupled structural-acoustic system are used here rather than the uncoupled modal shapes. One of the advantages of this treatment is that the basis will yield a set of uncoupled differential equations, instead of coupled equations.

The control portion of this study is to demonstrate that control laws can be applied to reduce acoustic transmission effectively. The linear quadratic regulator shows how much one can reduce the transmitted sound level in a theoretical sense. The feedforward least-mean-square control law is an attempt to design a more practical controller. The control formulations and numerical results are all given in Chapter 4. Concluding remarks and recommendations for future work are presented in Chapter 5.

Chapter 2
COUPLED FINITE ELEMENT AND BOUNDARY ELEMENT METHOD FOR STRUCTURAL-ACOUSTIC INTERACTION

In this chapter, the finite element method for a composite plate with embedded piezoelectric layers is developed, and the dual reciprocity boundary element formulation for acoustic problem is derived. Following this treatment, the finite element method and boundary element method are coupled together to form the discrete governing equations for the structural-acoustic interaction problem.

2.1 Coupled Finite Element Equation of Motion of Composite/Piezoelectric Materials

The finite element method has become a very powerful tool in the analysis of static and dynamic response of structures. This method is capable of handling structures having complex geometries, non-uniform materials, and complex boundary conditions. The objective here is to develop a finite element model to describe the coupling between a plate or structure and piezoelectric materials.

2.1.1 Piezoelectricity

It is well known that piezoelectric materials can be used as actuators and sensors due to their direct and converse effects[71]. To model these effects, a formulation with mechanical and electrical coupling should be considered. This electromechanical formulation presented here is based on the linear piezoelectricity theory[72, 73]. In this section, the general piezoelectric constitutive equations are briefly reviewed, and related piezoelectric constants are defined.

The electric enthalpy H is defined as the amount of energy stored in the material[72]

$$H = U - \vec{E} \cdot \vec{D} \tag{2.1}$$

where U is the total internal mechanical energy, $\vec{E}$ and $\vec{D}$ are the electric field and electric displacement vectors, respectively. Let $\vec{\sigma}$ and $\vec{\epsilon}$ be the mechanical stress and

strain tensors, they are related through the electric enthalpy as[72]

$$\vec{\sigma} = \frac{\partial H}{\partial \vec{\epsilon}} \tag{2.2}$$

Similarly, we have the relationship between the electric field vector and displacement vector as[72]

$$\vec{D} = -\frac{\partial H}{\partial \vec{E}} \tag{2.3}$$

The electric enthalpy H is assumed to have a homogeneous quadratic form in the linear piezoelectric theory, which includes the contributions from elastic strain energy, piezoelectric energy, and electric energy and is given by

$$H = \frac{1}{2}\{\epsilon\}^T[Q]\{\epsilon\} - \{E\}^T[e]\{\epsilon\} - \frac{1}{2}\{E\}^T[\varpi]\{E\} \tag{2.4}$$

where superscript T represents transpose, $[Q]$ is the stiffness matrix assumed independent on electric field, $[\varpi]$ is the dielectric matrix assumed independent on strain, and $[e]$ is the piezoelectric constant matrix which relates stress to applied electric field, and that is where the coupling electrical and mechanical features originate.

Substituting equation (2.4) into equations (2.2) and (2.3), the linear constitutive relations become

$$\{\sigma\} = [Q]\{\epsilon\} - [e]^T\{E\} \tag{2.5}$$

and

$$\{D\} = [e]\{\epsilon\} + [\varpi]^T\{E\} \tag{2.6}$$

Since the dielectric matrix $[\varpi]$ and the piezoelectric constant matrix $[e]$ are sometimes not available, the more commonly available constant matrix $[d]$ and the free dielectric matrix $[\varepsilon]$ are introduced, the relationship between those matrices are[73]

$$[e] = [d][Q] \tag{2.7}$$

and

$$[\varepsilon] = [\varpi] + [d][Q][d]^T \tag{2.8}$$

The constitutive equations of piezoelectric materials become

$$\{\sigma\} = [Q]\Big(\{\epsilon\} - [d]^T\{E\}\Big) \tag{2.9}$$

$$\{D\} = [d]\{\sigma\} + [\varepsilon]^T\{E\} \tag{2.10}$$

2.1.2 Constitutive Equations for Composite and Piezoelectric Laminae

For a thin laminated panel consisting of composite and piezoelectric layers (shown in Figure 2.1), the two-dimensional constitutive equation in principle material axes for an orthotopic piezoelectric layer can be obtained from equation (2.9) as[71]

$$\begin{Bmatrix} \sigma_1 \\ \sigma_2 \\ \tau_{12} \end{Bmatrix} = \begin{bmatrix} Q_{11} & Q_{12} & 0 \\ Q_{12} & Q_{22} & 0 \\ 0 & 0 & Q_{66} \end{bmatrix}_{\phi} \left(\begin{Bmatrix} \epsilon_1 \\ \epsilon_2 \\ \gamma_{12} \end{Bmatrix} - E_3 \begin{Bmatrix} d_{31} \\ d_{32} \\ 0 \end{Bmatrix} \right) \tag{2.11}$$

and the electrical displacement along the polling 3–axis, which is assumed to be the normal direction of the plate, from equation (2.10), is

$$D_3 = [d_{31} \;\; d_{32} \;\; 0] \begin{Bmatrix} \sigma_1 \\ \sigma_2 \\ \tau_{12} \end{Bmatrix} + E_3 \varepsilon_{33} \tag{2.12}$$

where E_3 is the electric field; d_{31}, d_{32} are the piezoelectric stress/charge constants; ε_{33} is the permittivity constant. For a composite lamina, the constitutive equation is

$$\begin{Bmatrix} \sigma_1 \\ \sigma_2 \\ \tau_{12} \end{Bmatrix} = \begin{bmatrix} Q_{11} & Q_{12} & 0 \\ Q_{12} & Q_{22} & 0 \\ 0 & 0 & Q_{66} \end{bmatrix}_{c} \begin{Bmatrix} \epsilon_1 \\ \epsilon_2 \\ \gamma_{12} \end{Bmatrix} \tag{2.13}$$

where $[Q]$ is the reduced stiffness matrix, and the subscripts ϕ and c denote for piezoelectric and composite laminae, respectively.

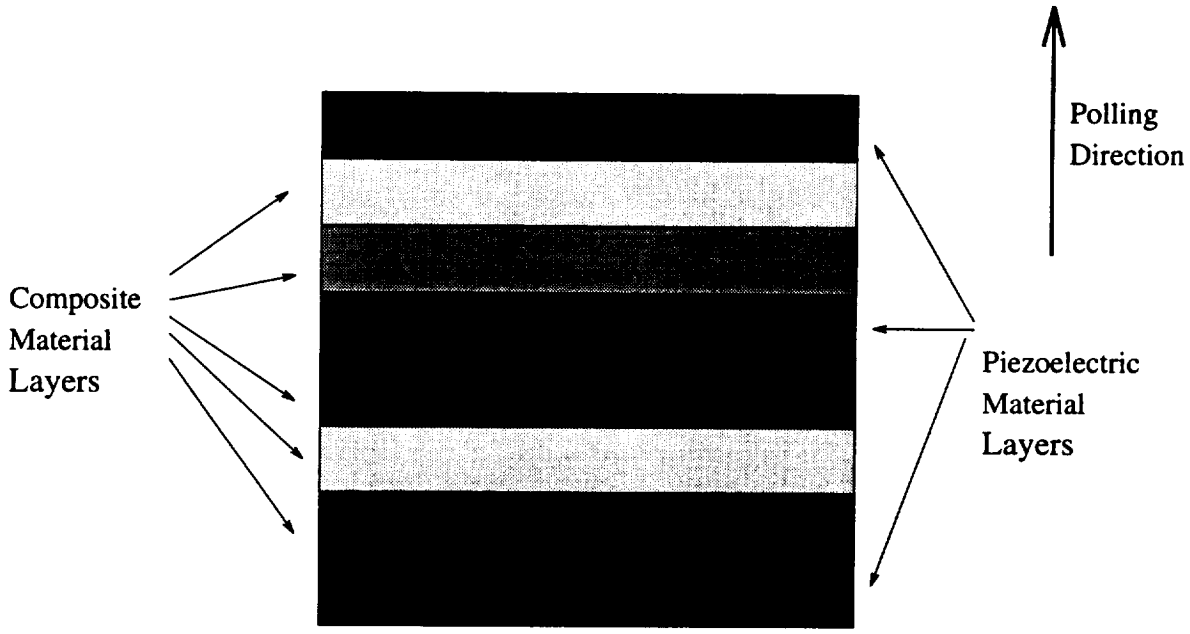

Figure 2.1 Composite and Piezoelectric Layers

Then the strain-stress relation for a general k-th layer with a lamination angle becomes

$$\begin{Bmatrix} \sigma_x \\ \sigma_y \\ \tau_{xy} \end{Bmatrix}_k = \begin{bmatrix} \bar{Q}_{11} & \bar{Q}_{12} & \bar{Q}_{16} \\ \bar{Q}_{12} & \bar{Q}_{22} & \bar{Q}_{26} \\ \bar{Q}_{16} & \bar{Q}_{26} & \bar{Q}_{66} \end{bmatrix}_k \left(\begin{Bmatrix} \epsilon_x \\ \epsilon_x \\ \gamma_{xy} \end{Bmatrix} - E_{3k} \begin{Bmatrix} d_x \\ d_y \\ d_{xy} \end{Bmatrix}_k \right) \tag{2.14}$$

where for composite layers,

$$\begin{aligned} [\bar{Q}] &= [\bar{Q}]_c \\ E_{3k} &= 0 \end{aligned} \tag{2.15}$$

and for piezoelectric layers,

$$\begin{aligned} [\bar{Q}] &= [\bar{Q}]_\phi \\ D_{3k} &= [d_x, d_y, d_{xy}]_k [\bar{Q}]_k \{\epsilon\} + E_{3k}\varepsilon_{33k} \end{aligned} \tag{2.16}$$

where $[\bar{Q}]$ is the transformed reduced stiffness matrix.

2.1.3 Finite Element Equations

The generalized Hamilton's principle for a coupled electromechanical system can be expressed as[74, 75]

$$\delta\left[\int_{t_1}^{t_2}(T - U_s + W_e - W_m + W)dt\right] = 0 \tag{2.17}$$

where

$$T = \frac{1}{2}\int_V \rho\frac{\partial\vec{w}}{\partial t}\frac{\partial\vec{w}}{\partial t}dV \tag{2.18}$$

is the kinetic energy;

$$U_s = \frac{1}{2}\int_V \{\epsilon\}^T\{\sigma\}dV \tag{2.19}$$

is the strain energy of the system;

$$W_e = \frac{1}{2}\int_V \{E\}^T\{D\}dV \tag{2.20}$$

is the electrical energy; W_m is the magnetic energy, which is negligible here; and

$$W = \int_V \vec{w}\vec{F}_b dV + \int_{s_1} \vec{w}\vec{F}_s dS + \vec{w}\vec{F}_c - \int_{s_2} \phi q dS \tag{2.21}$$

is the work done due to external forces and the applied surface charge. In equations (2.18) to (2.21), ρ is the density, $\vec{w}$ the displacement vector, $\vec{F}_b$ denotes the body force vector, $\vec{F}_s$ the surface traction vector, $\vec{F}_c$ the concentrated forces, ϕ the electric potential, and q the surface charge.

The linear strain-displacement relation is given as

$$\begin{Bmatrix}\epsilon_x\\ \epsilon_y\\ \gamma_{xy}\end{Bmatrix} = \begin{Bmatrix}u_{,x}\\ v_{,y}\\ u_{,y}+v_{,x}\end{Bmatrix} - z\begin{Bmatrix}w_{,xx}\\ w_{,yy}\\ 2w_{,xy}\end{Bmatrix} \tag{2.22}$$

and the relation between electric field and electrical potentials is

$$\{E_3\} = -[B_h]\{\phi\} \tag{2.23}$$

where $[B_h]$ is a diagonal matrix

$$[B_h] = \begin{bmatrix} h_1 & \dots & 0 \\ \vdots & \ddots & \vdots \\ 0 & \dots & h_{n\phi} \end{bmatrix}^{-1} \tag{2.24}$$

with h_k is the thickness of k-th piezoelectric layer, u, v are the in-plane displacements, w the transverse displacement, and n_ϕ is the number of piezoelectric layers.

Substituting equations (2.18) through (2.21) into equation (2.17), and using equations (2.14) to (2.16) and (2.23) to (2.25), we have the equation of motion for the composite plate with embedded piezoelectric layers in finite element form as

$$\begin{bmatrix} M_w & 0 \\ 0 & 0 \end{bmatrix} \begin{Bmatrix} \ddot{W} \\ 0 \end{Bmatrix} + \begin{bmatrix} K_w & K_{w\phi} \\ K_{\phi w} & K_\phi \end{bmatrix} \begin{Bmatrix} W \\ \Phi \end{Bmatrix} = \begin{Bmatrix} F_w \\ F_\phi \end{Bmatrix} \tag{2.25}$$

where $\{W\}$ and $\{\Phi\}$ are the system structural node degrees-of-freedom and electric potentials, $\{F_w\}$ and $\{F_\phi\}$ are the load vectors due to acoustic excitations and piezoceramic surface charge, and $[M]$ and $[K]$ are the system mass and stiffness matrices. The subscripts w and ϕ denote structural and electric field components, respectively. The detail derivation, element load vectors, and mass and stiffness matrices are given in Appendix A.

The equations of motion can then be rewritten as actuator equations as

$$\begin{aligned} [M_w]\{\ddot{W}\} + [K_w]\{W\} &= \{F_w\} + \{F_{w\phi}\} \\ \{F_{w\phi}\} &= -[K_{w\phi}]\{\Phi\} \end{aligned} \tag{2.26}$$

and as sensor equations as

$$[K_\phi]\{\Phi\} + [K_{\phi w}]\{W\} = \{F_\phi\} \tag{2.27}$$

where $\{F_{w\phi}\}$ is the load on structure due to electric potential $\{\Phi\}$.

2.1.4 Finite Element Specifications

Many rectangular and triangular type finite elements are currently being used in commercial and in-house codes. Any type of finite element can be applied to the present formulation. The element selected for this study is a four-node rectangular C^1 conforming element[76] and is shown in Figure 2.2. Each node of this element has four degrees of

freedom associated with the transverse displacements ($w, w_{,x}, w_{,y}, w_{,xy}$) and two in-plane displacements (u, v). The electric degrees of freedom are the electric potential ϕ of each piezoelectric layer. The displacement shape functions and other characteristics of this element are given in Appendix B.

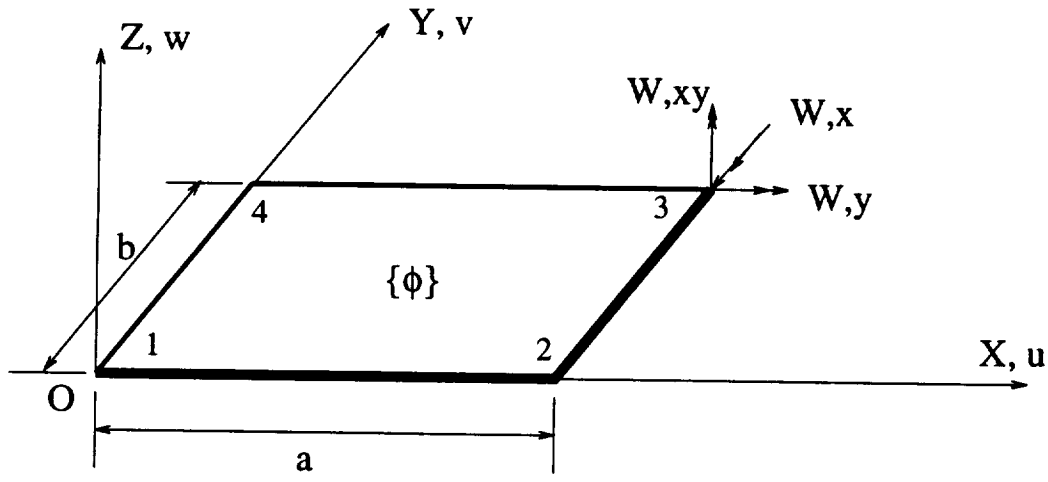

Figure 2.2 C^1 conforming rectangular finite element

2.2 Boundary Element Method for Acoustics

2.2.1 General Aeroacoustics Equations

The general governing equations of inviscid flow are formed by one continuity equation[77]

$$\frac{D\bar{\rho}}{Dt} + \bar{\rho}\frac{\partial \bar{u}_i}{\partial x_i} = 0 \tag{2.28}$$

three momentum equations

$$\bar{\rho}\frac{D\bar{u}_i}{Dt} + \frac{\partial \bar{p}}{\partial x_i} = \bar{\rho} f_i \tag{2.29}$$

and an energy equation

$$\frac{D\bar{p}}{Dt} = c^2 \frac{D\bar{\rho}}{Dt} \tag{2.30}$$

where c is the sound speed, $\bar{\rho}$ is the density of the medium, $\bar{u}_i(x_j,t)$, $i,j = 1,2,3$ are the velocity components, $\bar{p}(x_j,t)$ is the pressure, and f_i are body forces.

The change of density and pressure due to acoustic wave is usually much smaller than that due to fluid flow, so it is necessary to separate acoustic wave from the fluid flow, denote subscript 'o' as the variable of fluid flow (i.e., $\bar{\rho} = \rho + \rho_o$), the perturbation decomposition gives the governing equations of acoustic wave in a homogeneous medium with no mean flow as

$$\begin{aligned} &\frac{\partial \rho}{\partial t} + \rho_o \frac{\partial u_i}{\partial x_i} = 0 \\ &\rho_o \frac{\partial u_i}{\partial t} + \frac{\partial p}{\partial x_i} = 0 \qquad i = 1,2,3 \\ &\frac{\partial p}{\partial t} - c^2 \frac{\partial \rho}{\partial t} = 0 \end{aligned} \tag{2.31}$$

Eliminating the perturbation of density from above equations, we have the governing equation as

$$\frac{\partial^2 p}{\partial t^2} - c^2 \nabla^2 p = 0 \tag{2.32}$$

and the momentum equations give the relationship between acoustic pressure and velocity components as

$$\frac{\partial p}{\partial x_i} + \rho_o \frac{\partial u_i}{\partial t} = 0 \tag{2.33}$$

and at a boundary, the normal derivative of pressure is obtained as

$$q = \frac{\partial p}{\partial \vec{n}} = -\rho_o \frac{\partial u_i n_i}{\partial t} \tag{2.34}$$

where $\vec{n}$ is the unit outward normal vector.

Generally, it is more convenient to use a velocity potential to simplify the equations, but here, since both pressure and velocity are needed in the formulation of control theory, we use the pressure as the primary variable.

2.2.2 Dual Reciprocity Method

As one type of the boundary element method, the dual reciprocity method[69, 70] offers the advantage that it does not need any domain integrals which appear when

nonlinear problems or time dependent problems are considered (which does not mean no domain equations are needed). However, in this study, the main reason for using the dual reciprocity method instead of the general boundary element method is that we have to transform the coupled structural—acoustic equations into modal coordinates. To do so, some kind of uncoupled coordinates are required, and one commonly used set of coordinates are the eigenvectors. Generally, the boundary element method combines the frequency of the input excitation into its fundamental solution[48], making the identification of eigenvalues and eigenvectors extremely difficulty.

General formulation For a general boundary value problem,

$$\nabla^2 p(x,y,z,t) = b(x,y,z,t) \qquad in\ \ \Omega \tag{2.35}$$

Assume that the right-hand term, b, can be expressed as a linear combination of a set of independent functions, f_i, defined in the domain Ω and on the boundary Γ. That is,

$$b = \sum_{i=1}^{NN} \alpha_i f_i \tag{2.36}$$

where α_i are initially unknown coefficients, and NN is the number of independent functions. Defining a set of particular solutions, $\hat{p}_i$, as

$$\nabla^2 \hat{p}_i = f_i \qquad i = 1, 2, ..., NN \tag{2.37}$$

Then equation (2.35) becomes

$$\nabla^2 p = \sum_{i=1}^{NN} \alpha_i (\nabla^2 \hat{p}_i) \tag{2.38}$$

If we take the fundamental solution of the Laplace's equation

$$\nabla^2 p^*(\vec{r}) + \delta(\vec{r}_j) = 0 \tag{2.39}$$

that is

$$\begin{aligned} p^* &= \frac{1}{4\pi R}, \qquad R = |\vec{r} - \vec{r}_j| \\ q^* &= \frac{\partial p^*}{\partial \vec{n}} = -\frac{1}{4\pi R^2}\frac{\partial R}{\partial \vec{n}} \end{aligned} \tag{2.40}$$

as the weighting function, then the weighted-residual method applied to equation (2.38) requires

$$\int_{\Omega} (\nabla^2 p) p^* d\Omega = \sum_{i=1}^{NN} \alpha_i \int_{\Omega} (\nabla^2 \hat{p}_i) p^* d\Omega \tag{2.41}$$

Using Green's formula, we obtain an integral equation as

$$\int_{\Omega} (\nabla^2 p^*) p d\Omega + \int_{\Gamma} (pq^* - p^* q) d\Gamma = \sum_{i=1}^{NN} \alpha_i \left(\int_{\Omega} (\nabla^2 p^*) \hat{p}_i d\Omega + \int_{\Gamma} (\hat{p}_i q^* - p^* \hat{q}_i) d\Gamma \right) \tag{2.42}$$

where Γ is the boundary of the domain.

Using equation (2.39), and considering the singularity of the fundamental solution at the boundary, we obtain the integral equation for each point on the boundary as

$$c_j p_j + \int_{\Gamma} (pq^* - p^* q) d\Gamma = \sum_{i=1}^{NN} \alpha_i \left(c_j \hat{p}_{ij} + \int_{\Gamma} (\hat{p}_i q^* - p^* \hat{q}_i) d\Gamma \right) \tag{2.43}$$

where parameter c_j is the ratio of the exterior area outside the domain of a sphere surface with a small radius to the area of the entire sphere surface. For any interior point, we have $c_j = 1$ and

$$p_j = - \int_{\Gamma} (pq^* - p^* q) d\Gamma + \sum_{i=1}^{NN} \alpha_i \left(\hat{p}_{ij} + \int_{\Gamma} (\hat{p}_i q^* - p^* \hat{q}_i) d\Gamma \right) \tag{2.44}$$

Equation (2.43) is the basis of the boundary element method. Since we seek a time-dependent formulation, equations should be formed for nodes in the domain and on the boundary, but as can be seen from equation (2.44), no domain integrations are required. If the boundary is discretized into elements, and in each element, shape functions are assumed so that the variables defined on the boundary can be expressed in terms of their node values or

$$p = [N]\{p\} \tag{2.45}$$

then the integral equation becomes

$$- \sum_{k=1}^{N} H_{jk} p_k - \sum_{k=1}^{N} G_{ik} q_k = \sum_{i=1}^{NN} \left[\alpha_i \left(- \sum_{k=1}^{N} H_{jk} \hat{p}_k - \sum_{k=1}^{N} G_{ik} \hat{q}_k \right) \right] \tag{2.46}$$

where $[N]$ is the shape functions, and N is the number of boundary elements. In matrix form, we have

$$-[H]\{P\} - [G]\{Q\} = \left(-[H]\left[\hat{P}\right] - [G]\left[\hat{Q}\right]\right)\{\alpha\} \tag{2.47}$$

where matrices $\left[\hat{P}\right]$ and $\left[\hat{Q}\right]$ contain $\hat{p}_i$ and $\hat{q}_i$ as their columns, respectively, matrices $[H]$ and $[G]$ are globe acoustic influence matrices assembled from the corresponding element matrices which are defined as

$$\begin{aligned} [g]_k &= \int_{\Gamma_k} p^*[N]d\Gamma \\ [h]_k &= -c_j\delta_{jk} - \int_{\Gamma_k} q^*[N]d\Gamma \end{aligned} \tag{2.48}$$

Functions As expressed in equation (2.36), when function b satisfies certain continuous conditions, there will be a set of functions and correspond coefficients such that

$$\{b\} = [F]\{\alpha\} \tag{2.49}$$

where each column of $[F]$ consists of a vector which contains the value of the function f_i at the (NN) collocation points. Then if matrix $[F]$ is invertible, we have

$$\{\alpha\} = [F]^{-1}\{b\} \tag{2.50}$$

Substitute the above equation into equation (2.47), and denote

$$[S] = \left(-[H]\left[\hat{P}\right] - [G]\left[\hat{Q}\right]\right)[F]^{-1} \tag{2.51}$$

we obtain

$$-[H]\{P\} - [G]\{Q\} = [S]\{b\} \tag{2.52}$$

Matrix $[S]$ is a function of $f_i, \hat{q_i}$, and $\hat{p}_i$ only, where the requirement on functions f_i, except some continuous requirements, is to allow that matrix $[F]$ to be invertible. One choice for those functions is to let [78, 79]

$$f_i(\hat{r}) = 1 + R_i, \qquad R_i = |\hat{r} - \hat{r}_i| \tag{2.53}$$

and for a three-dimensional problem, we have

$$\hat{p}_i = \frac{R_i^3}{12} + \frac{R_i^2}{6} \tag{2.54}$$

and

$$\hat{q}_i = \frac{\partial \hat{p}_i}{\partial \vec{n}} = \left(\frac{R_i^2}{4} + \frac{R_i}{3}\right)\frac{\partial R_i}{\partial \vec{n}} \tag{2.55}$$

When these three sets of functions are obtained, matrices $[H]$, $[G]$ and $[S]$ are known, and with the function b, equation (2.52) can be solved with suitable boundary conditions and initial conditions.

2.2.3 Boundary Element Method Equations

For a time-dependent acoustic problem, equation (2.32) is the governing equation, comparing to equation (2.35), we set

$$b = \frac{1}{c^2}\ddot{p} \tag{2.56}$$

so from equation (2.52), we have

$$[M_a]\left\{\ddot{P}\right\} + [H]\{P\} + [G]\{Q\} = 0 \tag{2.57}$$

where

$$[M_a] = \frac{1}{c^2}[S] \tag{2.58}$$

2.2.4 Boundary Element Specifications

Similar to the finite element method, many types of boundary elements are available. In this study, we selected one of the simplest two dimensional elements, the constant rectangular element (shown in Figure 2.3), to demonstrate the capability of boundary element method in solving acoustic problems.

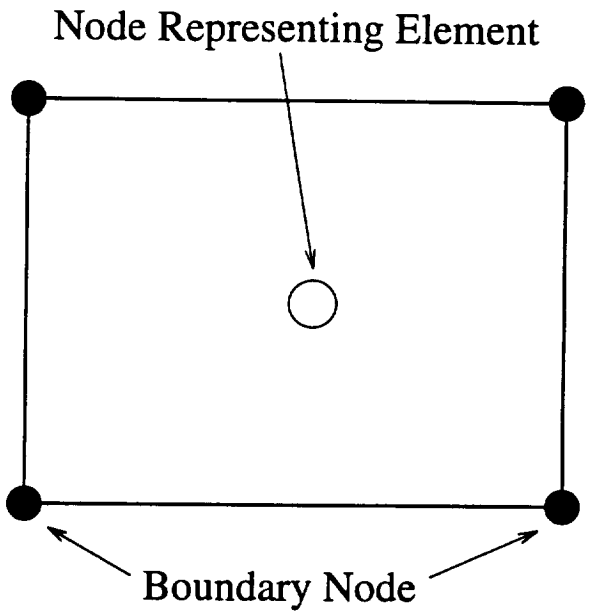

Figure 2.3 Two dimensional constant boundary element

2.3 Coupled Structure/Acoustic Equations

The boundary element equations of acoustic wave inside the cavity can be rewritten here as

$$\begin{bmatrix} M_c & M_{cb} \\ M_{bc} & M_b \end{bmatrix} \begin{Bmatrix} \ddot{P}_c \\ \ddot{P}_b \end{Bmatrix} + \begin{bmatrix} H_c & H_{cb} \\ H_{bc} & H_b \end{bmatrix} \begin{Bmatrix} P_c \\ P_b \end{Bmatrix} + \begin{bmatrix} G_c & G_{cb} \\ G_{bc} & G_b \end{bmatrix} \begin{Bmatrix} Q_c \\ Q_b \end{Bmatrix} = 0 \qquad (2.59)$$

where the pressure and its normal derivative are divided into two parts,

$$\{P\} = \begin{Bmatrix} P_c \\ P_b \end{Bmatrix}, \quad \{Q\} = \begin{Bmatrix} Q_c \\ Q_b \end{Bmatrix} \qquad (2.60)$$

the subscript c denotes the quantities on the inner surface of the structure which will be coupled with the finite element structure equation, and b at all the other locations. The governing finite element equation of the structure, equation (2.26), is

$$[M_w]\left\{\ddot{W}\right\} + [K_w]\{W\} = \{F_{ex}\} - \{F_{in}\} + \{F_{w\phi}\} \qquad (2.61)$$

where the acoustic load is separated into external excitation load and inside acoustic load, $\{F_w\} = \{F_{ex}\} - \{F_{in}\}$.

Those two set of equations will be coupled by using the compatibility of displacement and pressure on the inner surface of the plate.

2.3.1 Coupled Equation in Structure DOF

Because of the continuity of the displacement, the normal component of acoustic velocity on the inner surface of the plate must be equal to that of the plate at the same location, or

$$\{u_{nc}\} = [\beta]\{u_c\} = [\beta][T]\left\{\dot{W}\right\} \tag{2.62}$$

where the matrix $[\beta]$ transforms the acoustic velocity on the inner surface of the plate $\{u_c\}$ to its normal component $\{u_{nc}\}$, and matrix $[T]$ is a transformation, which depends on the primary variables and meshes of finite element and boundary element models. The element matrices $[\beta_e]$ and $[T_e]$ for constant boundary elements are derived in Appendix C. Since equation (2.34) gives a relation between pressure and acceleration components, we have

$$\{Q_c\} = -\rho_o\{\dot{u}_{nc}\} = -\rho_o[\beta][T]\left\{\ddot{W}\right\} = [T_1]\left\{\ddot{W}\right\} \tag{2.63}$$

The second loading term on right side of equation (2.61) is due to the acoustic pressure inside the cavity, its element node value can be related to the inside acoustic pressure (see equation A.16) as

$$\{f_{in}\} = [T_b]^T \int_A p_c\{H_w\}dA \tag{2.64}$$

Form this, we can obtain the relationship on a global level as

$$\{F_{in}\} = \sum \left([T_b]^T \int_A \{H_w\}dA \right) \{P_c\} = [T_2]\{P_c\} \tag{2.65}$$

Substituting equations (2.63) and (2.65) into equations (2.59) and (2.61), we have the coupled equation for a structural—acoustic system as

$$\begin{bmatrix} M_w & 0 & 0 \\ M_{cw} & M_c & M_{cb} \\ M_{bw} & M_{bc} & M_b \end{bmatrix} \begin{Bmatrix} \ddot{W} \\ \ddot{P}_c \\ \ddot{P}_b \end{Bmatrix} + \begin{bmatrix} C_w & 0 & 0 \\ 0 & 0 & 0 \\ 0 & 0 & 0 \end{bmatrix} \begin{Bmatrix} \dot{W} \\ \dot{P}_c \\ \dot{P}_b \end{Bmatrix} +$$
$$\begin{bmatrix} K_w & K_{wc} & 0 \\ 0 & H_c & H_{cb} \\ 0 & H_{bc} & H_b \end{bmatrix} \begin{Bmatrix} W \\ P_c \\ P_b \end{Bmatrix} = \begin{Bmatrix} F_{ex} \\ -G_{cb}Q_b \\ -G_bQ_b \end{Bmatrix} + \begin{Bmatrix} F_{w\phi} \\ 0 \\ 0 \end{Bmatrix} \tag{2.66}$$

or

$$[M]\{\ddot{\chi}\} + [C]\{\dot{\chi}\} + [K]\{\chi\} = \{F_1\} + \{F_2\} \tag{2.67}$$

where $\{\chi\} = [W, P_c, P_b]^T$ and

$$\begin{aligned} ([M_{cw}], [M_{bw}]) &= ([G_c], [G_{bc}])[T_1] \\ [K_{wc}] &= [T_2] \end{aligned} \tag{2.68}$$

Notice that the generalized mass matrix $[M]$ and the generalized stiffness matrix $[K]$ are all no longer symmetric, and for generality, a damping term $[C_w]\left\{\dot{W}\right\}$ is included in equation (2.66). The force $\{F_1\}$ consists of external excitation to the structure and normal derivative of pressure in the cavity, and $\{F_2\}$ is the force acting on structure due to applied electric potential.

2.3.2 Coupled Equations in Modal Coordinates

There are at least two different modal coordinate systems that can be used to transform the governing equation in node DOF to truncated modal coordinates. One is taking the natural modal shapes of the uncoupled system, defined by equation (2.59) and equation (2.61). This allows the nodal DOF to be expressed as

$$\{\chi\} = \begin{Bmatrix} W \\ P \end{Bmatrix} = \begin{bmatrix} \Psi_w & 0 \\ 0 & \Psi_a \end{bmatrix} \begin{Bmatrix} \eta_w \\ \eta_a \end{Bmatrix} = [\Psi]\{\eta\} \tag{2.69}$$

where $[\Psi_w]$ is the modal matrix for plate equation, $[\Psi_a]$ $\left([\Psi_a] = [\Psi_c, \Psi_b]^T\right)$ is the modal matrix for acoustic equation, and $\{\eta_w\}$ and $\{\eta_a\}$ are the modal variables of plate

displacement and acoustic pressure, respectively. Another transformation is based on the truncated natural modal shapes of the coupled equation (2.66), which gives

$$\{\chi\} = [\Psi]\{\eta\} \tag{2.70}$$

where $\{\eta\}$ is the vector of modal variables, and $[\Psi]$ is the modal matrix.

The first transformation will end with a set of coupled ordinary differential equations because of the coupling between structure and acoustics even when no damping is involved. Further, cases with all rigid acoustic boundary condition require some special treatment for the rigid acoustic mode. Meanwhile, although more computing time is needed to form coupled modes, the second transformation will give a set of independent ordinary differential equations in the case without damping, and no judgement is needed to select modes. Therefore, the second transformation, using coupled modes as modal coordinates, is applied here.

Substitute equation (2.70) into equation (2.67), and pre-multiply by the transpose of corresponding modal matrix, or

$$[M]^*\{\ddot{\eta}\} + [C]^*\{\dot{\eta}\} + [K]^*\{\eta\} = \{L_1\} + \{L_2\} \tag{2.71}$$

where the modal matrices and modal vectors are

$$\begin{aligned} ([M]^*, [C]^*, [K]^*) &= [\Psi]^T([M], [C], [K])[\Psi] \\ (\{L_1\}, \{L_2\}) &= [\Psi]^T(\{F_1\}, \{F_2\}) \end{aligned} \tag{2.72}$$

Equation (2.71) is the so-called time-domain modal formulation.

CHAPTER 3
RESULTS FOR THE MODELING OF COUPLED STRUCTURAL-ACOUSTIC SYSTEM

In this chapter we present the results based on the formulation previously developed and also some additional discussion. The results are subdivided into three sections: acoustic results using the dual reciprocity boundary element method, the coupled structural-acoustic response using the coupled boundary element and finite element method, and results using the time-domain modal formulation. The purpose of this chapter is to show that the dual reciprocity boundary element method is a powerful numerical technique that can be used to solve a wide range of acoustic problems. The coupling of the boundary element method and the finite element method, and its time-domain modal formulation, lead to powerful tools that can be readily used to analyze structural-acoustic interaction problems.

3.1 Interior Domain Analysis

In this section, three example problems are solved and results are compared with exact solutions. Those problems are derived from a typical rectangular duct as shown in Figure 3.1. The inlet is assumed to be at $z = 20cm$ and the outlet at $z = 0$, while the four duct side walls, with length of $20cm$, are all assumed to be acoustically rigid in all three examples, that is $\frac{\partial p}{\partial \vec{n}} = 0$. The outlet has different boundary conditions.

The input acoustic wave, that is the acoustic field at the inlet, is assumed to be a unit plane wave, thus the one-dimensional exact solution becomes valid[80]. While for the dual reciprocity boundary element approach, the inlet, outlet, and the four duct walls are all discretized by constant two—dimensional boundary elements, and internal nodes are uniformly distributed inside the duct. Two different models with different mesh are employed for each problems. The first model (model–1) discretizes the inlet, outlet, or each wall by a 5×5 mesh (or 150 boundary elements for the whole boundary) and $5 \times 5 \times 5$ (or 125) internal nodes. The second model (mode–2) discretizes the inlet, outlet, or each wall by a 7×7 mesh (or 294 boundary elements for the whole boundary)

and also $5 \times 5 \times 5$ (or 125) internal nodes. In the following example problems, the pressure obtained at location $x = y = z = 10\ cm$ is compared with the exact solution at different input frequencies.

In the first example, a null pressure field is applied at the duct outlet, the results are given in Figure 3.2. It can be seen that the boundary element method gives very accurate results compared to the exact solution. However, at the acoustic natural frequency of the duct, the boundary element results vary from the exact solution slightly. The source of this discrepant is the coefficient matrix singularity at this frequency.

The second example problem uses the same duct and the same acoustic assumption, but the outlet boundary condition is assumed to be a rigid wall. Once again, from Figure 3.3, the boundary element method gives very accurate approximation, except at the acoustic natural frequency.

In the third example problem, an impedance boundary condition is applied at the outlet of the duct. A non-reflection condition, that is no reflection from the outlet, is used here, which assumes the relationship between pressure and velocity at the outlet to be $v = \rho_o c$ based on the plane wave assumption. The density of air is taken as $\rho_o = 1.21 kg/m^3$ and the speed of sound in air is given as $c = 343 m/sec$. The results are shown in Figure 3.4. Compared to the exact solution[48], observe that the boundary element method results are quite accurate.

Generally, when the input frequency increases, the boundary element method results tend to diverge from the exact solution. At high frequency, the higher acoustic modes become significant while the current boundary element mesh may not be fine enough to describe the higher acoustic modes. Thus, a finer mesh is needed to resolve the solution.

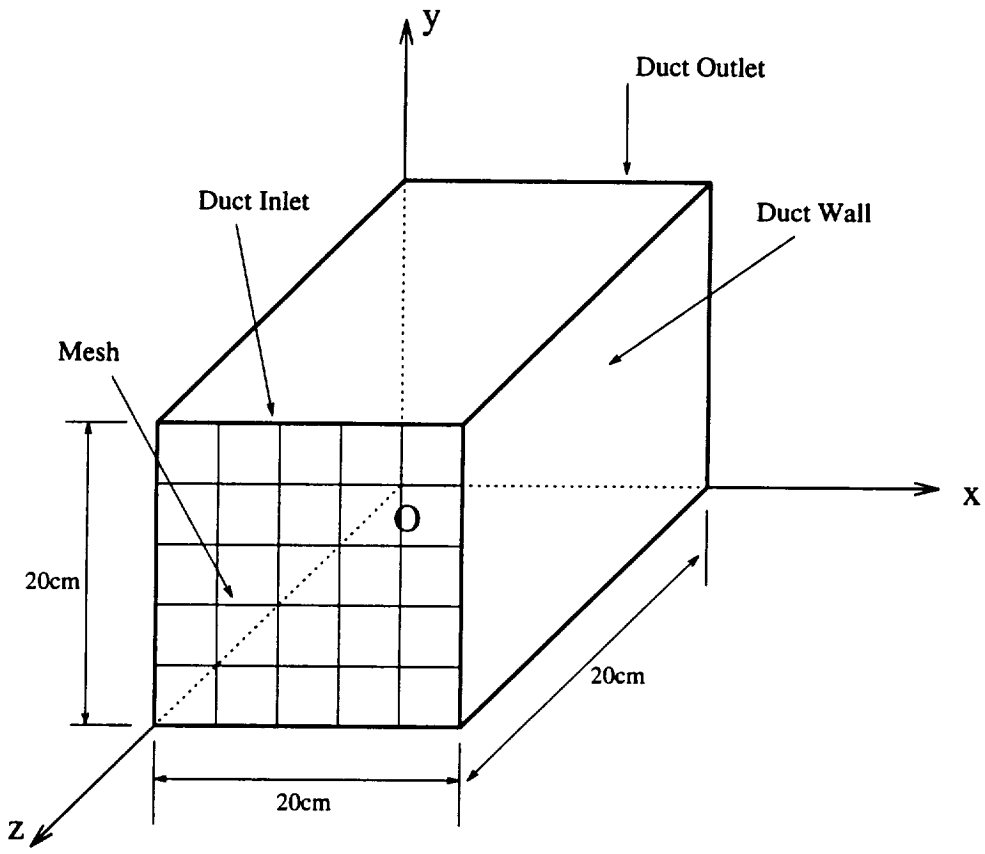

Figure 3.1 Three dimensional rectangular duct

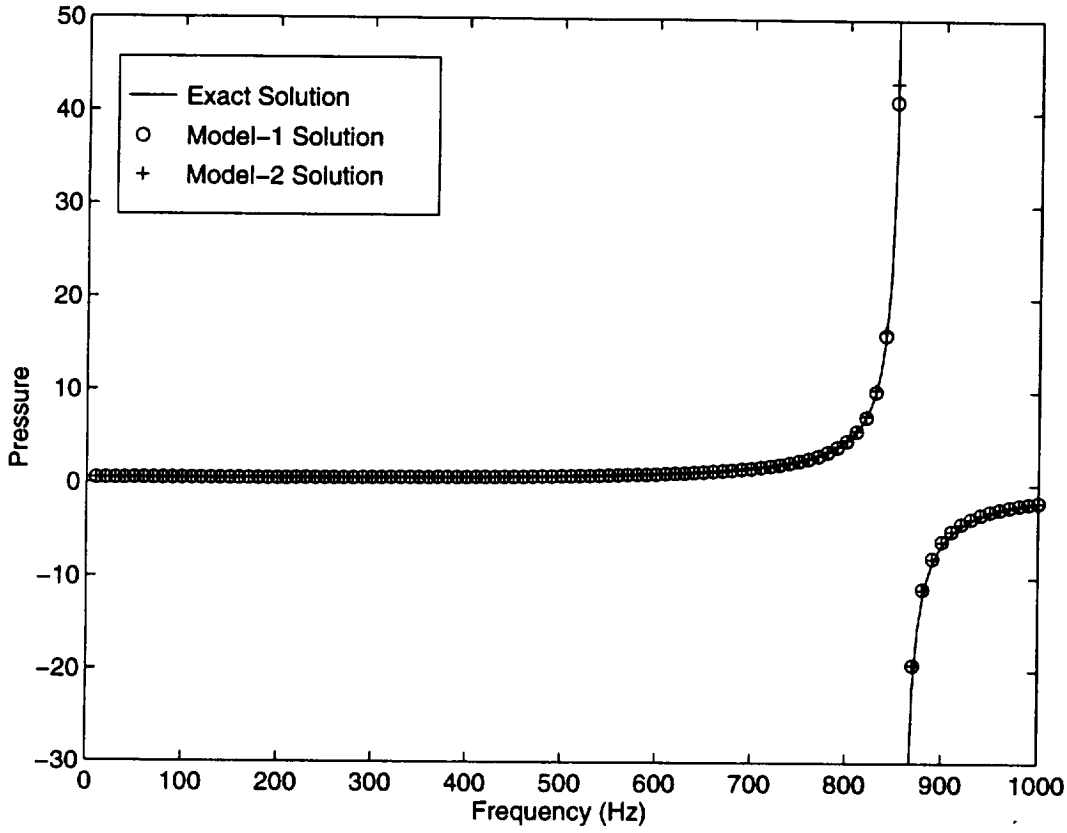

Figure 3.2 Results for three-dimensional duct with null pressure at outlet

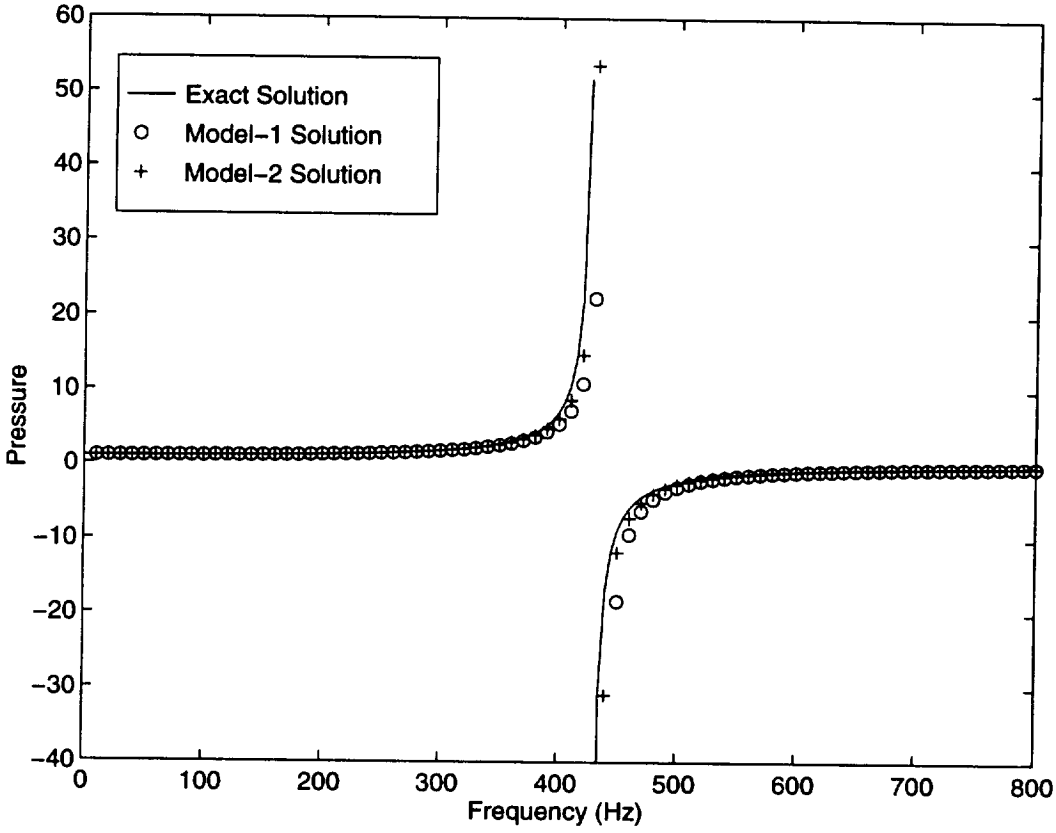

Figure 3.3 Results for three-dimensional duck with rigid wall outlet

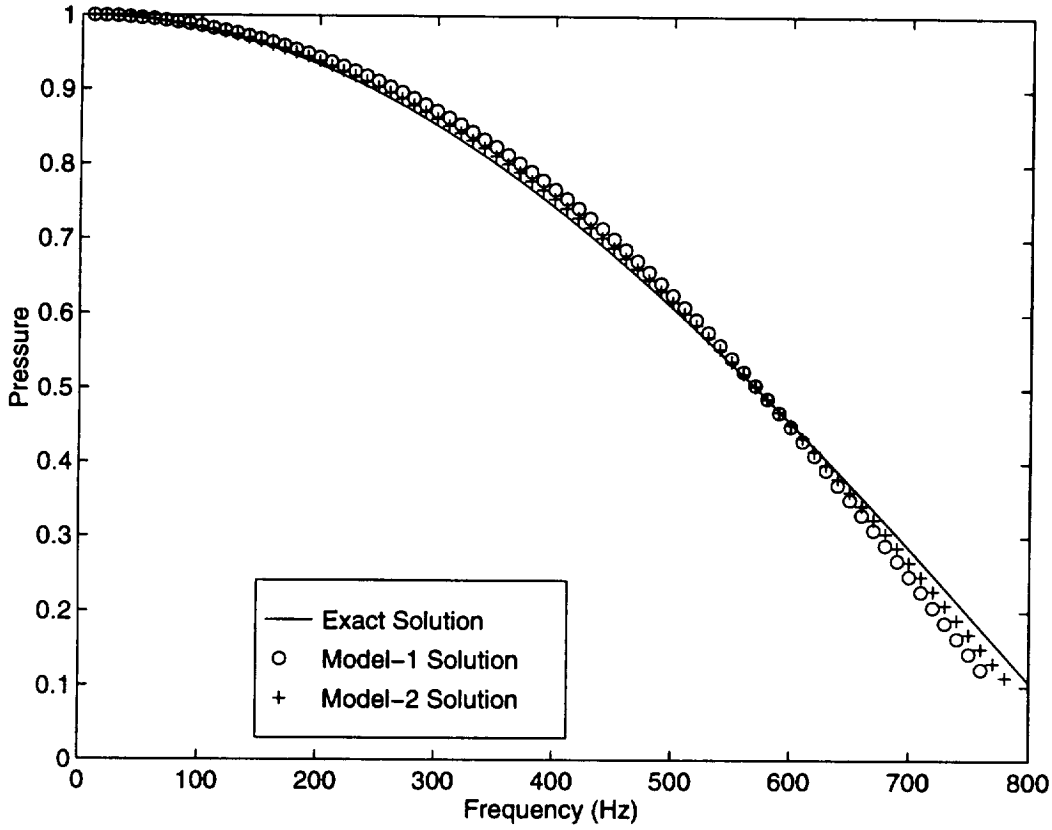

Figure 3.4 Result for three-dimensional duck with non-reflection outlet

3.2 Structural—Acoustic Interaction Response by Coupled FE/BE Method

Coupling the structural and acoustic domains is essential when trying to accurately model harsh environments. As mentioned in Chapter 1, the coupling between a flexible plate and the acoustic cavity under harmonic acoustic inputs has been investigated by many researchers using different approaches. The first objective of this section is to validate the present coupled FE/BE method by comparing with known analytical and experimental results for a system consisting of an isotropic plate and a cubic acoustic cavity. Then this coupled FE/BE method is extended to other systems with composite plates.

As shown in Figure 3.5, the coupled structural-acoustic system studied in this section consists of a square plate and a cubic acoustic cavity with all other five walls acoustically rigid. The plate is subjected to a uniformly distributed external pressure loading. Two different plate models are considered.

The first coupled structural—acoustic system studied here consists of a cubic cavity and a simply supported brass panel with the following plate and cavity characteristics:

Panel/Cavity Problem-Simply Supported Brass Plate

Cavity

X axis length $L_x = 20 \quad cm$

Y axis length $L_y = 20 \quad cm$

Z axis length $L_z = 20 \quad cm$

Density of Air $\rho_o = 1.21 \times 10^{-3} \quad g/cm^3$

Sound speed $c = 34300 \quad cm/sec.$

Brass

Young's Modulus $= 10.4 \times 10^{10} \quad psi$

Poisson's Ratio $= 0.37$

Density $\rho_b = 8.5 \quad g/cm^3$

Brass Plate

X axis length = 20 cm.

Y axis length = 20 cm.

Thickness = 0.09144 cm.

Two different mesh cases were used in modeling this coupled system. One case (mesh-1) consisted of 25 (5x5 mesh) finite elements for the plate, 150 (5x5 mesh for each of the six cavity walls) boundary elements for cavity, and 125 (5x5x5) internal nodes; the second case (mesh-2) used 49 (7x7 mesh) finite elements for the plate, 294 (7x7 mesh for each of the six cavity walls) boundary elements, and 343 (7x7x7) internal nodes. The pressure at the center of the cavity back wall (at $x = y = 10\ cm,\ z = 0$) is considered as the output pressure (p_{out}) and the transmission loss (TL) is calculated using the pressure on the exterior surface of the plate (at $z = 20\ cm$) as the input pressure (p_{in})

$$TL = 10 \log_{10} \left(\frac{p_{in}}{p_{out}} \right)^2 \tag{3.1}$$

The present FE/BE method results are shown in Figure 3.6 and exact solutions[17] and experimental data[9] in Figure 3.7[17]. Note the FE/BE method results are of comparable accuracy even for the first mesh case.

The second example considered analyzes the same plate/cavity system as the previous one. The cavity is still cubic with all five walls being acoustically rigid; however, this time the panel is made of composite materials. The cavity and composite plate used in this example have the following properties:

Panel/Cavity Problem — Simply Supported Composite Plate

Cavity

X axis length $L_x = 8\ in.$

Y axis length $L_y = 8\ in.$

Z axis length $L_z = 8\ in.$

Density of Air $\rho_o = 0.1138 \times 10^{-6}\ lb/in.^3$

Sound speed $c = 1.3504 \times 10^4 \quad in./sec.$

Composite Plate

X axis length = 8 in.

Y axis length = 8 in.

Thickness = 0.036 in.

Graphite/Epoxy

$$E_{11} = 2.25 \times 10^7 \ psi$$

$$E_{22} = 1.17 \times 10^6 \ psi$$

$$\nu_{12} = 0.22$$

$$G_{12} = 0.66 \times 10^6 \ psi$$

$$\rho = 0.1458 \times 10^{-3} \ lb/in.^3$$

Three 6–layer composite plates of different stacking sequences are investigated. The plate is simply supported. The transmission losses are plotted in Figures 3.8 to 3.10 versus frequency. It can be seen that, in the three different stacking sequences, the fundamental natural frequencies increase from uncoupled 115.3 Hz for $(0/30/0)_s$ plate, 114.9 Hz for $(0/60/0)_s$ plate, 109.5 for $(0/90/0)_s$ plate (obtained by 7x7 mesh), to coupled 143.9 Hz, 143.9 Hz, and 139.7 Hz, respectively.

Boundary conditions are another factor affecting coupled natural frequencies. Figure 3.11 shows the transmission losses of the system with the same $(0/90/0)_s$ laminated plate, but with different supported conditions. The 7x7 mesh is used. The coupled fundamental natural frequency increases to around 240 Hz for the clamped case. Generally, the transmission loss for the clamped case is larger than that of the simply supported case.

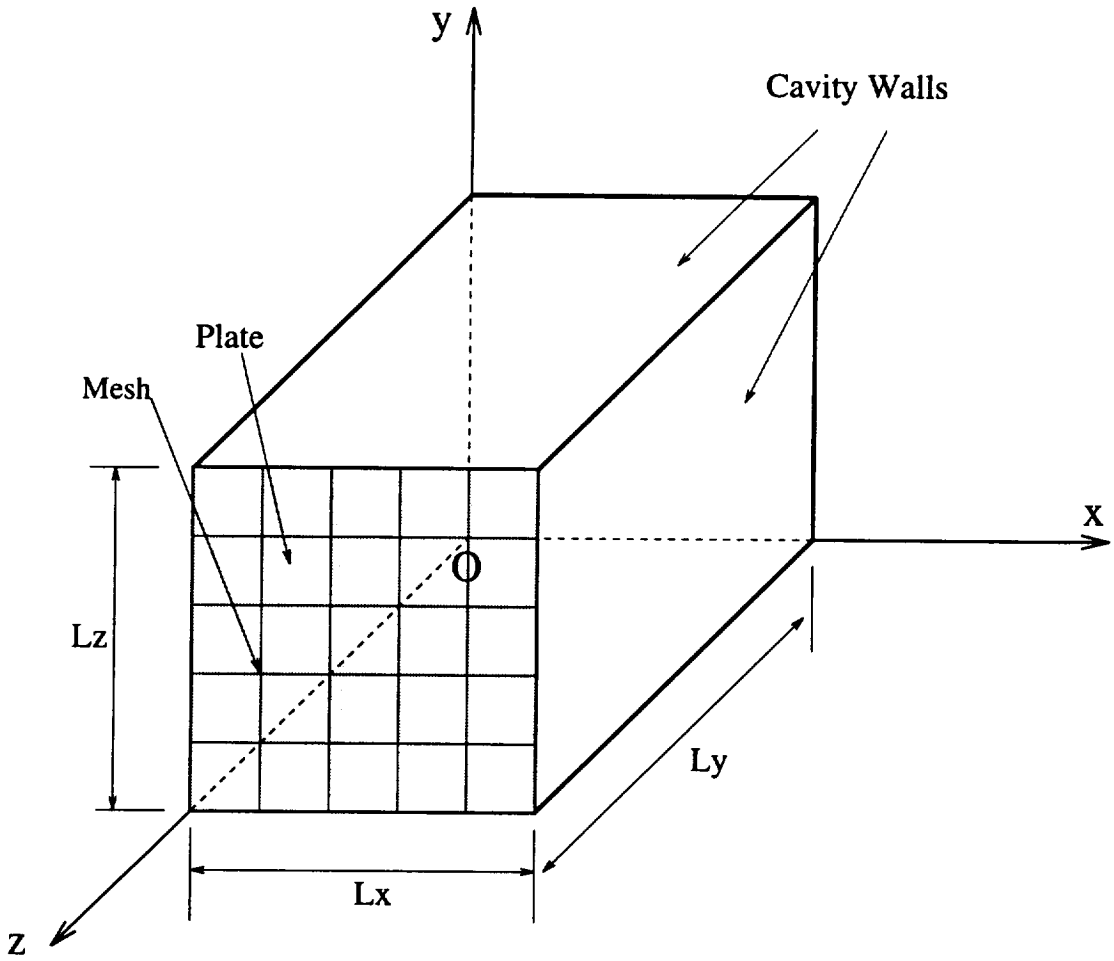

Figure 3.5 Structural-acoustic system: plate and cavity

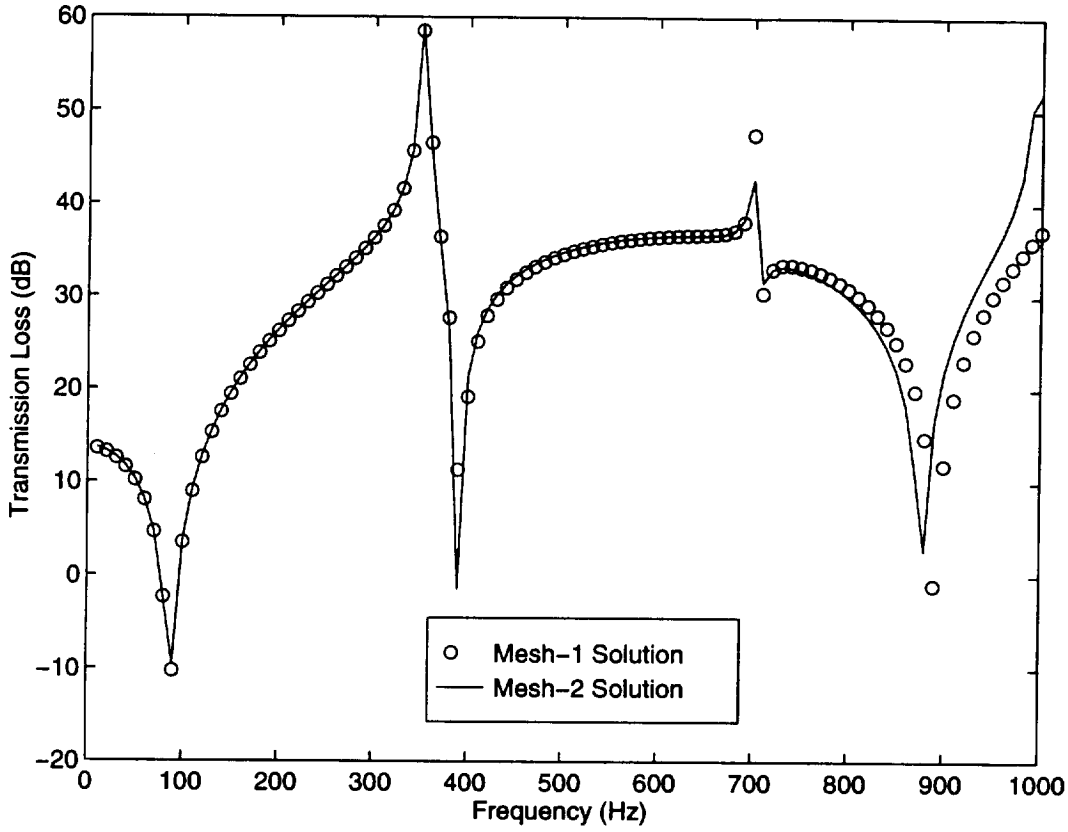

Figure 3.6 Transmission loss for the system consists of a simply supported isotropic plate and a cubic cavity: Present results

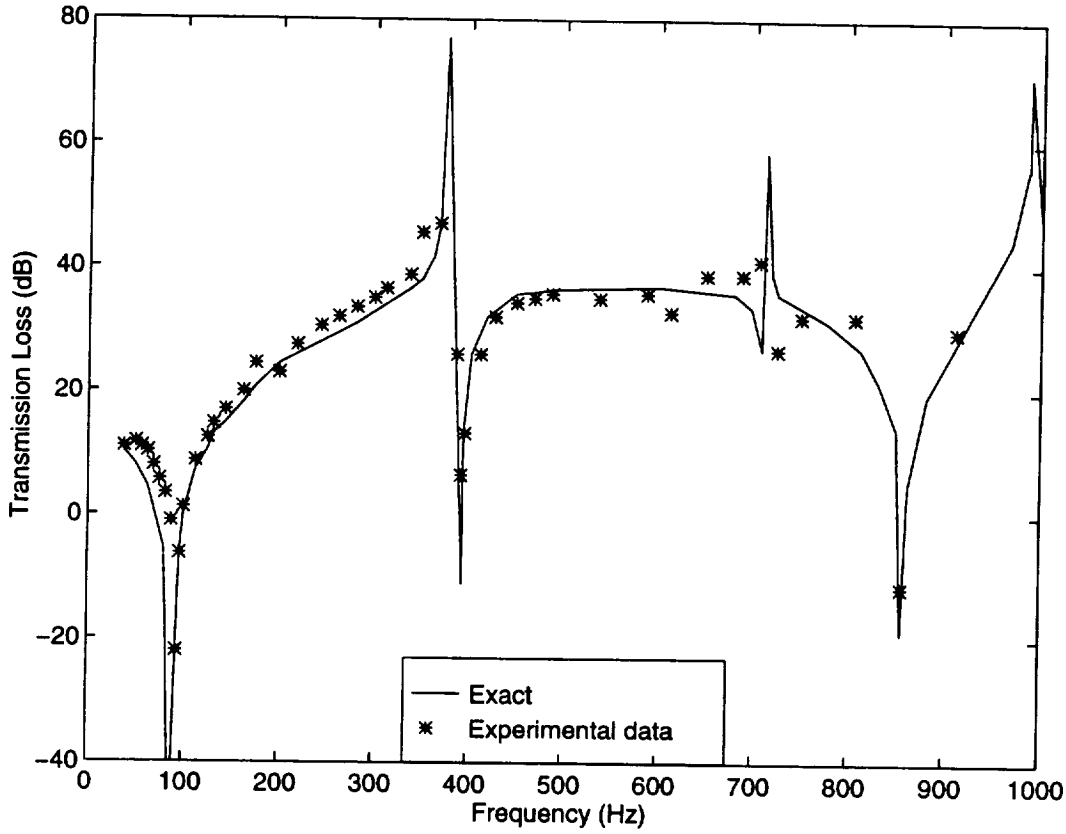

Figure 3.7 Transmission loss for the system consists of a simply supported isotropic plate and a cubic cavity: Exact solution[17] and experimental data[9] (Ref. 17)

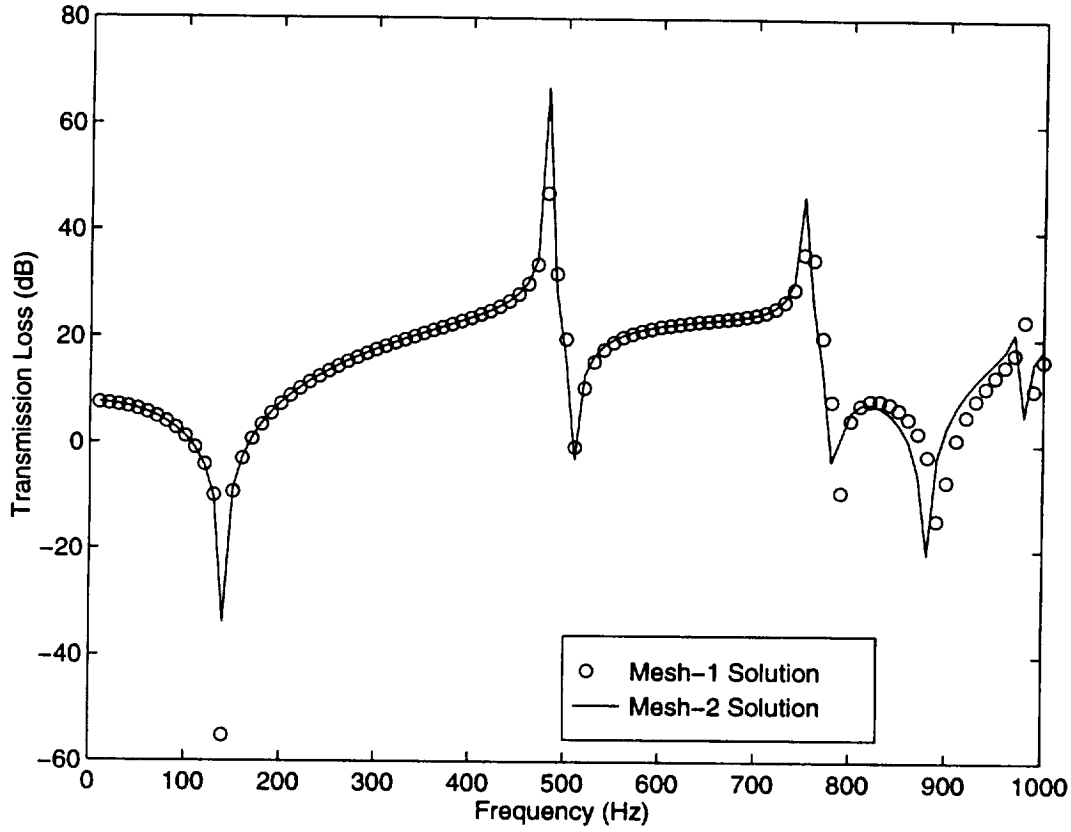

Figure 3.8 Transmission loss for the system consists of a simply supported $(0/90/0)_s$ plate and a cubic cavity

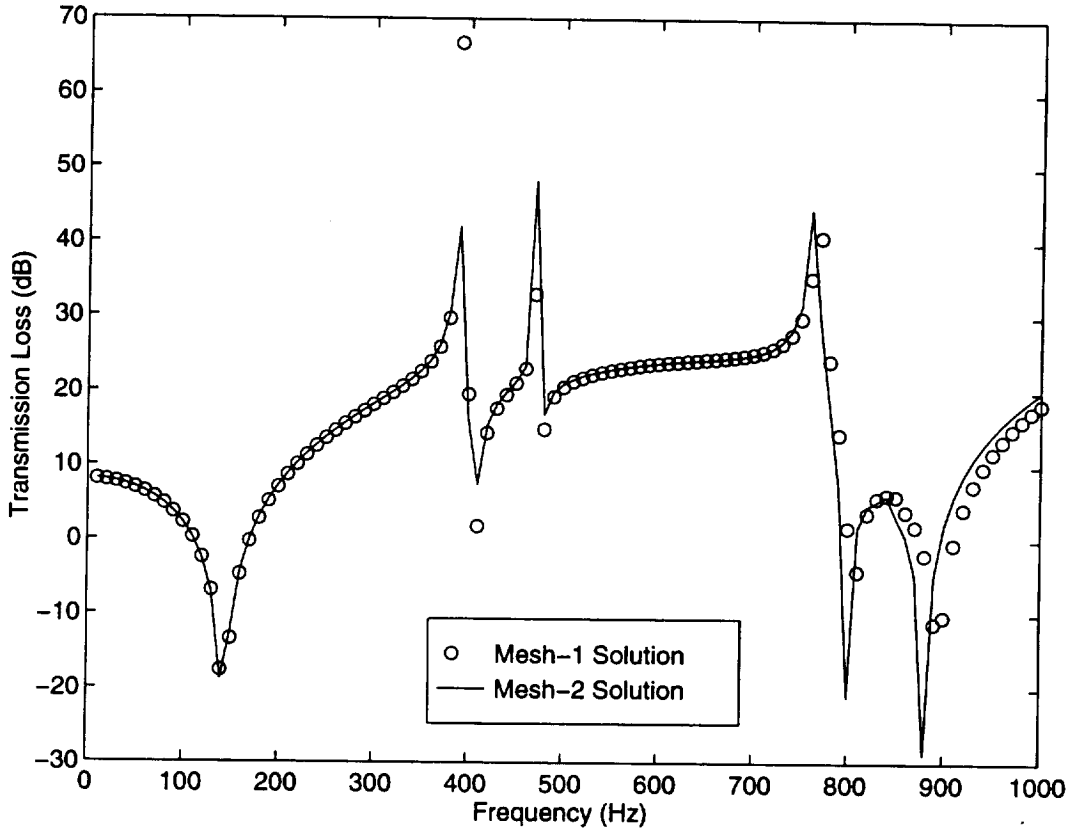

Figure 3.9 Transmission loss for the system consists of a simply supported $(0/60/0)_s$ plate and a cubic cavity

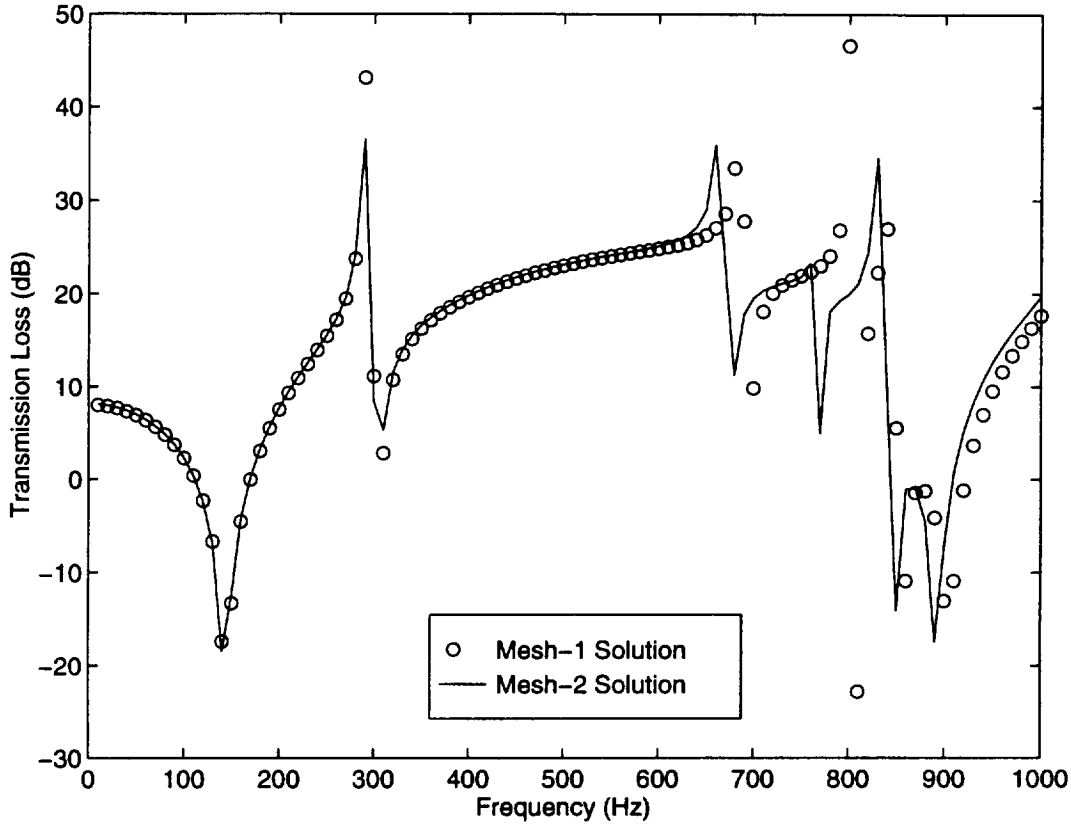

Figure 3.10 Transmission loss for the system consists of a simply supported $(0/30/0)_s$ plate and a cubic cavity

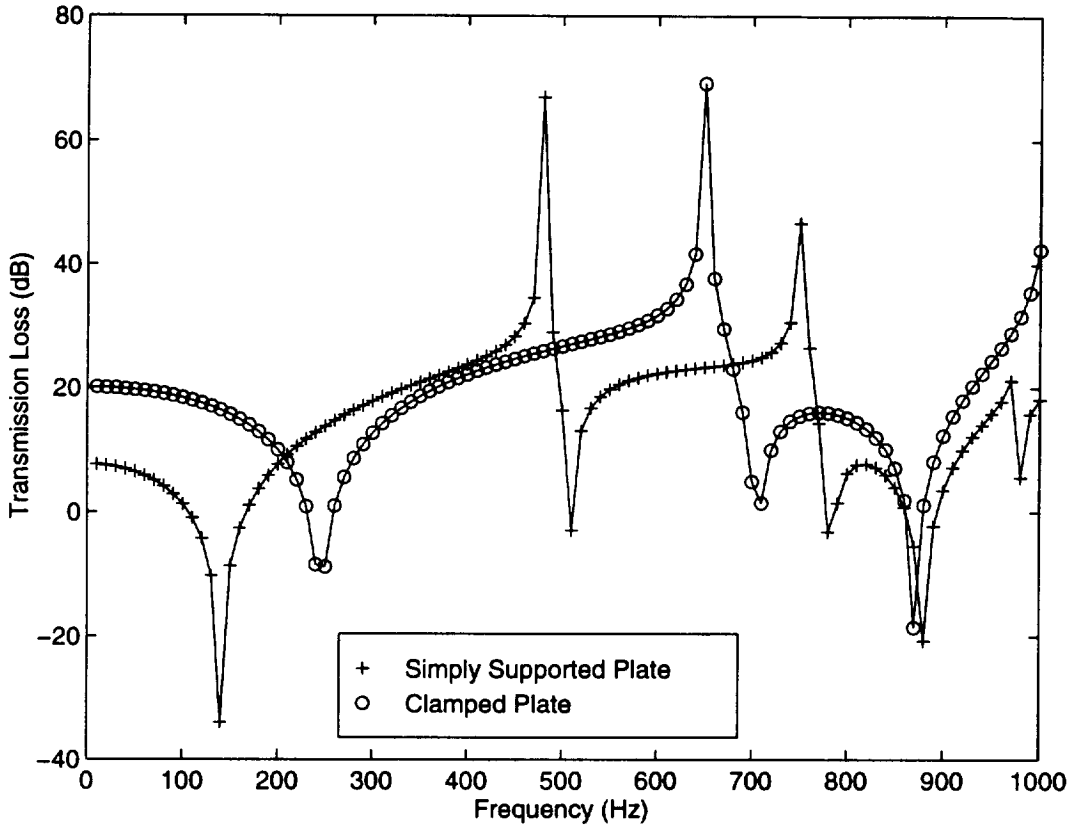

Figure 3.11 Transmission loss for the system consists of a simply supported $(0/90/0)_s$ plate and a cubic cavity, Comparison of different plate boundary conditions.

3.3 Structural-Acoustic Interaction Response by Modal Formulation

The next objective is to form the model in modal coordinates for the coupled system consisting of a 6–layer $(0/90/0)_s$ composite plate and a cubic acoustic cavity, and to investigate the response of this coupled system under transient acoustic pressure. It is essential for a mathematical model to accurately represent transient behavior if the model is to be used as the basic equation for control. Even under harmonic inputs, there is a transient period immediately following controller activation. Although the final response of the coupled system will be harmonic under harmonic disturbance, the capability of the coupled equations to model the response under transient load is necessary. Meanwhile, to predict transient response itself is rather important for structural-acoustic interactions.

Although the coupled finite element and boundary element formulation developed in Chapter 2 can be applied to transient problems directly, the current formulation is not convenient because of the large number of equations, and it is very difficult, if not impossible, to use this formulation in any control attempt. Hence, the coupled equations have to be transformed into the modal formulation.

3.3.1 Coupled Natural Frequency and Mode Shape

To transform the coupled finite element and boundary element equations in terms of physical coordinates into modal coordinates, a transformation matrix is required. As mentioned in Chapter 2, we use the eigenvectors of the coupled system as the transformation matrix. Generally, not all boundary element methods applied in acoustics can be used to obtain the natural frequency and/or modal shape of the system, because the frequency of the external load is embedded in the fundamental solution[48]. But the dual reciprocity boundary element method is one of those which can isolate eigenvalues and eigenvectors. In fact, assuming the load term and damping term in equation (2.67) are zero, we obtain an eigenvalue problem.

Table 3.1 gives a comparison of the natural frequency results for the coupled system consisting of a cubic acoustic cavity with all five walls rigid and a simply supported brass

plate obtained from experiment[9], analytical approach[17], and present method. The table indicates the coupled FE/BE method gives rather accurate results.

Table 3.1 Natural frequencies (Hz): Exact solution, Experiment data, and Present Results

Exact [17]	Experiment [9]	Present FEM/BEM		Uncoupled
		FE-25, BE-125	FE-49, BE-294	
87.0	91.0	87.7	87.4	78.1
390.4	397.0	394.7	392.1	390.3
702.5	730.0	710.9	704.3	702.5
860.0	864.0	891.8	872.9	857.5

The convergence of the time-domain modal formulation, that is how many modes should be retained in the analysis, was studied. Figure 3.12 shows the transmission loss of the system consisting of a cubic acoustic cavity with all five wall rigid and a simply supported brass plate under uniformly distributed external pressure. It indicates that the lowest five modes are sufficient to give an accurate result. For the system with a 6–layer, simply supported $(0/90/0)_s$ composite plate, the number of modes needed for accurate results is also five as shown in Figure 3.13. The non-dimensional plate deflection and transmitted acoustic pressure on the cavity back wall and one side wall (for example, x = 8 in.) for the first mode are plotted in Figures 3.14 to 3.16 to show the coupling affect on both the deflection mode of plate and the acoustic pressure mode of the cavity. We thus will take five modes for all subsequent calculations using modal formulation.

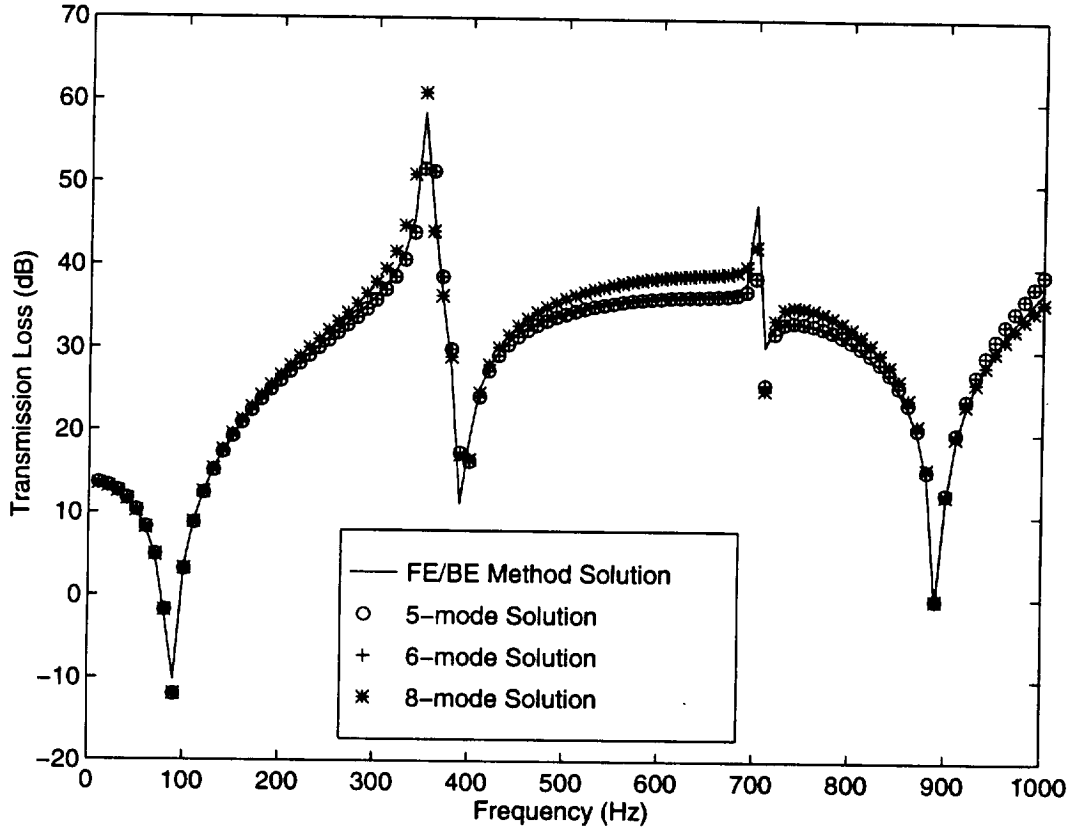

Figure 3.12 Convergence of the time-domain formulation for the system consists of a simply supported brass plate and a cubic cavity

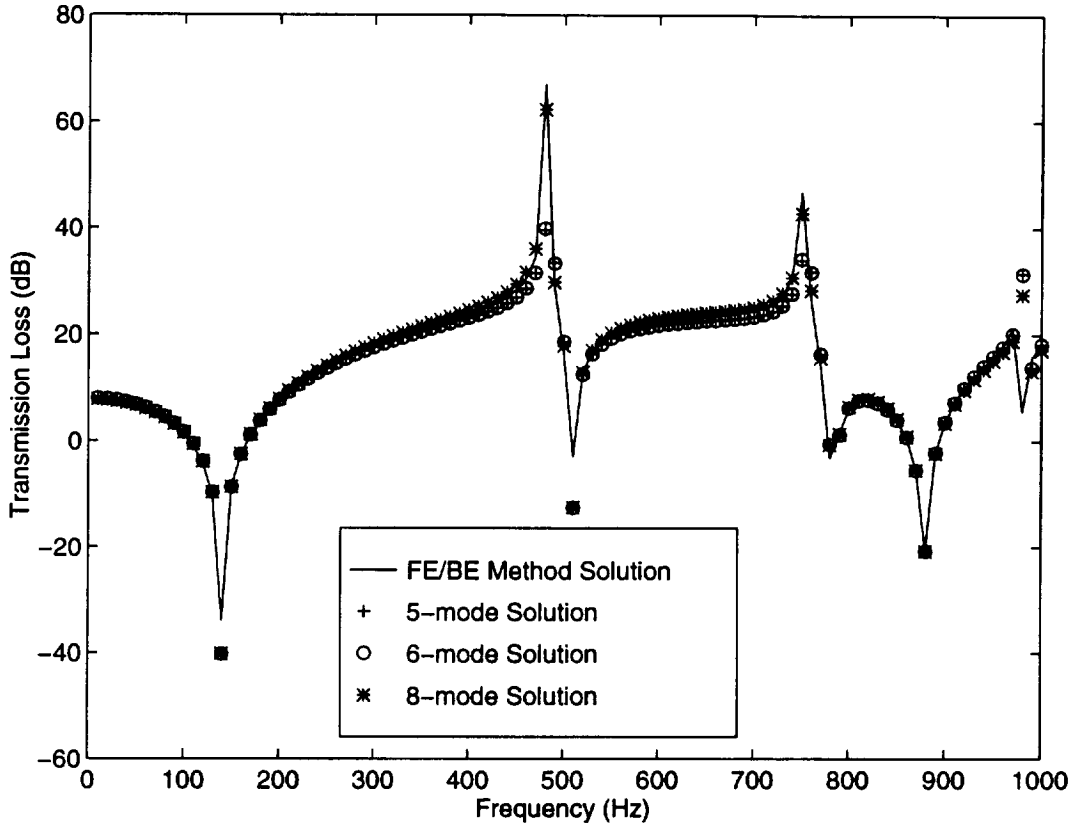

Figure 3.13 Convergence of the time-domain formulation for the system consists of a simply supported $(0/90/0)_s$ plate and a cubic cavity

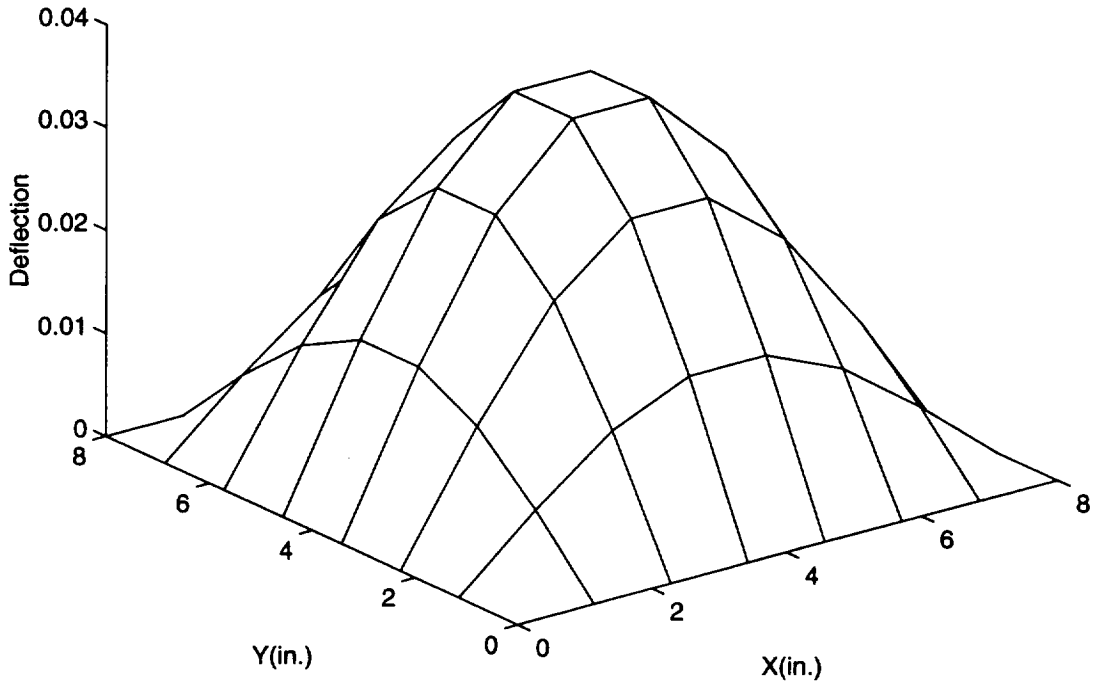

Figure 3.14 The first modal shape of the system consisting of a simply supported $(0/90/0)_s$ plate and a cubic cavity: plate deflection

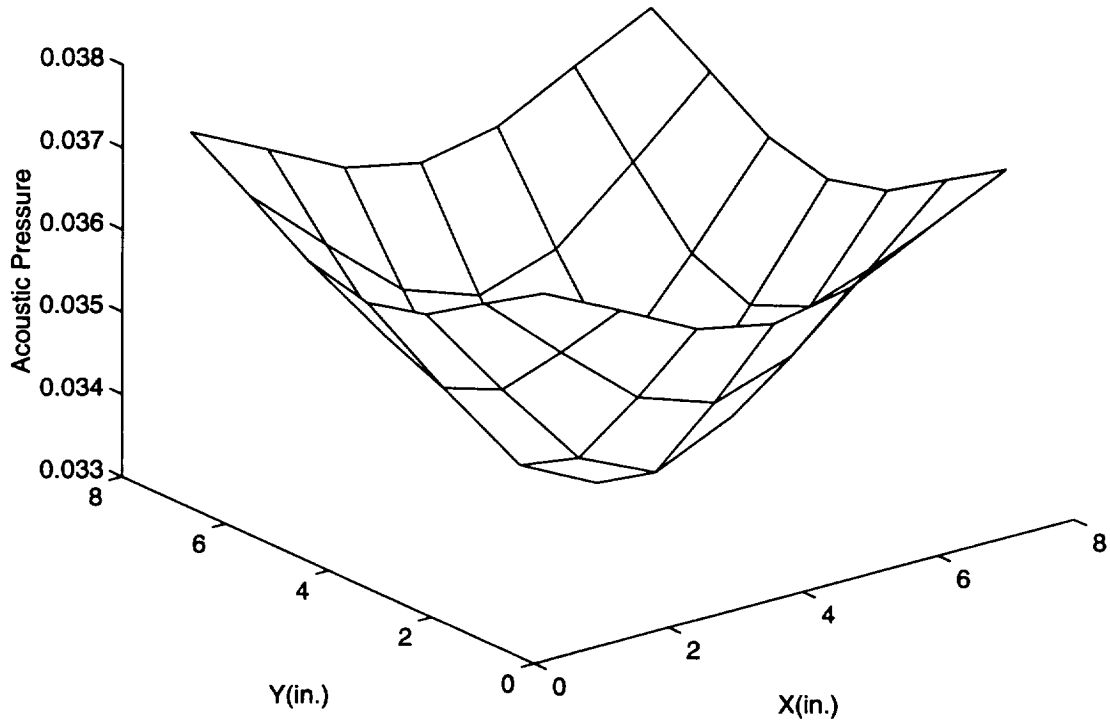

Figure 3.15 The first modal shape of the system consisting of a simply supported $(0/90/0)_s$ plate and a cubic cavity: pressure on the back wall of the cavity

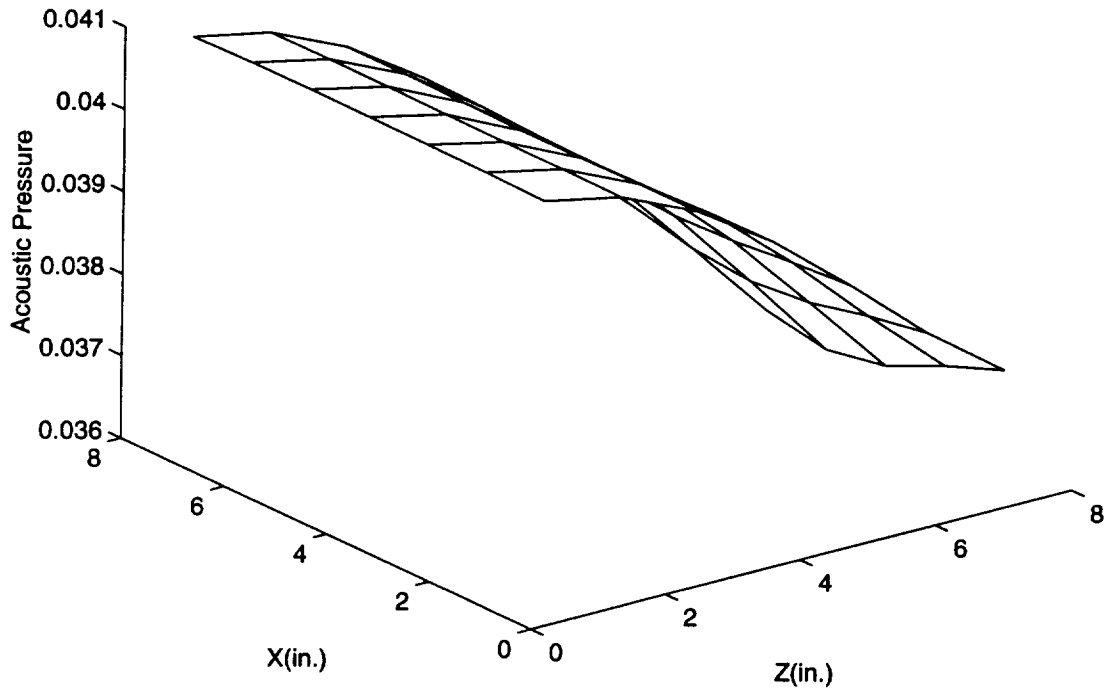

Figure 3.16 The first modal shape of the system consisting of a simply supported $(0/90/0)_s$ plate and a cubic cavity: pressure on a side wall of the cavity

3.3.2 Time-Domain Modal Results

When modal coordinates, or modes, are selected, we are ready to predict the response of the coupled structural-acoustic system. The time-domain modal formulation is actually a set of ordinary differential equations (for transient problem). Since the number of equations in the modal formulation is small (here it is five), a classical Runge-Kutta numerical integration scheme can be easily employed.

What we study here is the coupled structural-acoustic system consisting of a 6–layer, $(0/90/0)_s$ composite plate and a cubic cavity given in Section 3.2 under uniformly distributed pressure on the external surface of the plate. The initial conditions in all three examples are static. The first example problem is the response to an impulse, that is, the forcing function is assumed to be

$$F(x,y,t) = 1.5\delta(t) \times 10^{-3} \ (lb/in.^2) \tag{3.2}$$

The time history of the displacement at the center of the plate, the transmitted acoustic pressure at the center of the cavity back wall ($x = y = 4\ in.\ \ z = 0$), and the forcing function are shown in Figure 3.17. It can be seen that multiple modes are excited.

Multiple resonant excitation of this coupled structural—acoustic system is studied next. The forcing function is

$$f(x,y,t) = 1.5[\sin(300\pi t) + \sin(1760\pi t)] \times 10^{-3} \ \ (lb/in.^2) \tag{3.3}$$

and, hence, it excites the first and fourth system modes which have natural frequencies of 139.7 Hz and 879.0 Hz, respectively. This forcing function represents a periodic plane wave with a sound pressure level of 126 dB. The time histories of the forcing function, the displacement at the center of the plate, and the transmitted acoustic pressure at the center of the cavity back wall are shown in Figure 3.18.

The last example of this chapter is the response under a forcing function defined as

$$f(x,y,t) = 1.5 \times \left\{ \begin{array}{ll} 95t & 0 \le t \le 0.01 \\ 0.95 & 0.01 \le t \le 0.03 \\ 0.95 - 55(t - 0.03) & 0.03 \le t \le 0.04 \\ 0.4 & t \ge 0.04 \end{array} \right\} (lb/in.^2) \tag{3.4}$$

The forcing function, the displacement at the center of the plate and the transmitted acoustic pressure at the center of the cavity back wall are shown in Figure 3.19. Those examples demonstrated the capability of handling time-dependent problems of the present method.

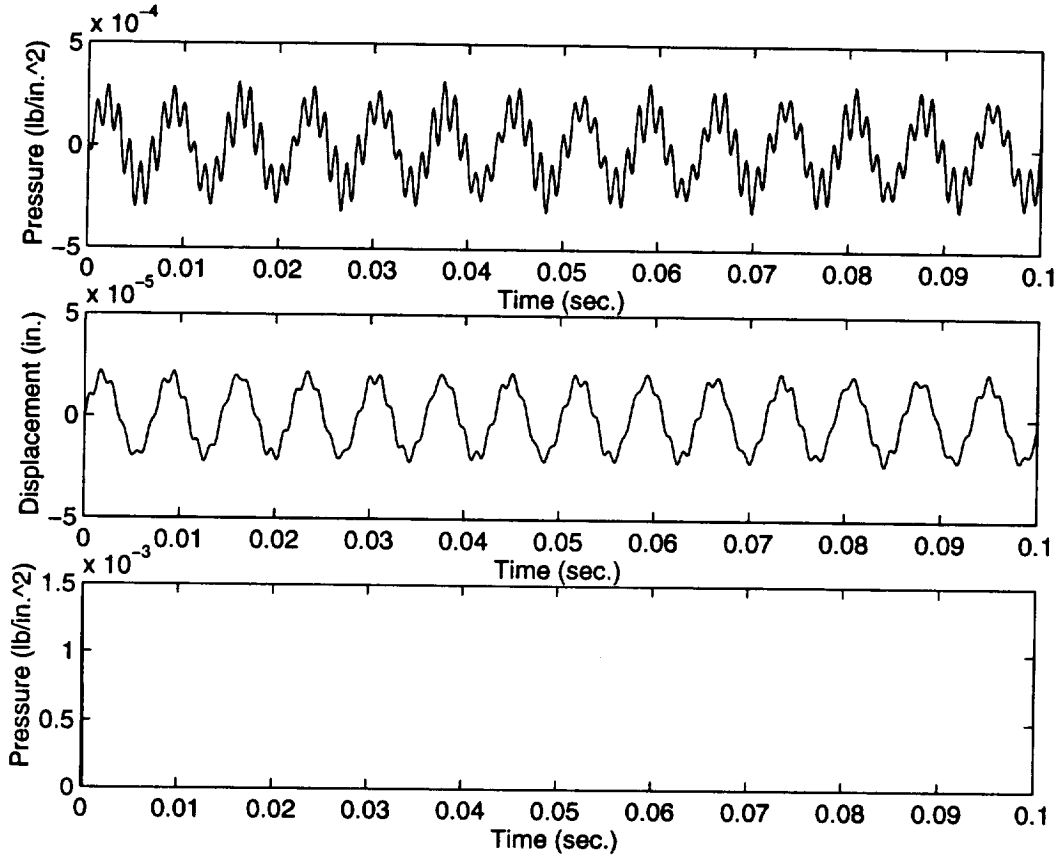

Figure 3.17 Displacement at the center of the plate and transmitted pressure at the center of the cavity back wall: Forcing function (bottom) equation (3.2)

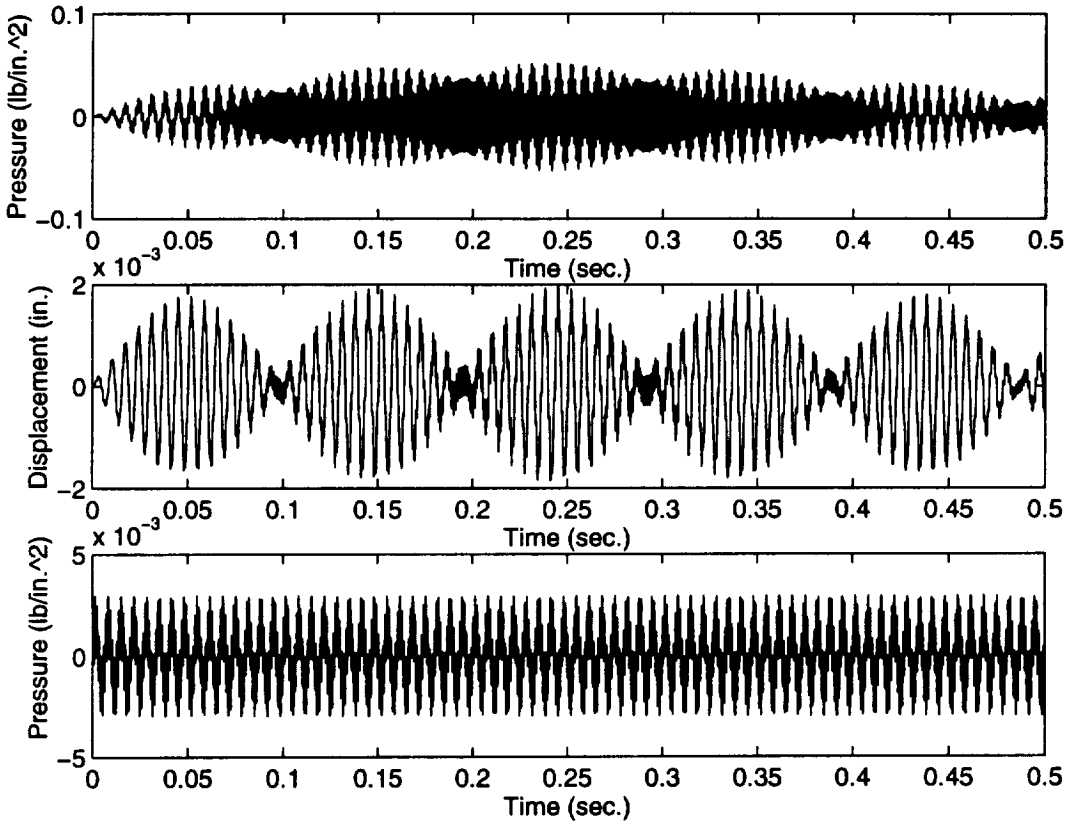

Figure 3.18 Displacement at the center of the plate and transmitted pressure at the center of the cavity back wall: Forcing function (bottom) equation (3.3)

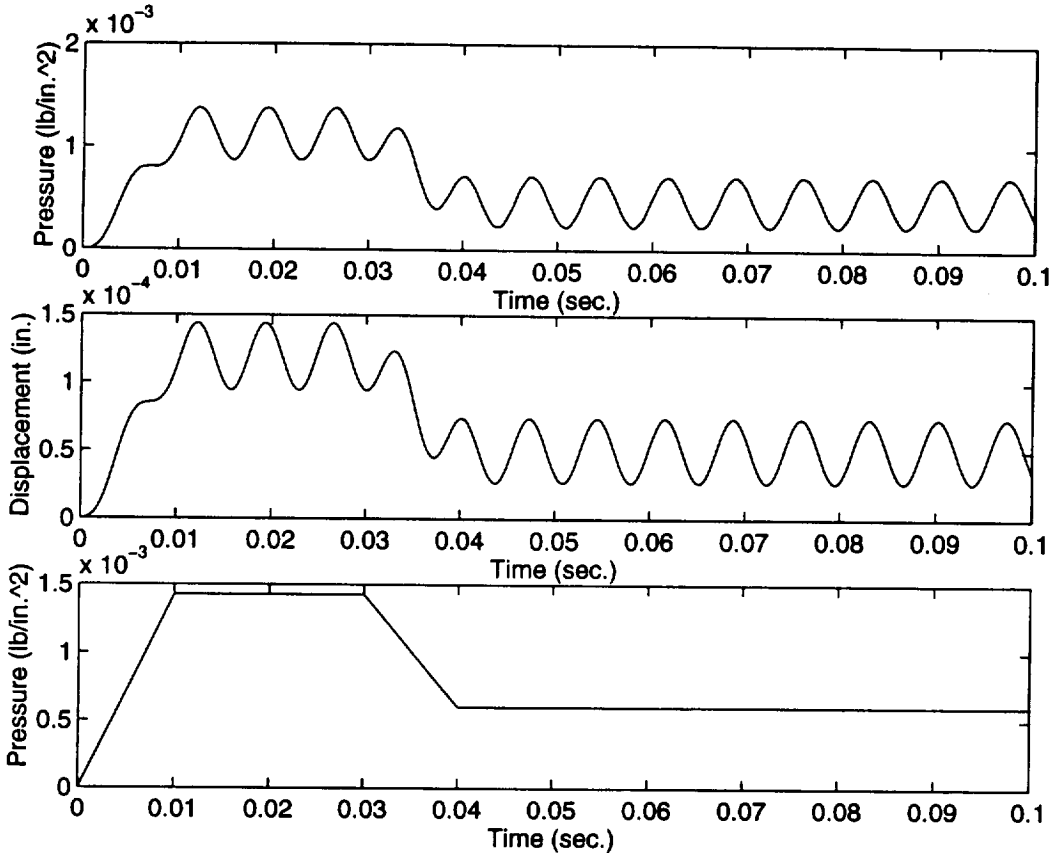

Figure 3.19 Displacement at the center of the plate and transmitted pressure at the center of the cavity back wall: Forcing function (bottom) equation (3.4)

3.4 Conclusions

The numerical examples given in this chapter show that the dual reciprocity boundary element method, the coupled boundary element-finite element method and its time-domain formulation, developed in Chapter 2, can be used to solve acoustic or coupled structural-acoustic problems accurately and efficiently. Although we did not give any example with complex geometry, based on the versatility of the boundary element method and the finite element method, and the general approach employed in this chapter for the structural-acoustic coupling, we can expect that it is not difficult to extend this method to problems of complex geometry. In fact, the example problems investigated in this chapter show little difficulty in applying this method to different plates, different plate boundary conditions, and different acoustic boundary conditions.

Chapter 4
CONTROL OF INTERIOR ACOUSTIC PRESSURE LEVEL

The second step of this investigation is to control the interior acoustic pressure level based on the governing equations in the time-domain derived in Chapter 2. The control force is applied through the piezoelectric patches bonded on the two surfaces of the plate.

The governing equations in time-domain are first rewritten in state space form. Then a feedback controller, the linear quadratic regulator, and a feedforward controller based on the concept of least mean square (LMS) are employed to reduce the acoustic pressure field inside the cavity via transmission through the flexible plate using piezoelectric patches as actuators.

4.1 State Space Formulation

The time-domain modal formulation is rewritten here as

$$[M]^*\{\ddot{\eta}\} + [C]^*\{\dot{\eta}\} + [K]^*\{\eta\} = \{L_1\} + \{L_2\} \tag{4.1}$$

where $\{L_1\}$ is due to external acoustic pressure and $\{L_2\}$ is due to piezoelectric actuators. If we denote the system response due to external pressure as $\{\eta_e\}$ and that due to actuators as $\{\eta_a\}$, then we have

$$[M]^*\{\ddot{\eta}_e\} + [C]^*\{\dot{\eta}_e\} + [K]^*\{\eta_e\} = \{L_1\} \tag{4.2}$$

$$[M]^*\{\ddot{\eta}_a\} + [C]^*\{\dot{\eta}_a\} + [K]^*\{\eta_a\} = \{L_2\} \tag{4.3}$$

and

$$\{\eta\} = \{\eta_e\} + \{\eta_a\} \tag{4.4}$$

Define

$$\mathbf{x_o} = [\eta_e, \dot{\eta}_e]^T, \qquad \mathbf{x} = [\eta_a, \dot{\eta}_a]^T \tag{4.5}$$

Then we have the state space form of the governing equations (4.3) as

$$\dot{\mathbf{x}} = \mathbf{A}\mathbf{x} + \mathbf{B}\mathbf{u} \tag{4.6}$$

where $\mathbf{u} = \{E_3\}/E_{3max}$ is the control variable vector, E_{3max} is the maximum allowable operating electric field of the piezoelectric material,

$$\mathbf{A} = \begin{bmatrix} 0 & I \\ -M^{*-1}K^* & -M^{*-1}C^* \end{bmatrix}, \mathbf{B} = \begin{Bmatrix} 0 \\ M^{*-1}G \end{Bmatrix} \tag{4.7}$$

and $[G]$ is the control inference matrix which is obtained from

$$\{L_2\} = [G]\mathbf{u} \tag{4.8}$$

4.2 Linear Optimal Controller

The linear quadratic regulator is considered in this section to reduce the acoustic pressure level inside the cavity. The objective here is to minimize the global acoustic pressure using the piezoelectric patches bonded on the two surfaces of the plate. The control mathematical models based on the time-domain state space formulation are presented first, then numerical results are obtained.

4.2.1 Mathematical model

Define the linear quadratic performance index for optimal control as[81]

$$J = \frac{1}{2}\int_0^\infty \left[(\mathbf{x}+\mathbf{x_0})^{\mathrm{T}}\mathbf{Q}(\mathbf{x}+\mathbf{x_0}) + \mathbf{u}^{\mathrm{T}}\mathbf{R}\mathbf{u}\right]dt \tag{4.9}$$

where $\mathbf{Q}$ is a real symmetric positive semi-definite matrix and $\mathbf{R}$ is a real symmetric positive definite matrix. Then the optimal control for this linear quadratic problem can be obtained as a function of the costate[81], and if we assume the relation between the costate and the state variable is linear, we have the control effort as

$$\mathbf{u} = -\mathbf{R}^{-1}\mathbf{B}^{\mathrm{T}}\mathbf{P}(\mathbf{x}+\mathbf{x_o}) \tag{4.10}$$

while the Riccati matrix $\mathbf{P}$, which is symmetric and positive definite, can be obtained from the Riccati equation[82]

$$\mathbf{A}^{\mathrm{T}}\mathbf{P} + \mathbf{P}\mathbf{A} - \mathbf{P}\mathbf{B}\mathbf{R}^{-1}\mathbf{B}^{\mathrm{T}}\mathbf{P} = -\mathbf{Q} \tag{4.11}$$

Consider a maximum electric field that can be applied to the piezoelectric material, where the constraint for equation (4.11) is

$$|u_i| < 1, \quad i = 1, 2, \ ..., \ Np \tag{4.12}$$

and Np is the number of piezoelectric actuators. Then equations (4.9), (4.10), and (4.11) form a bounded optimization problem.

Since our objective is to control the inside acoustic pressure level, we define the weighting matrix $\mathbf{Q}$ so that the $(\mathbf{x}+\mathbf{x_o})^T\mathbf{Q}(\mathbf{x}+\mathbf{x_o})$ term in the linear quadratic performance index represents the acoustic potential energy in the cavity

$$\frac{1}{2}\int_V \frac{p^2}{\rho_o c^2} dV = \frac{1}{2\rho_o c^2}\{\eta\}^T[\Psi_\Omega]^T[\Psi_\Omega]\{\eta\} \tag{4.13}$$

where $[\Psi_\Omega]$ is the modal shape matrix evaluated inside the cavity, it relates to the NN interior points in the cavity and can be obtained from the coupled modal matrix $[\Psi]$ in equation (2.70). Then we have

$$[\mathbf{Q}] = \begin{bmatrix} \mathbf{Q_{11}} & \mathbf{0} \\ \mathbf{0} & \mathbf{Q_{22}} \end{bmatrix} \tag{4.14}$$

where

$$\begin{aligned} \mathbf{Q_{11}} &= \frac{1}{2\rho_o c^2}[\Psi_\Omega]^T[\Psi_\Omega] \\ \mathbf{Q_{22}} &= \mathbf{0} \end{aligned} \tag{4.15}$$

4.2.2 Numerical Results

Based on the above mathematical model, several example problems are solved. The coupled structural-acoustic system is the cubic cavity backed by a simply supported 6–layer $(0/90/0)_s$ composite plate given in Section 3.2. The results are presented as follows.

Piezoelectric Layers

Before the discussion of control results, the coupled structural-acoustic system is modified by bonding a piezoelectric layer on each of the external and internal surfaces completely of the composite plate. The piezoelectric material is considered as isotropic. The characteristics of the piezoceramic layer are:[71]

Piezoelectric Layer (PZT)

$$Modulus\ of\ Elasticity \quad E_p = 0.9 \times 10^7 \ psi$$

$$Poisson's\ Ratio \quad \gamma_p = 0.3$$

$$Density \quad \rho_p = 0.7101 \times 10^{-3} \ lb/in.^3$$

$$Stress/Charge\ Constant \quad d_{31} = d_{32} = -7.51 \times 10^{-9} \ in./v$$

$$Max.\ Electric\ Field \quad E_{3max} = 1.52 \times 10^4 \ v/in.$$

The thickness of the piezoelectric layer is assumed to be the same as the composite layer; that is, 0.006 inch. Following the same procedure given in Chapter 3, the responses of the full coupled acoustic/composite/piezoelectric system under harmonic acoustic pressure with different frequency content are obtained. The transmission loss at the center of the cavity back wall is compared with that of the system without piezoelectric layers in Figure 4.1. The natural frequencies of the systems with or without piezoelectric layers are tabulated in Table 4.1. Two conclusions can be obtained from this result: 1) the mass and stiffness of the piezoceramic layers have to be considered, the responses of the structural-acoustic systems with and without the piezoceramic layers are rather different, the natural frequencies of the system are changed, the fundamental frequency decreases 10Hz and the second increases because of the isotropic property of the piezoelectric layers; and 2) five modes are sufficient for the time-domain modal formulation to obtain accurate results for input frequency up to 1000 Hz.

Table 4.1 Natural frequencies (Hz) of the system with and without piezoelectric layers

	mode 1	mode 2	mode 3	mode 4	mode 5
With PZT Layers	129.6	574.7	685.0	867.9	1060.1
Without PZT Layers	139.7	509.8	783.5	878.6	985.4

Resonant Excitation

The forcing function for this example is assumed to be

$$f(x,y,t) = 3.0 \sin(280\pi t) \times 10^{-3} \ (lb/in^2.) \tag{4.16}$$

which corresponds to the frequency of 140 Hz and, hence, the fundamental natural frequency of the coupled structural-acoustic system with piezocermatic layers which is 129.6 Hz is excited. Consider the reflection, equation (4.16) models a periodic exterior plane wave with a maximum pressure level of 120 dB. The initial condition of the system is assumed to be at rest. The weighting matrix $\mathbf{R}$ is taken to be diagonal, and each diagonal element is equal to 10^{-4}.

Table 4.2 Modal coefficients for controlled and uncontrolled system for resonant excitation

	mode 1	mode 2	mode 3	mode 4	mode 5
uncontrolled	1.77E-01	1.27E-04	1.87E-04	-6.34E-04	-2.34E-05
controlled	3.91E-03	4.56E-04	5.29E-04	-5.11E-04	-8.56E-05

Control is implemented via piezoelectric patches covering the two surfaces of the composite plate. The time histories of the displacement at the center of the plate, the pressure at the center of the cavity back wall, the norm of the pressure field inside the cavity ($||[\Psi_\Omega]\{\eta\}||$), and the control effort are given in Figure 4.2. The amplitude of the acoustic pressure at the center of the cavity back wall decreases from 7.22×10^{-3} $lb/in.^2$ to 1.37×10^{-4} $lb/in.^2$ after the controller is turned on, that means a 34.4 dB increase in the transmission loss. At the same time, the amplitude of the maximum deflection of the plate reduced from 7.93×10^{-4} $in.$ to 1.14×10^{-5} $in.$ It can be seen form Figure 4.2, the acoustic pressure and the displacement of the plate are all reduced when the control force is applied. Figures 4.3 and 4.4 give the comparison of the maximum acoustic pressure inside the cavity and the maximum plate displacement between the controlled and uncontrolled system at the instant of maximum acoustic pressure at the center of the cavity back wall. It can be seen that, for the uncontrolled system, the response is dominated by the first coupled mode. After the controller is turned on, multi-mode behavior appears. Table 4.2 gives the values of the modal variables corresponding to maximum acoustic pressure at the center of the cavity back wall for the controlled and

uncontrolled systems, those results indicate the dominated fundamental mode is reduced with active control.

Multi-Resonant Excitation

The forcing function for this example is

$$f(x,y,t) = 3.0[\sin(280\pi t) + \sin(1760\pi t)] \times 10^{-3} \quad (lb/in.^2) \tag{4.17}$$

Hence, the fundamental and the fourth coupled natural frequency, the later corresponds to the uncoupled cavity frequency at 867.9 Hz, are excited. This function models a periodic plane wave of maximum pressure level around 126 dB. The initial condition of the coupled system is at rest.

Table 4.3 Modal coefficients for controlled and uncontrolled system for multi-resonant excitation

	mode 1	mode 2	mode 3	mode 4	mode 5
uncontrolled	1.78E-01	3.68E-04	5.48E-04	-4.43E-02	-6.48E-05
controlled	4.01E-03	6.15E-04	9.10E-04	-2.82E-03	-4.61E-05

The same cost function as in the resonant excitation case is applied in this example. The time histories of the displacement at the center of the plate, the pressure at the center of the cavity back wall, the norm of the pressure field inside the cavity, and the control effort are given in Figure 4.5. Notice that the pressure and displacement are both reduced dramatically after the controller is turned on. The amplitude of the acoustic pressure at the center of the cavity back wall decreases from 9.56×10^{-3} $lb/in.^2$ to 2.33×10^{-4} $lb/in.^2$ after the controller was turned on, that means a 32.3 dB increase in the transmission loss, and the amplitude of the maximum deflection of the plate reduced from 8.05×10^{-4} $in.$ to 1.50×10^{-5} $in.$ Figures 4.6 and 4.7 give the comparison of acoustic pressure inside the cavity and plate displacement of the controlled and uncontrolled system at the instant of maximum acoustic pressure at the center of the cavity back wall. Table 4.3 tabulates the modal coefficients corresponding to maximum acoustic pressure at the center of the cavity back wall for the controlled and uncontrolled systems. It can be seen that the fundamental and fourth modes are the dominate and both are reduced.

Off-Resonant Excitation

In this example, the forcing function was taken to be

$$f(x,y,t) = 3.0\sin(500\pi t) \times 10^{-3} \ \ (lb/in.^2) \tag{4.18}$$

with a frequency of 250 Hz which is between the natural frequencies of the first (129.6 Hz) and the second (574.7 Hz) system modes. As noted before, this models a periodic plane wave of maximum pressure level around 120 dB. The initial condition of the system is again at rest.

The same quadratic cost as before is applied in this example. The time histories of the displacement at the center of the plate, the pressure at the center of the cavity back wall, the norm of the pressure field inside the cavity, and the control effort are given in Figure 4.8. Figures 4.9 and 4.10 give the comparison of acoustic pressure inside the cavity and the plate displacement of the controlled and uncontrolled system. The amplitude of the acoustic pressure at the center of the cavity bottom decreases from 6.49×10^{-4} $lb/in.^2$ to 1.40×10^{-4} $lb/in.^2$ after the controller was turned on, that means a 13.3 dB increase in the transmission loss, and the amplitude of the maximum deflection of the plate reduced from 6.49×10^{-5} $in.$ to 1.92×10^{-5} $in.$ Notice that the reduction of acoustic pressure and the plate deflection in this off-resonant excitation example is much smaller than in the resonant or multi-resonant examples, this phenomena is reasonable because, the pressure or deflection of the off-resonant case themselves are much small comparing to resonant or multi-resonant cases. This can be observed by comparing Table 4.4 with Tables 4.2 and 4.3.

Table 4.4 Modal coefficients for controlled and uncontrolled system for off-resonant excitation

	mode 1	mode 2	mode 3	mode 4	mode 5
uncontrolled	1.52E-02	1.54E-04	2.02E-04	-9.13E-04	-2.36E-05
controlled	3.46E-03	4.01E-04	4.40E-04	-7.86E-04	-5.89E-05

Effect of Weighting Matrix Q

Weighting matrix **Q** determines the linear quadratic response term in the cost function. Consequently, different definitions of **Q** will give different performance. Here we defined another weighting matrix to compare the performance with the cavity acoustic potential energy given in equation (4.15). The elements in equation (4.14) are defined here as

$$\begin{aligned} \mathbf{Q_{11}} &= [K]^* \\ \mathbf{Q_{22}} &= [\mathrm{M}]^* \end{aligned} \tag{4.19}$$

The results of the system response under external excitations given in equations (4.16) to (4.18) are obtained using the same **R** matrix as before. The time histories of the displacement at the center of the plate, the pressure at the center of the cavity back wall, the norm of the pressure field inside the cavity, and the control effort are given in Figures 4.11 to 4.13 for the three loads, respectively. Table 4.5 compares the increase of sound transmission loss at the center of the cavity back wall and the displacement reduction at the center of the plate for those two **Q** matrices. The displacement reduction is defined as the ratio of the controlled and the uncontrolled displacement amplitudes. It can be seen that the performance from the two different cost functions are comparable to each other.

Table 4.5 The increase of sound transmission loss (ITL) at the center of the cavity back wall and the displacement reduction (DR) at the center of the plate: comparison of different weighting matrices **Q**

	Q matrix in Eq. (4.15)		**Q** matrix in Eq. (4.19)	
	ITL (dB)	DR (%)	ITL (dB)	DR (%)
Resonant	34.4	1.44	27.8	4.04
Multi-Resonant	32.3	1.86	29.2	4.35
Off-Resonant	13.3	29.4	12.4	29.3

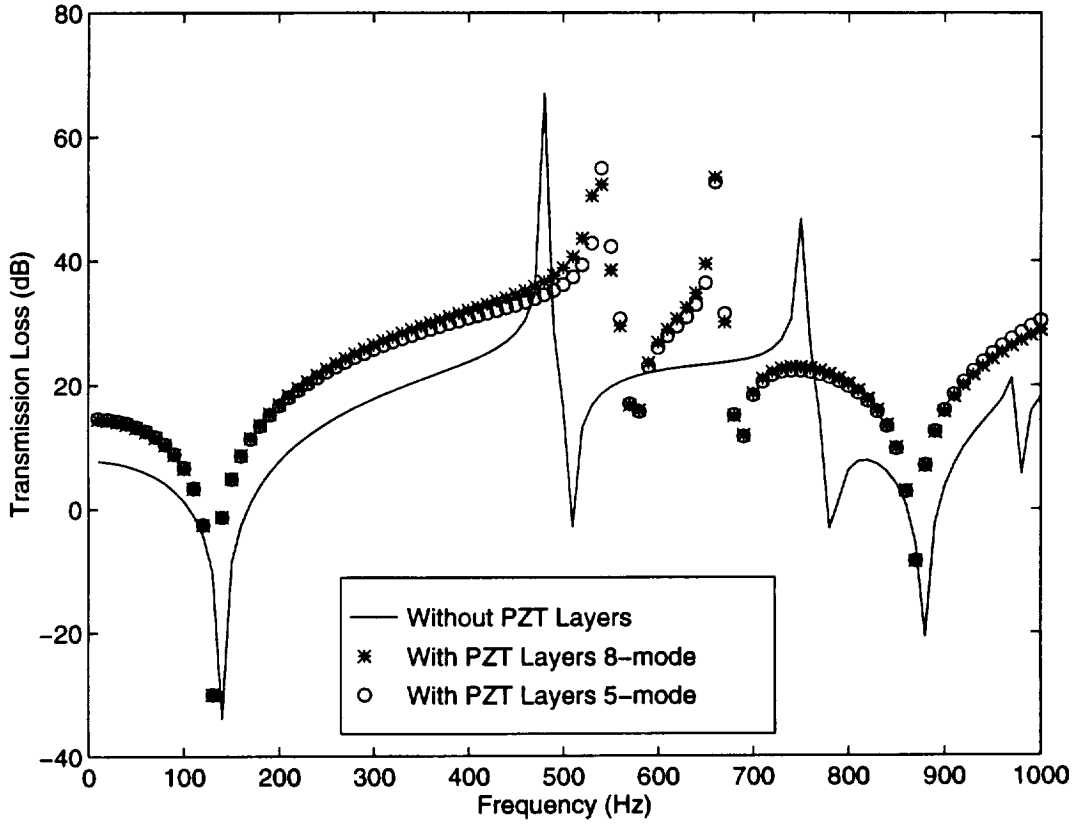

Figure 4.1 Comparison of responses to harmonic external excitations for the coupled structural-acoustic system with or without piezoelectric layers.

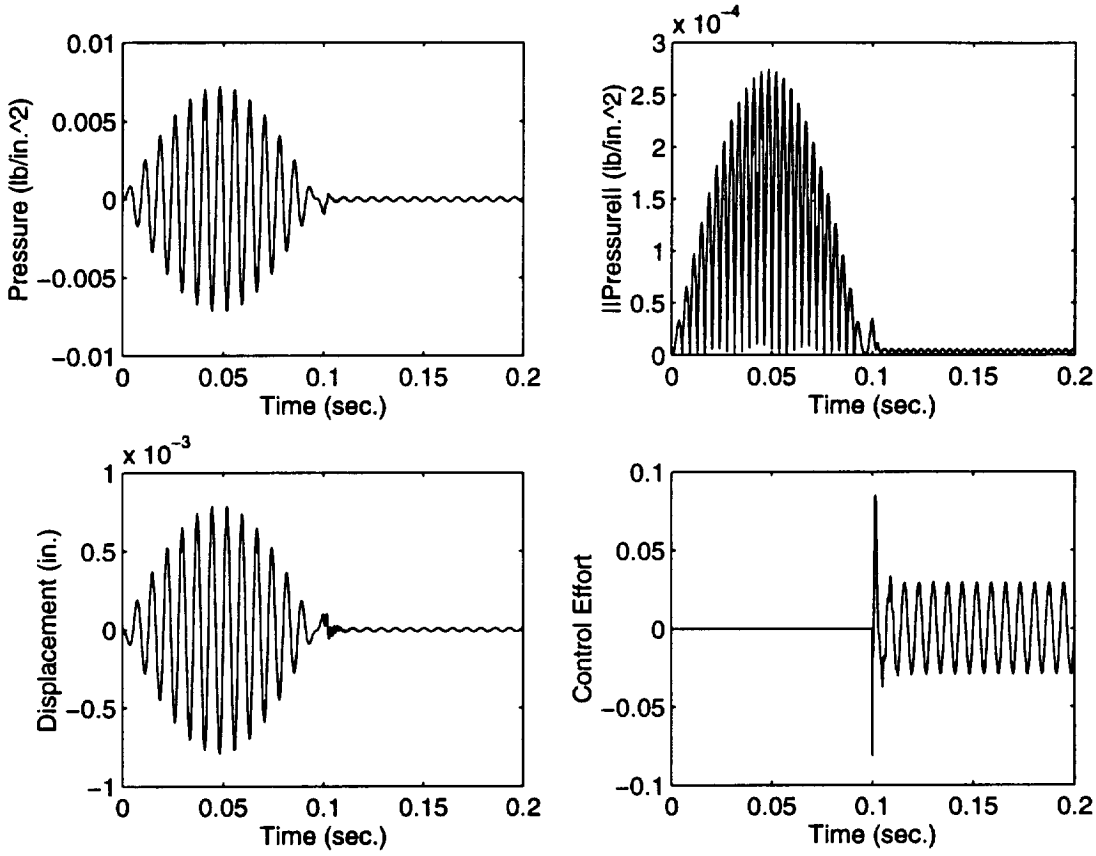

Figure 4.2 Time history of the pressure at the center of the cavity back wall, the displacement at the center of the plate, the norm of the cavity pressure field, and the control effort: Resonant excitation

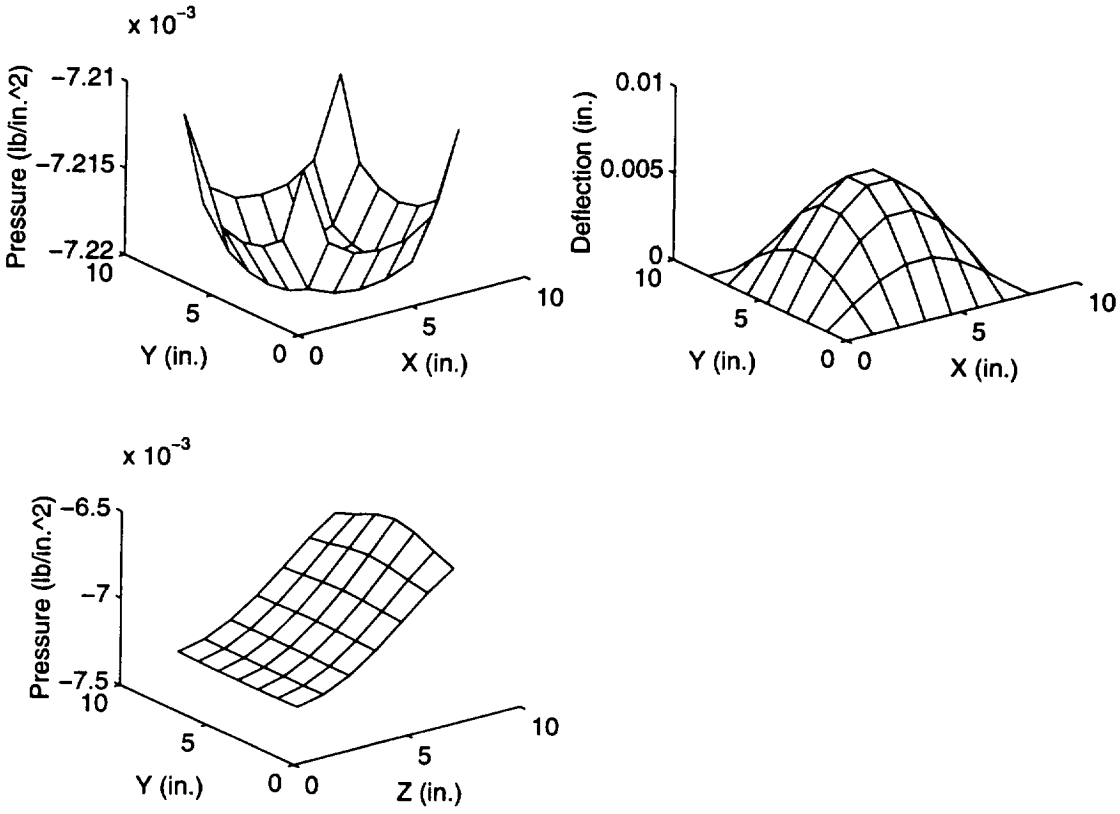

Figure 4.3 Uncontrolled pressure field and plate deflection: Resonant excitation

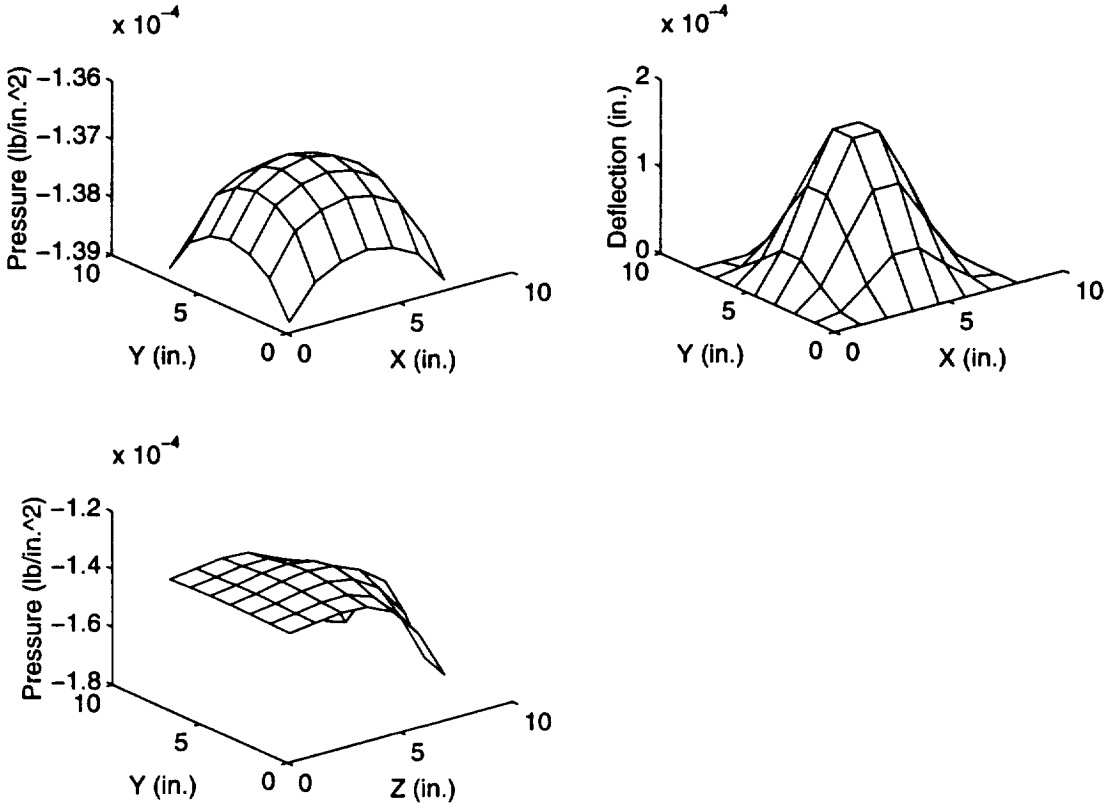

Figure 4.4 Controlled pressure field and plate deflection: Resonant excitation

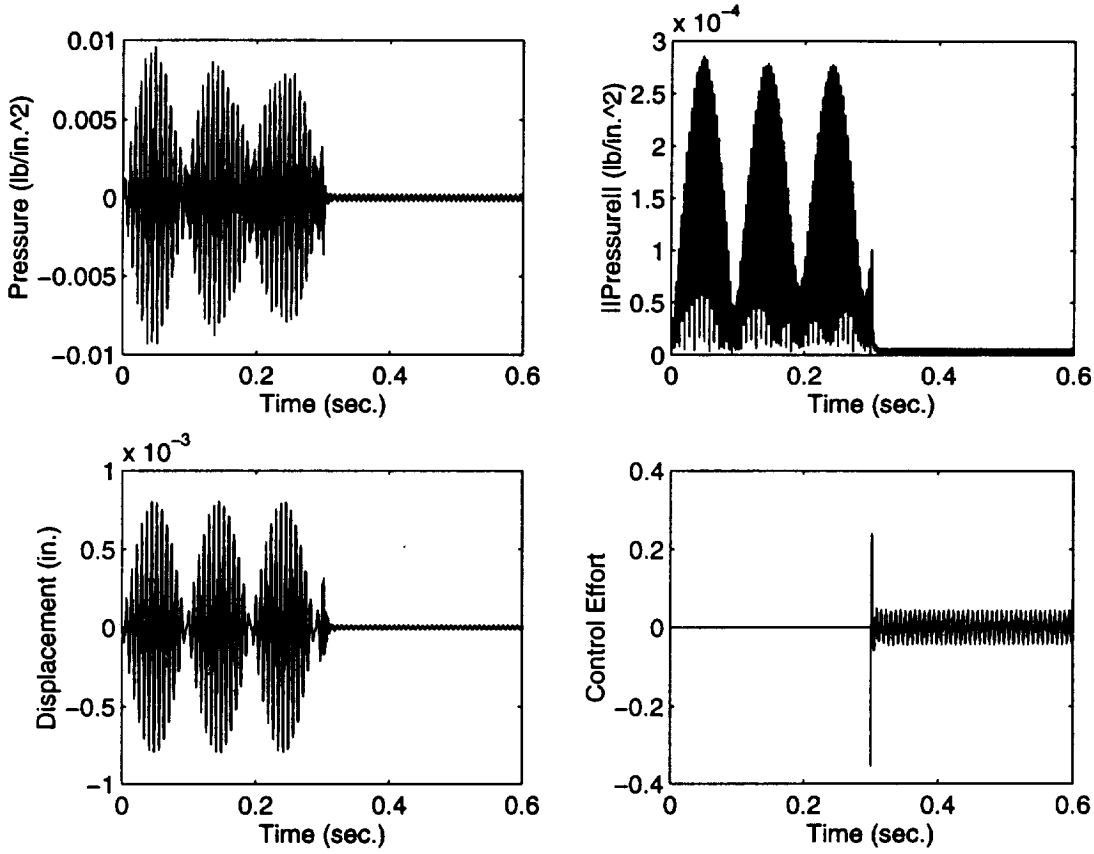

Figure 4.5 Time history of the pressure at the center of the cavity back wall, the displacement at the center of the plate, the norm of the cavity pressure field, and the control effort: Multi-Resonant excitation

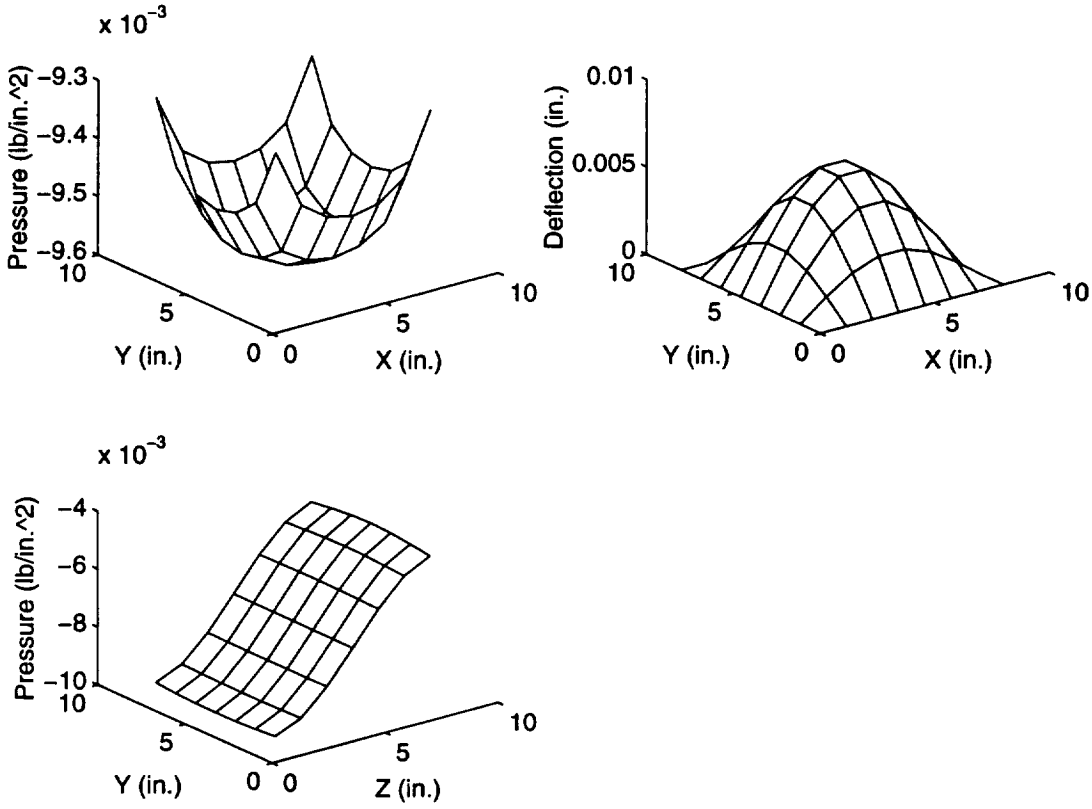

Figure 4.6 Uncontrolled pressure field and plate deflection: Multi-Resonant excitation

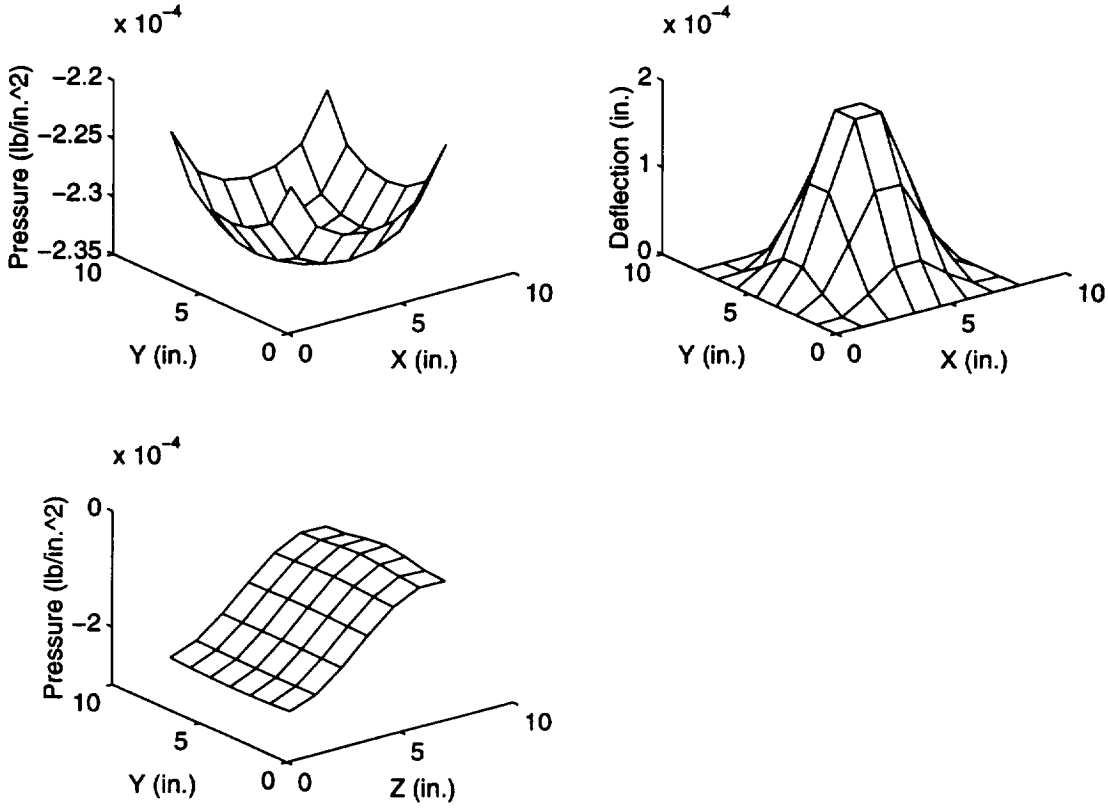

Figure 4.7 Controlled pressure field and plate deflection: Multi-Resonant excitation

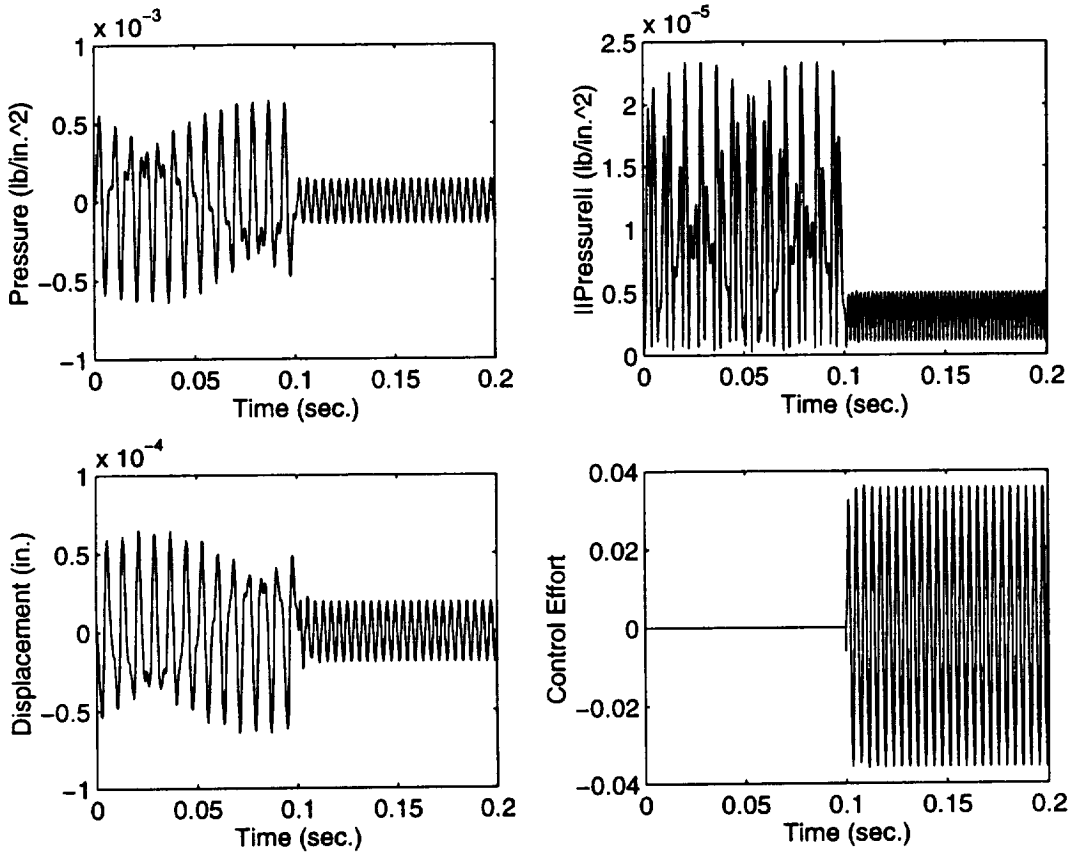

Figure 4.8 Time history of the pressure at the center of the cavity back wall, the displacement at the center of the plate, the norm of the cavity pressure field, and the control effort: Off-Resonant excitation

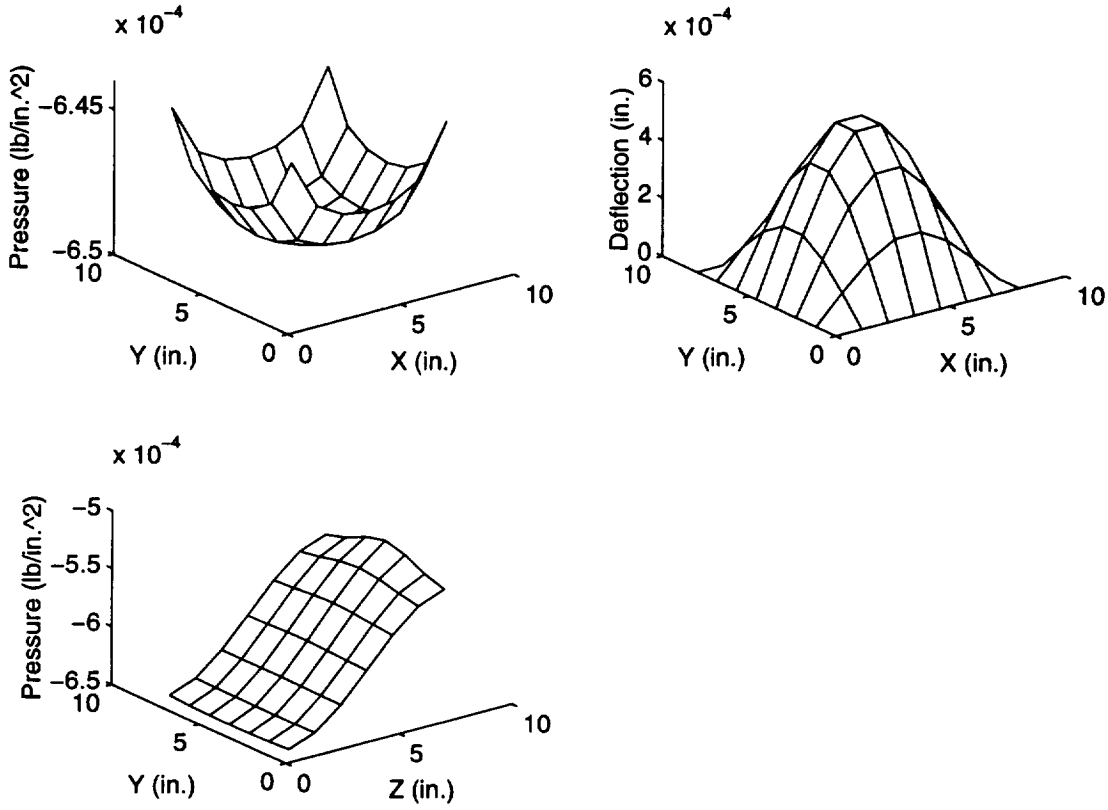

Figure 4.9 Uncontrolled pressure field and plate deflection: Off-Resonant excitation

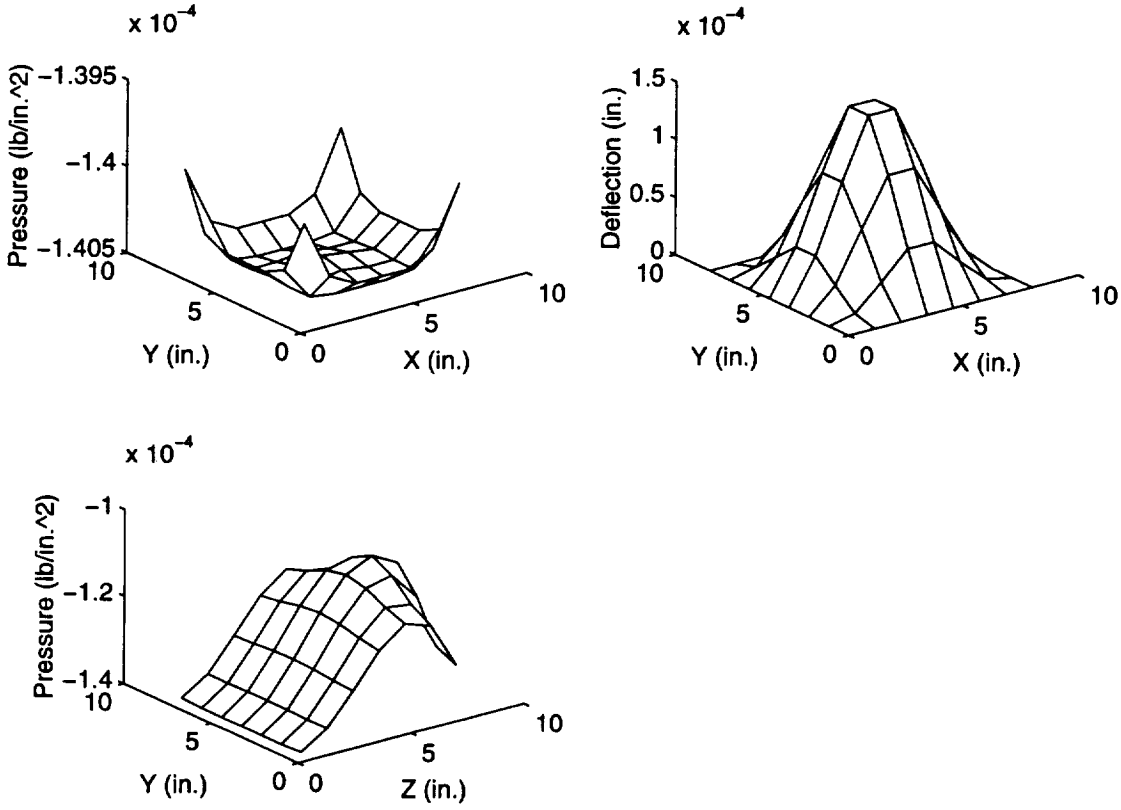

Figure 4.10 Controlled pressure field and plate deflection: Off-Resonant excitation

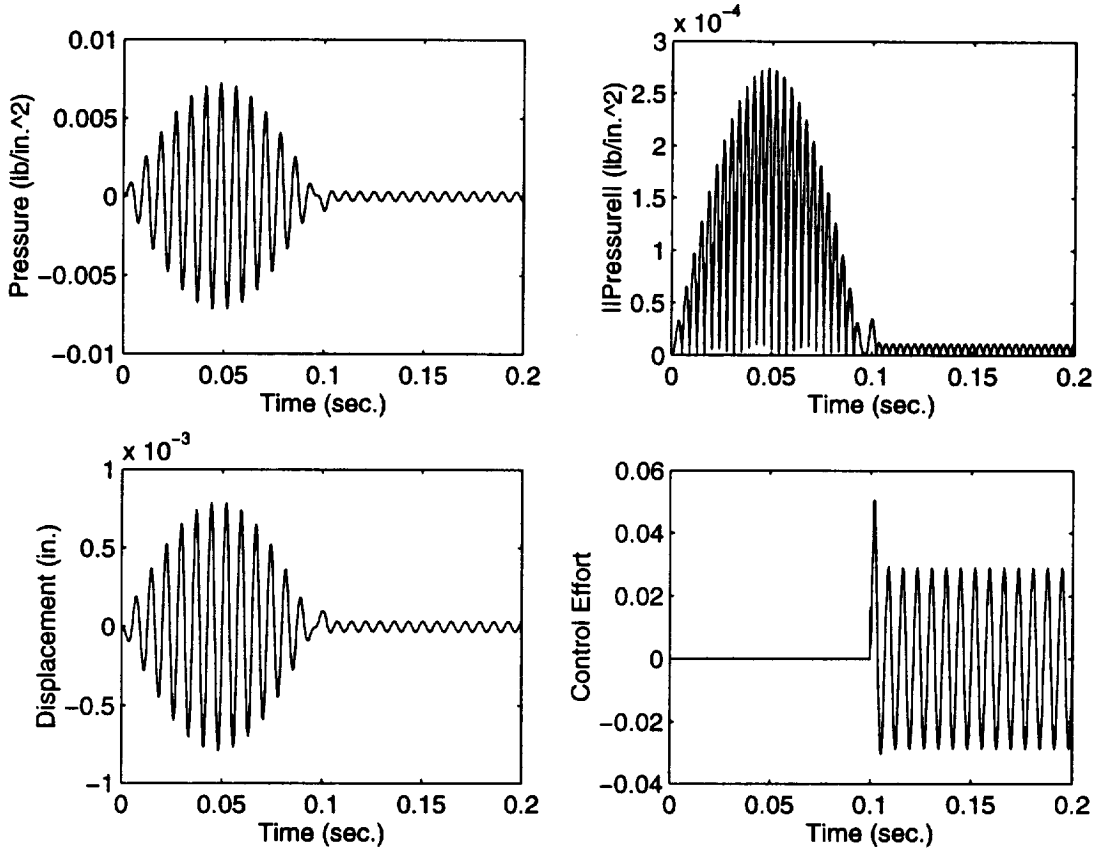

Figure 4.11 Time history of the pressure at the center of the cavity back wall, the displacement at the center of the plate, the norm of the cavity pressure field, and the control effort: Resonant excitation and **Q** matrix in equation (4.19)

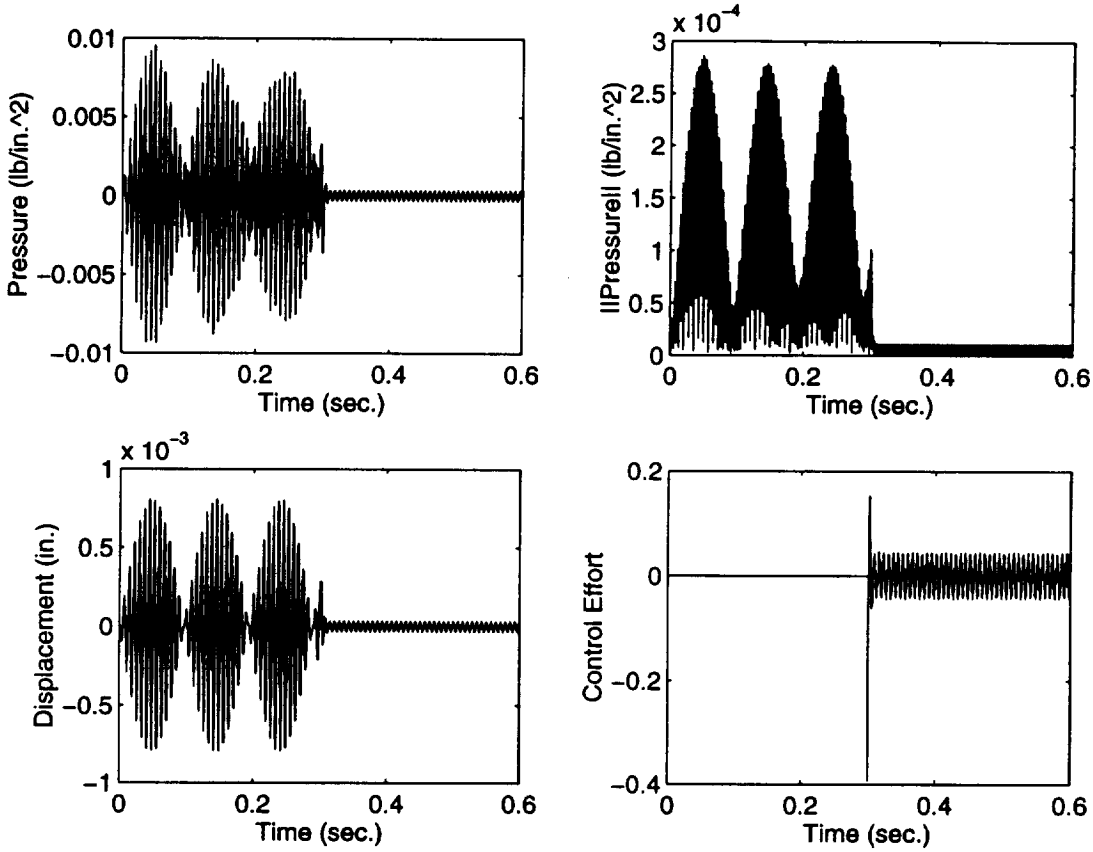

Figure 4.12 Time history of the pressure at the center of the cavity back wall, the displacement at the center of the plate, the norm of the cavity pressure field, and the control effort: Multi-Resonant excitation and **Q** matrix in equation (4.19)

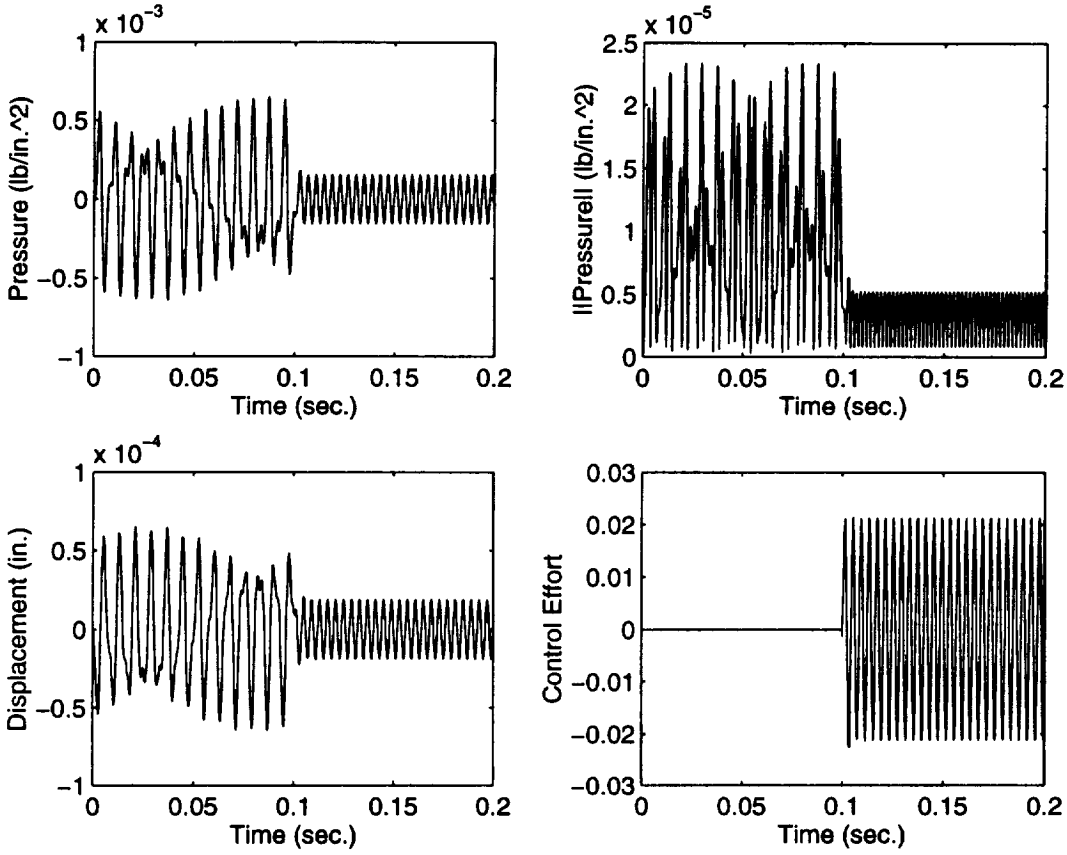

Figure 4.13 Time history of the pressure at the center of the cavity back wall, the displacement at the center of the plate, the norm of the cavity pressure field, and the control effort: Off-Resonant excitation and **Q** matrix in equation (4.19)

4.2.3 Optimal Location of the Piezoelectric Patch

We are now trying to investigate the best location of the piezoelectric patch. In this study, we will utilize the finite element method to determine the locations where piezoelectric patches can most affect the inside acoustic pressure. To assess the effect of the different patch locations, a norm of the feedback control gain (NFCG) is defined. The feedback control gain matrix can be determined from equation (4.10) as[71]

$$[G_a] = [R]^{-1}[B]^T[P] \tag{4.20}$$

the norm of the feedback control gain is defined from the norm of matrix $[G_a]$ as

$$NFCG = \sum_{i=1}^{Np} \left[\sum_{j=1}^{2m} (g_a)_{ij}^2 \right]^{\frac{1}{2}} \tag{4.21}$$

where Np is the number of piezoelectric actuators, and $2m$ is the total number of state variables in equation (4.6).

Assuming that we use a pair of piezoelectric patches ($Np = 2$) having the same shape and area of a finite element and bonded to the two surfaces of the composite plate. The NFCGs for the piezoelectric patches covering each element alone are calculated. The same weighting matrices $\mathbf{Q}$ and $\mathbf{R}$ as previously defined are used. After normalization with the maximum norm to be unity, they are plotted in Figure 4.14. Only 16 elements are marked and the others can be obtained by symmetry. It can be seen that placing the actuators at the center of the plate will give the best performance.

The results of using a pair of actuators at the center of the plate for the three external loads are given in Figures 4.15 to 4.17, respectively, and, as shown in Table 4.6, they are compared with the previous results in the sense of using the same weighting matrices. Notice that the optimally located actuators uses only 2% of the piezoelectric material as the earlier analysis and computations with piezoelectric layers covered the complete surfaces.

Table 4.6 The increase of sound transmission loss (ITL) at the center of the cavity back wall and the displacement reduction (DR) at the center of the plate: Comparison of the performance of optimal located actuators and previous ones.

	Actuators cover two surfaces of plate		Actuators cover two surfaces of center element	
	ITL (dB)	DR (%)	ITL (dB)	DR (%)
Resonant	34.4	1.44	18.1	13.3
Multi-Resonant	32.3	1.86	23.1	13.9
Off-Resonant	13.3	29.4	8.70	40.0

0.09	0.18	0.06	0.31			
0.23	0.26	0.13	0.40			
0.23	0.23	0.21	0.61			
0.53	0.55	0.41	1.00			

Figure 4.14 NFCGs for different locations of piezoelectric actuator.

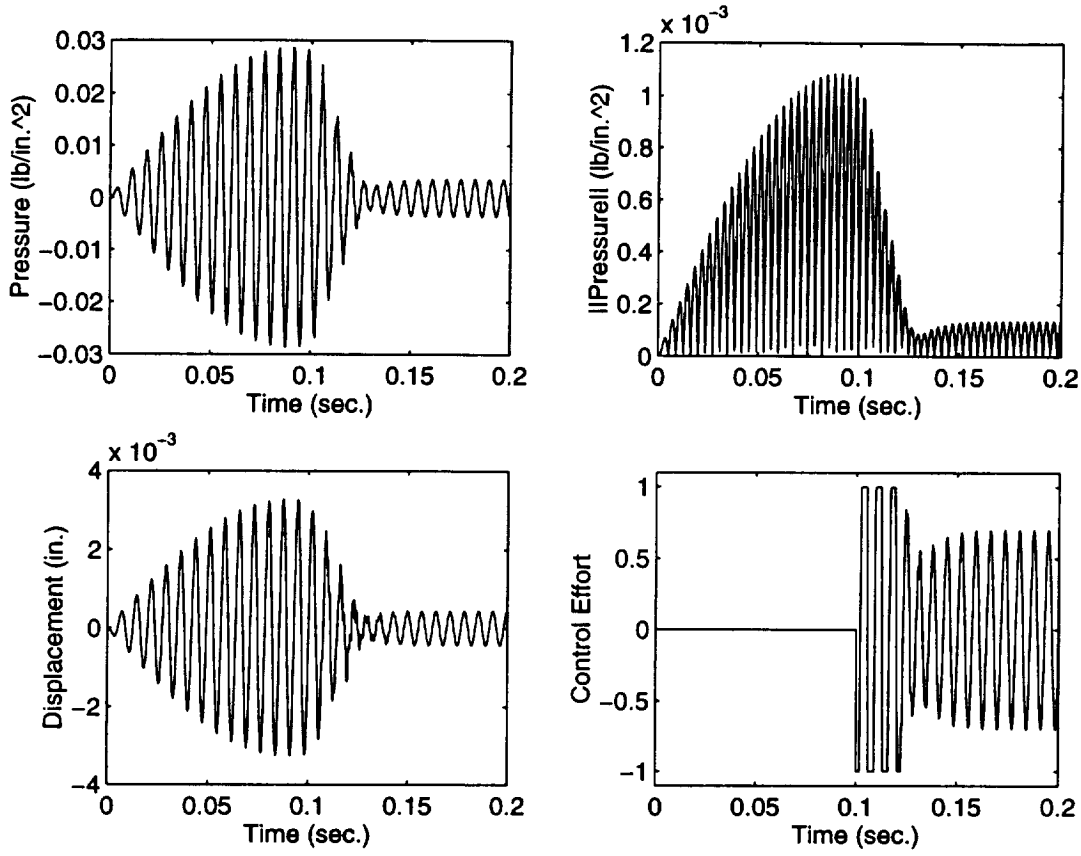

Figure 4.15 Time history of the pressure at the center of the cavity back wall, the displacement at the center of the plate, the norm of the cavity pressure field, and the control effort: Resonant excitation and best location

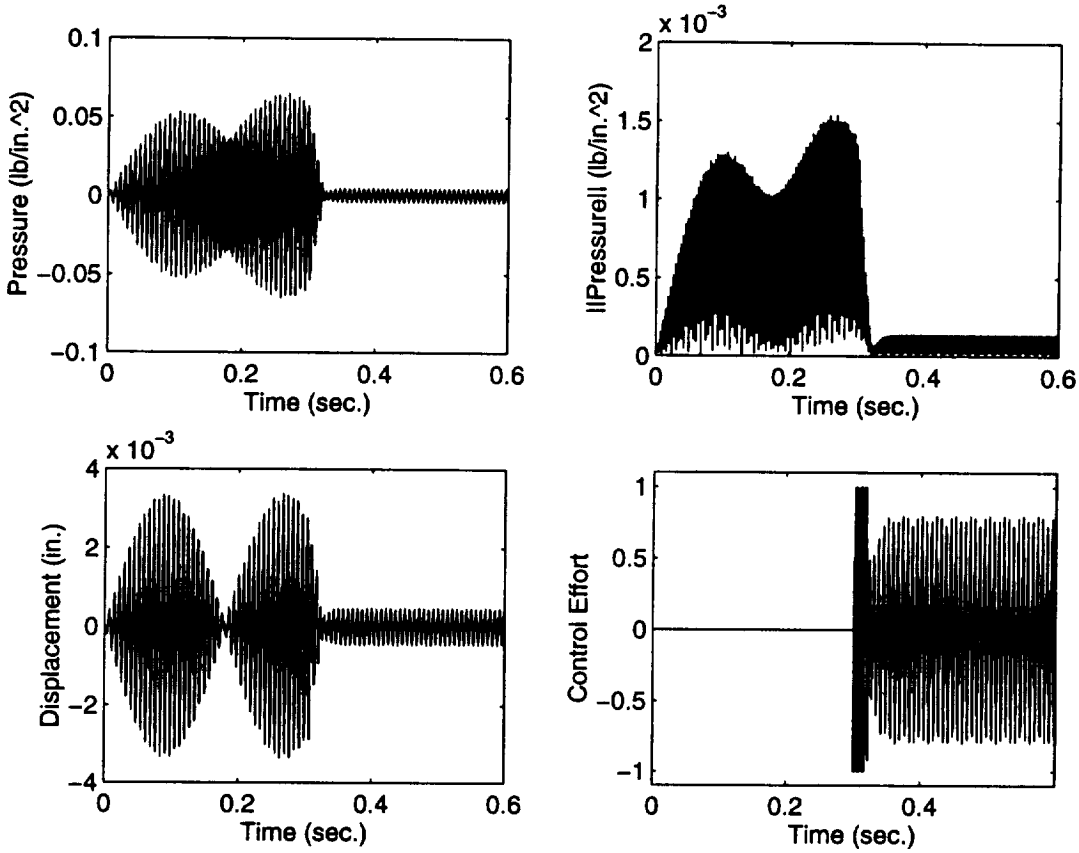

Figure 4.16 Time history of the pressure at the center of the cavity back wall, the displacement at the center of the plate, the norm of the cavity pressure field, and the control effort: Multi-Resonant excitation and best location

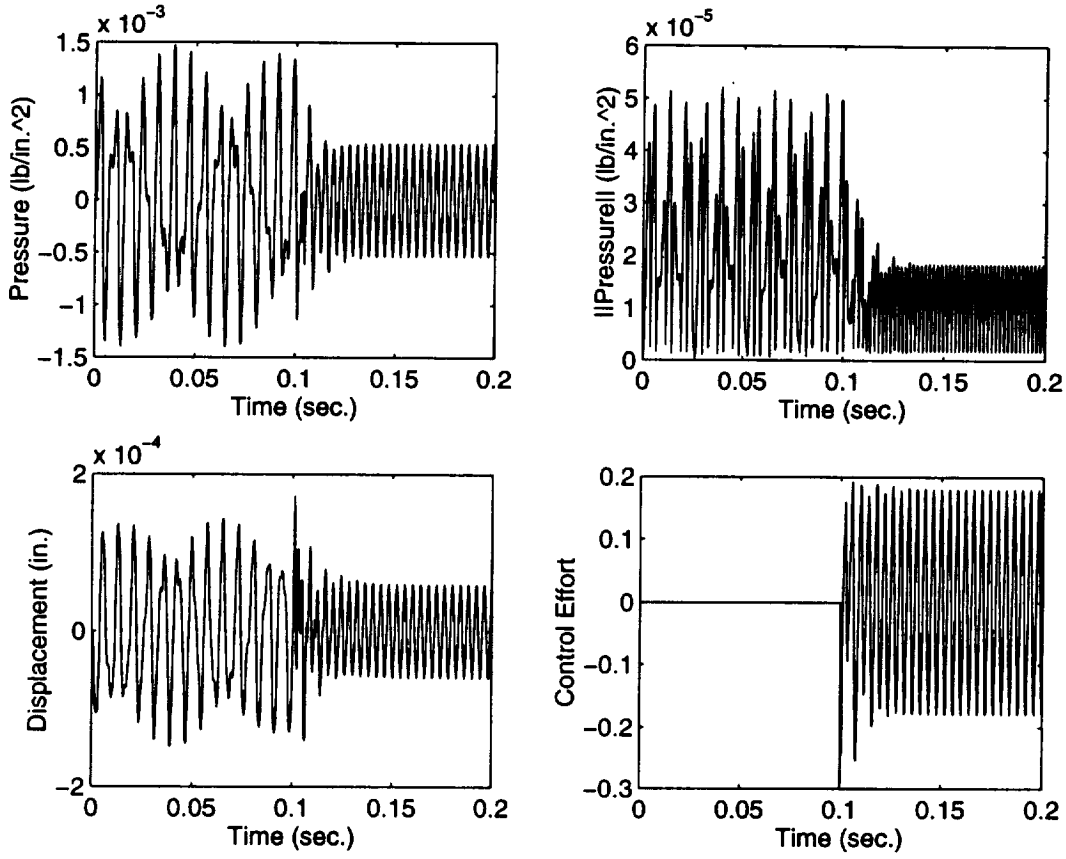

Figure 4.17 Time history of the pressure at the center of the cavity back wall, the displacement at the center of the plate, the norm of the cavity pressure field, and the control effort: Off-Resonant excitation and best location

4.3 Feedforward Controller

In linear quadratic regulator, the control gain is sought to give the best trade-off between performance level and cost of control. However, this controller requires full state feedback which in reality is hard to achieve[83]. In this section, a more practical controller design, feedforward control[58], is investigated.

Assume the external acoustic wave is measurable, we try neutralize the external disturbance by applying a control force (from piezoelectric actuators) in the weighted least-mean-square sense which counteracts the external pressure disturbance.

4.3.1 Mathematical Model

Assume that the external wave is a plane wave, and the measured pressure on the plate can be expressed as a Fourier series

$$P(x,y,t) = \sum_{k=1}^{N_L} P_k \sin \omega_k t \tag{4.22}$$

where P_k are known coefficients, and ω_k are the input frequencies. Then the load term in equation (4.2) can be expressed as

$$\{L_1\} = \{\bar{L}_1\} \sum_{k=1}^{N_L} P_k \sin \omega_k t \tag{4.23}$$

where $\{\bar{L}_1\}$ is the modal force corresponding to uniformly distributed unit pressure.

To suppress the acoustic field inside the cavity, we assume that the control force has the form of

$$\{L_2\} = [G]\{\beta\} \sum_{k=1}^{N_L} P_k \sin \omega_k t \tag{4.24}$$

where $[G]$ is the modal force matrix corresponding to the maximum operating electrical field as defined in equation (4.8). Each column of $[G]$ corresponds to each actuator. Further, $\{\beta\}$ is the undetermined coefficient vector.

After substituting equation (4.23) and (4.24) into equation (4.1), we have

$$[M]^*\{\ddot{\eta}\} + [C]^*\{\dot{\eta}\} + [K]^*\{\eta\} = \left(\{\bar{L}_1\} + [G]\{\beta\}\right) \sum_{k=1}^{N_L} P_k \sin \omega_k t \tag{4.25}$$

If we ignore the damping term when we determine the control effort, and notice that matrices $[M]^*$ and $[K]^*$ are all diagonal, we have

$$\{\eta\} = \sum_{k=1}^{N_L} \{\alpha\}_k \sin\omega_k t = \sum_{k=1}^{N_L} [O]_k (\{\bar{L}_1\} + [G]\{\beta\}) \sin\omega_k t \tag{4.26}$$

where matrix $[O]_k$ is also diagonal and

$$(o_k)_{ii} = \frac{P_k}{k^*_{ii} - \omega_k^2 m^*_{ii}} \tag{4.27}$$

To reduce the acoustic pressure level, we desire the inside acoustic pressure caused by external acoustic waves at each frequency to be null, that is

$$[\Psi_\Omega]\{\alpha\}_k \sin\omega_k t = \{0\}, \qquad k = 1, 2, ..., N_L \tag{4.28}$$

Generally, the number of the actuators is not the same as the number of frequencies in the exciting wave, and there is no proportional relation between $\{\bar{L}_1\}$ and $[G]$. Thus, equation (4.28) is impossible to achieve. Instead, $\{\beta\}$ will be designed to reduce the internal pressure waves as much as possible in the least mean square sense, or

$$\Pi = \sum_{k=1}^{N_L} \|[\Psi_\Omega]\{\alpha\}_k\|^2 = \sum_{k=1}^{N_L} \left\|[\Psi_\Omega][O]_k (\{\bar{L}_1\} + [G]\{\beta\})\right\|^2 \rightarrow min. \tag{4.29}$$

The resulting $\{\beta\}$ is

$$\{\beta\} = -\frac{\sum_{k=1}^{N_L} [G]^T [O]_k^T [\Psi_\Omega]^T [\Psi_\Omega][O]_k}{\sum_{k=1}^{N_L} [G]^T [O]_k^T [\Psi_\Omega]^T [\Psi_\Omega][O]_k [G]} \{\bar{L}_1\} \tag{4.30}$$

4.3.2 Numerical Results

The example problems in Section 4.2 using three different excitation forces investigated are studied again here using the feedforward controller. As in the LQR, only one pair of actuators covering the external and internal surfaces of the composite plate are used. The results are presented as follows.

Resonant Excitation

The comparison of the controlled and uncontrolled responses is given in Figures 4.18 and 4.19. The feedforward controller reduced the maximum pressure at the center of the cavity back wall from the uncontrolled 7.22×10^{-3} $lb/in.^2$ to controlled 5.69×10^{-5} $lb/in.^2$ This is a 42.1 dB increase in the transmission loss. At the same time, the amplitude of the maximum deflection of the plate is reduced from 7.93×10^{-4} $in.$ to 2.05×10^{-5} $in.$ Higher performance has been achieved here relative to the LQR case.

Multi-Resonant Excitation

The results are compared in Figures 4.20 and 4.21. The feedforward controller reduced the maximum pressure at the center of the cavity back wall from the uncontrolled 9.56×10^{-3} $lb/in.^2$ to controlled 2.62×10^{-3} $lb/in.^2$ This is a 11.2 dB increase in the transmission loss. The amplitude of the maximum deflection of the plate is reduced from 8.05×10^{-4} $in.$ to 1.23×10^{-4} $in.$

Off-Resonant

The results are given in Figures 4.22 and 4.23. The feedforward controller reduced the maximum pressure at the center of the cavity back wall from the uncontrolled 6.49×10^{-4} $lb/in.^2$ to controlled 1.17×10^{-4} $lb/in.^2$ This is a 14.9 dB increase in the transmission loss. At the same time, the amplitude of the plate deflection is reduced from 6.51×10^{-5} $in.$ to 3.34×10^{-5} $in.$

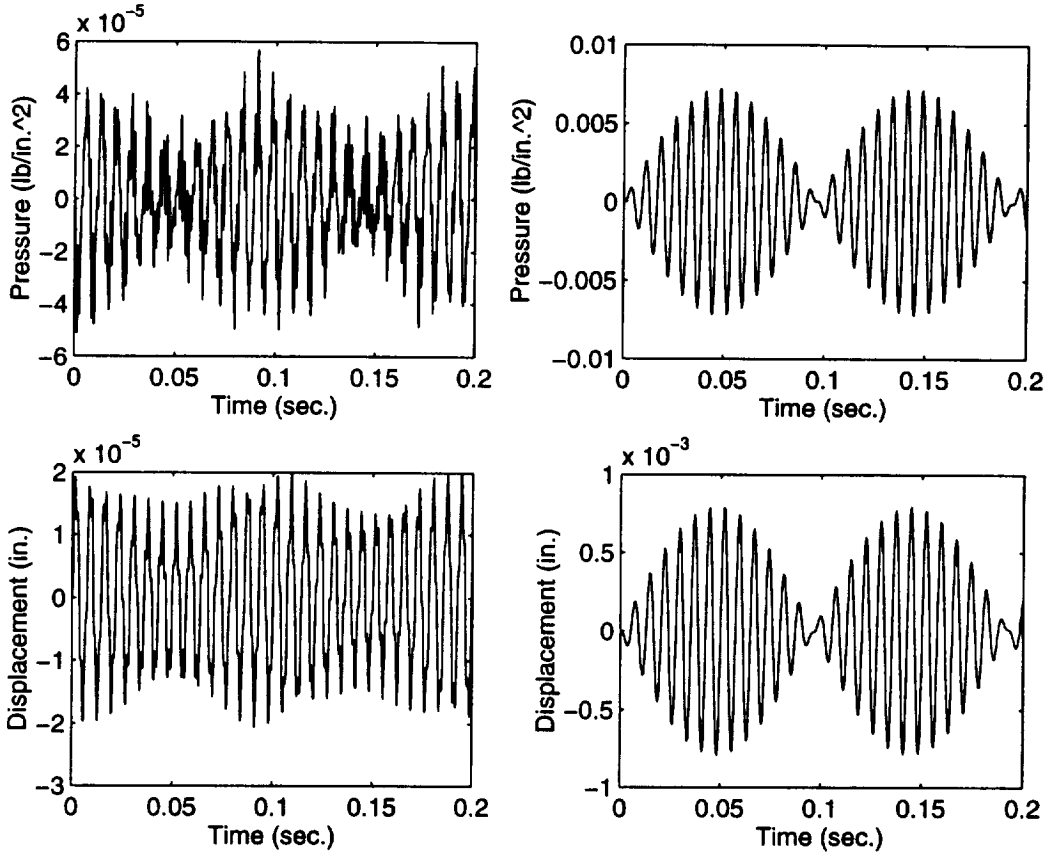

Figure 4.18 Comparison of controlled (left) and uncontrolled (right) system response to resonant excitation: Time history of the pressure at the center of the cavity back and displacement at the center of the plate

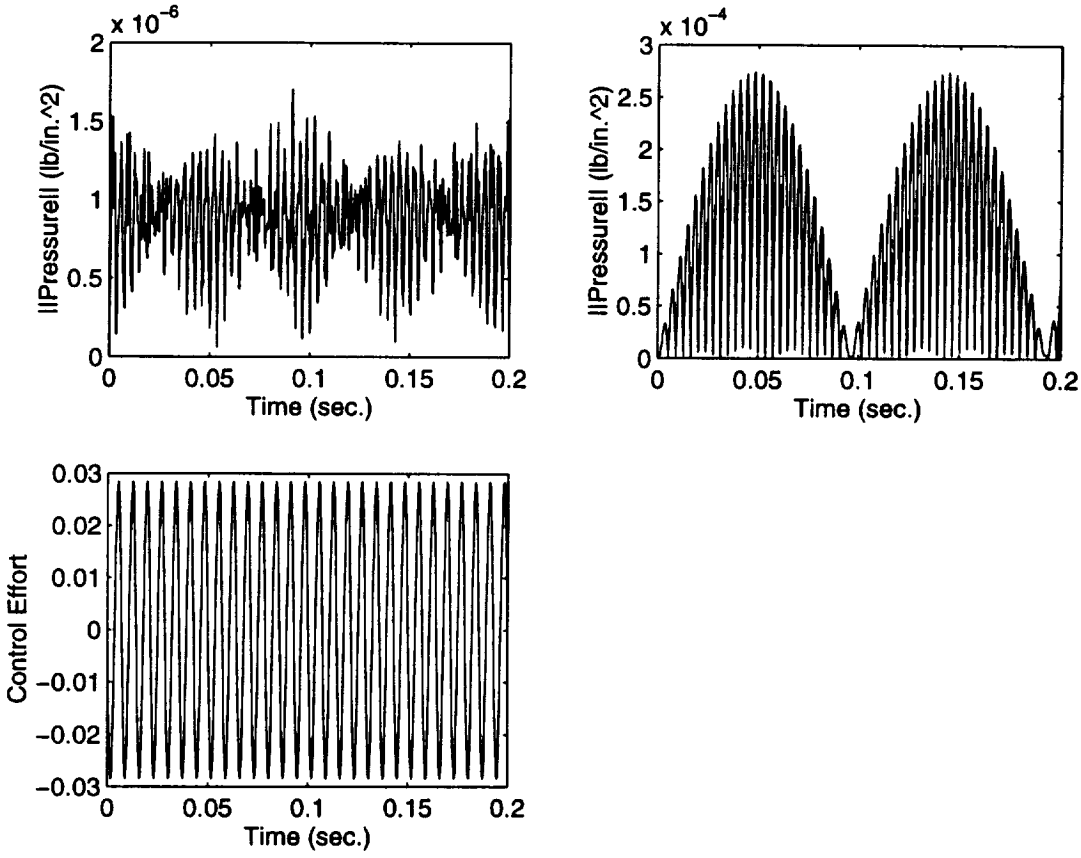

Figure 4.19 Comparison of controlled (left) and uncontrolled (right) system response to resonant excitation: norm of the cavity pressure field, and control effort

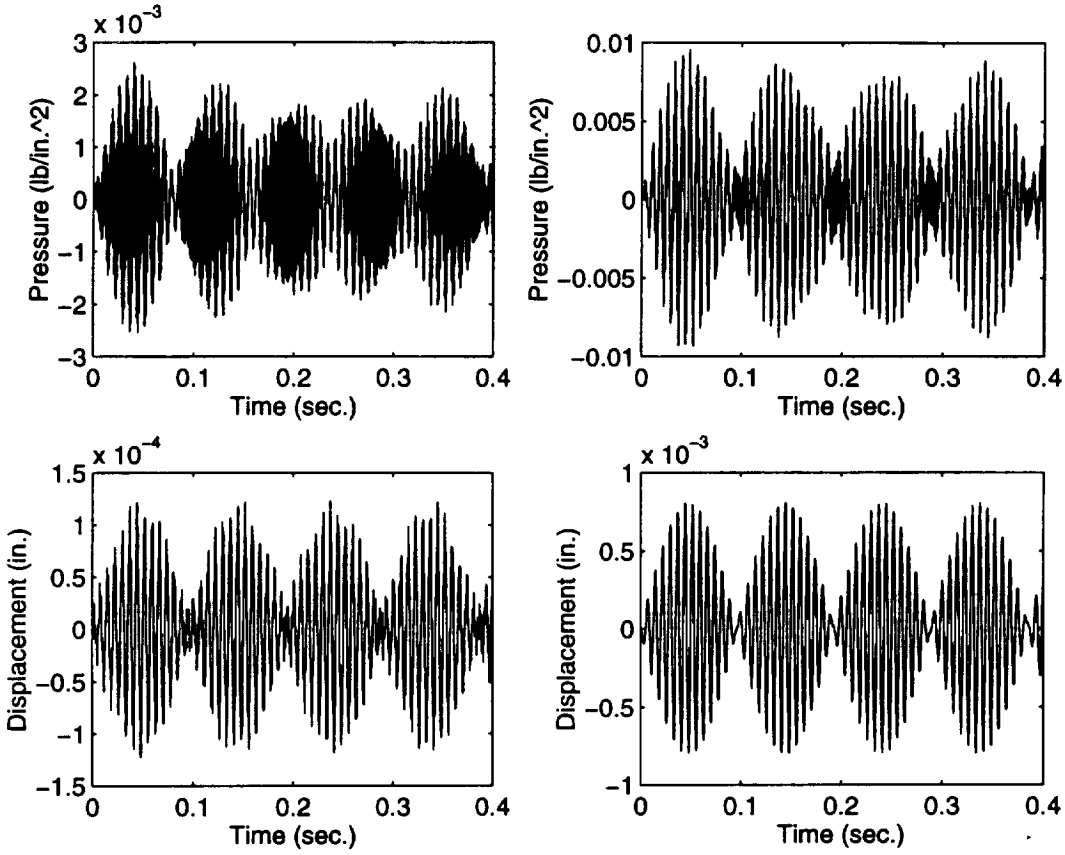

Figure 4.20 Comparison of controlled (left) and uncontrolled (right) system response to multi-resonant excitation: Time history of the pressure at the center of the cavity back wall and displacement at the center of the plate

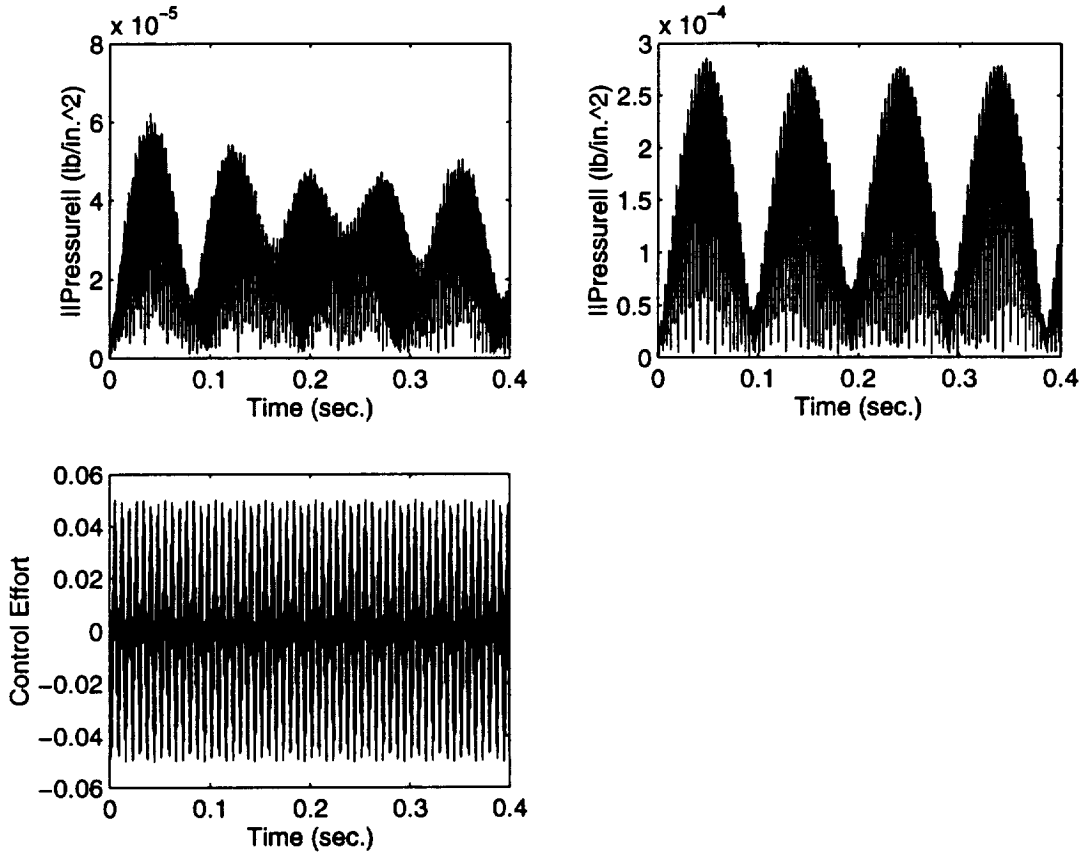

Figure 4.21 Comparison of controlled (left) and uncontrolled (right) system response to multi-resonant excitation: norm of the cavity pressure field, and control effort

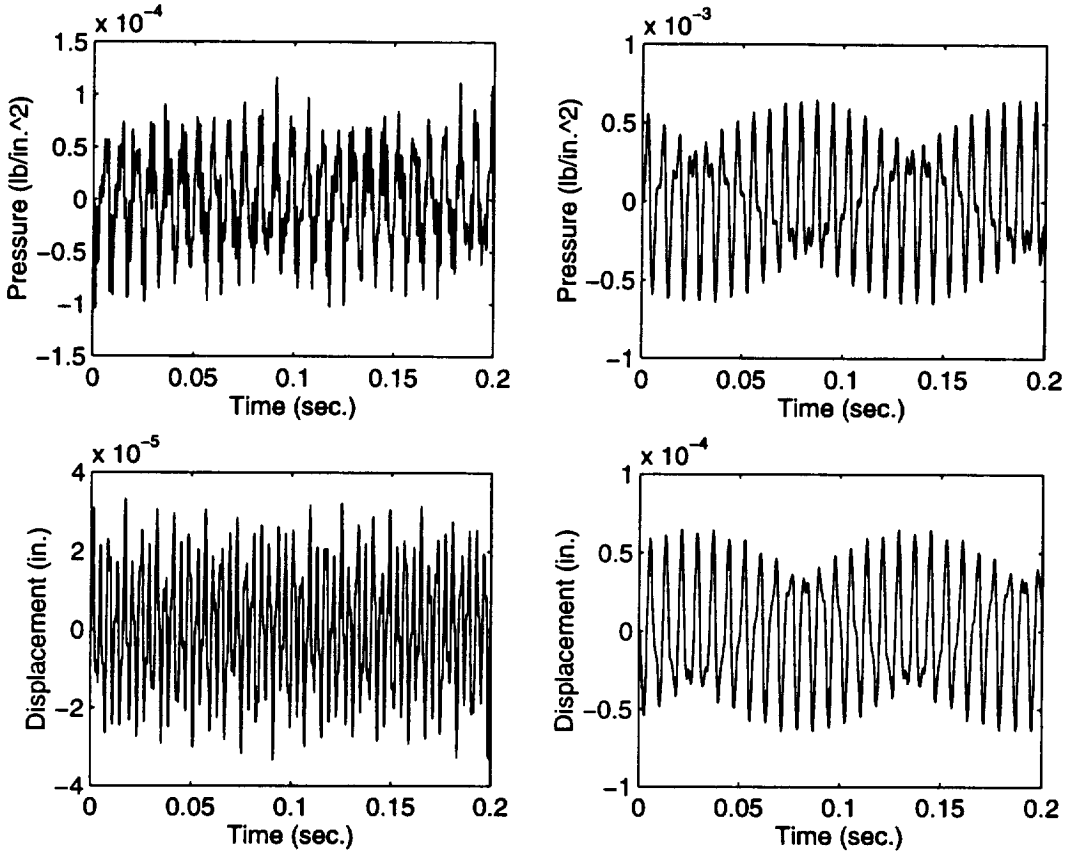

Figure 4.22 Comparison of controlled (left) and uncontrolled (right) system response to off-resonant excitation: Time history of the pressure at the center of the cavity back wall and the displacement at the center of the plate

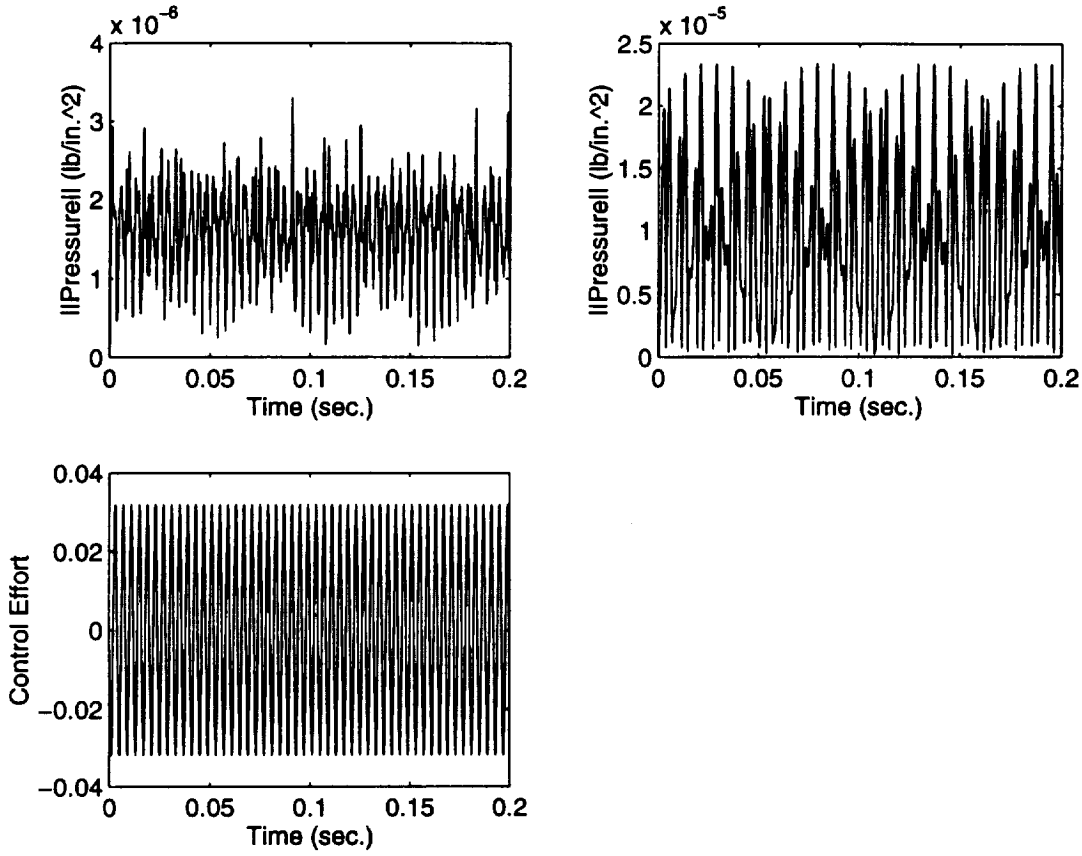

Figure 4.23 Comparison of controlled (left) and uncontrolled (right) system response to off-resonant excitation: the norm of the cavity pressure field and the control effort

4.3.3 Optimal Location of the Piezoelectric Patch

Once again, we try to find the optimal location of the piezoelectric patches. As we mentioned in Section 4.2, the mass and stiffness of the piezoceramic patches will affect the characteristics of the coupled system. Thus, the different location and shape of the piezoelectric actuators will mathematically change the system and the response. So in this study, we only try to investigate the optimal location when the external excitation is a simple harmonic plane wave at frequency of 140 Hz. And similar to Section 4.2, we try only one pair of piezoelectric patches bonded to the two surfaces of the plate, and each patch occupies only one finite element.

The criteria of the performance in this section is defined as the increase of the transmission loss for the norm of the inside acoustic pressure field between controlled and uncontrolled systems. The results are given in Figure 4.24 after normalization with the maximum value. Notice the best location of the piezoceramtic actuator is at the center of the plate again. The time histories of the displacement at the center of the plate, the pressure at the center of the cavity back wall, the norm of the pressure field inside the cavity, and the control effort when the actuator is at the best location are given in Figures 4.25. The comparison of the increase of sound transmission loss at the center of the cavity back wall and displacement reduction at the center of the plate between actuators at the best location and actuators covering two surfaces of the plate are given in Table 4.7.

Table 4.7 The increase of sound transmission loss (ITL) at the center of the cavity back wall and the displacement reduction (DR) at the center of the plate: Comparison of the performance of optimal located actuators and the one covering two surface of the plate.

Actuators cover two surfaces of plate		Actuators cover center element	
ITL (dB)	DR (%)	ITL (dB)	DR (%)
42.1	2.59	33.8	5.37

0.46	0.06	0.56	0.45			
0.05	0.15	0.55	0.84			
0.57	0.24	0.12	0.89			
0.20	0.20	0.46	1.00			

Figure 4.24 The normalized increase of transmission loss obtained from different location of piezoelectric actuators.

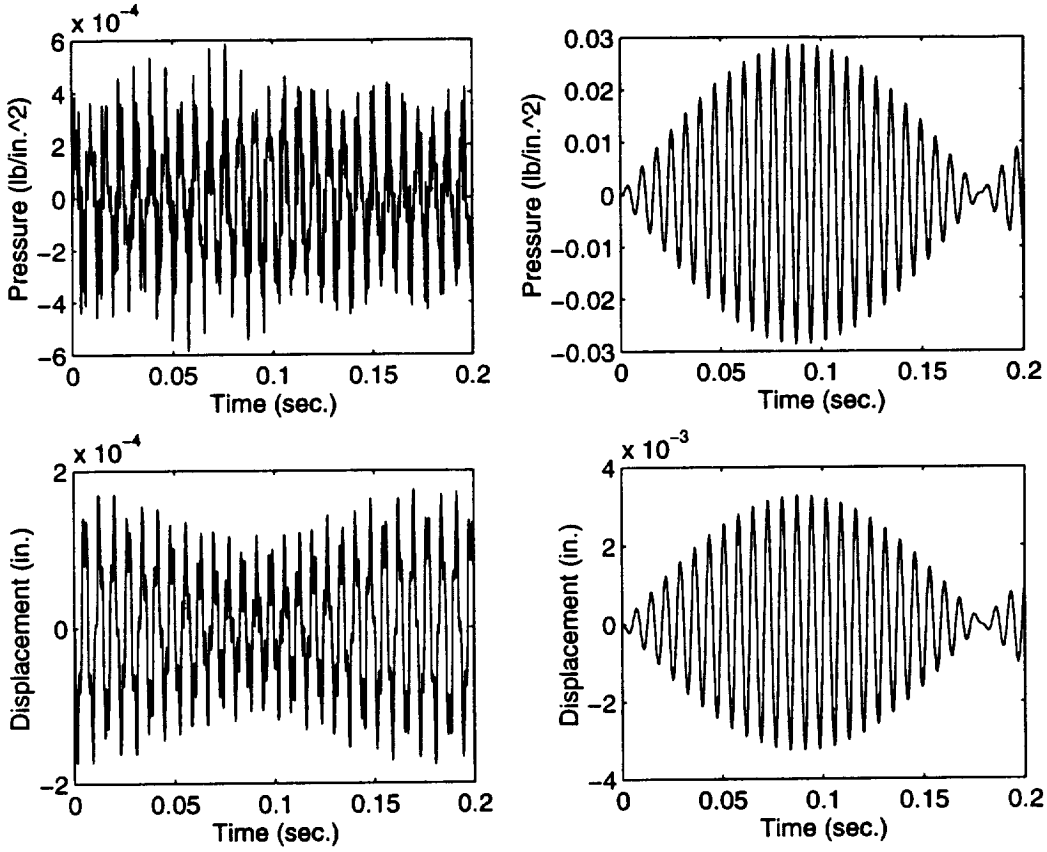

Figure 4.25 Comparison of controlled (left) and uncontrolled (right) system responses to resonant excitation: Time history of the pressure at the center of the cavity back and displacement at the center of the plate: Best location

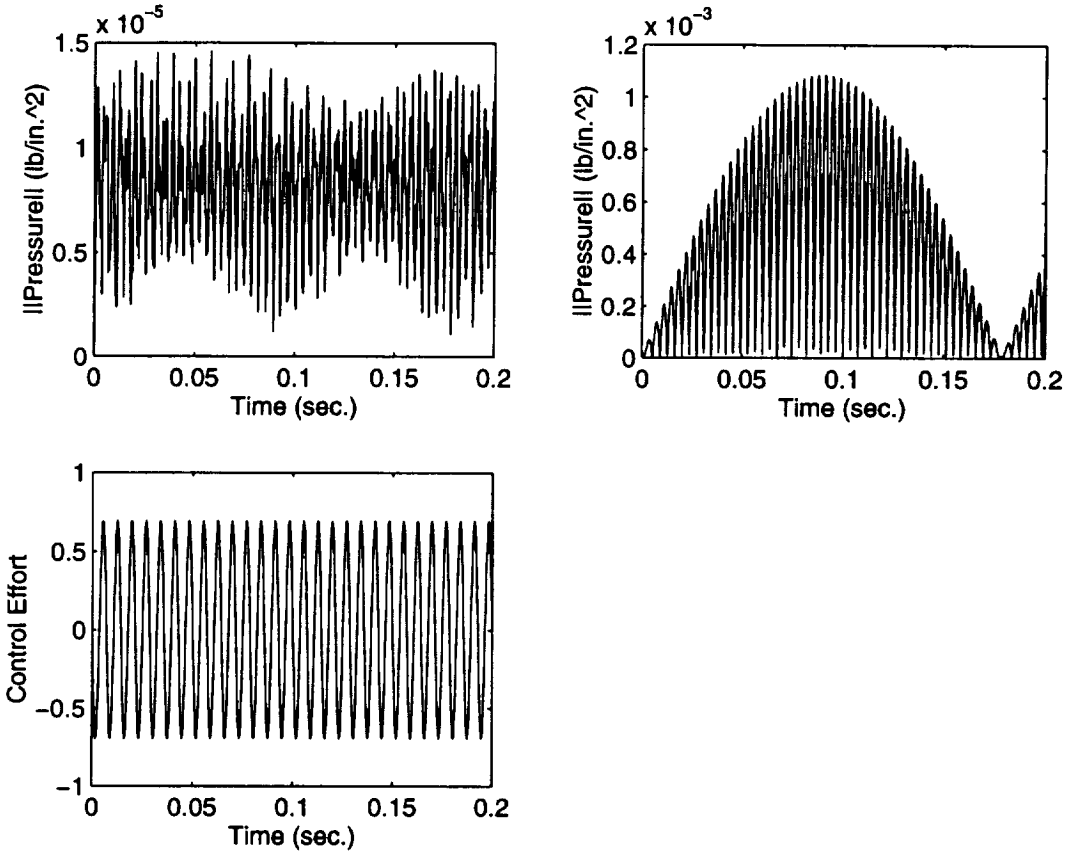

Figure 4.26 Comparison of controlled (left) and uncontrolled (right) system responses to resonant excitation: norm of the cavity pressure field, and control effort: Best location

4.4 Conclusions

The linear quadratic regulator and a feedforward controller based on the concept of least mean square are applied with the intent to reduce the acoustic pressure field inside the cavity for the coupled plate/cavity system under different external disturbances. The piezoelectric patches bonded on the plate surfaces are used as the actuators, and the total acoustic potential energy inside the cavity is used as the control objective. The pressure level inside the cavity and the plate deflection are reduced successfully for both controllers. The optimal location of the piezoelectric actuators are investigated based on those two controllers.

Chapter 5
Summary and Conclusions

5.1 Concluding Remarks

The contributions of this dissertation consists of two parts, one is the modeling of the acoustic-structure interaction using the coupled finite element and boundary element methods, the other is the suppression of interior acoustic pressure levels transmitted through composite plates using bonded piezoelectric actuators.

To predict the response of the coupled structural-acoustic system under external acoustic excitation, the C^1 conforming finite element method is used to model the plate, and the dual reciprocity boundary element method is used to model the interior acoustic domain. Based on the continuity requirement on the interior surface of the plate, the boundary element method and finite element method are coupled together to form a powerful tool which can be used to solve structural-acoustic interaction problems. Interior acoustic problems are analyzed first using only the boundary element method, serving to verify that the boundary element method is an accurate and versatile approach in solving acoustic problems. The coupled method is then applied to a cubic acoustic cavity backed by a brass plate, the results are compared with the analytical solution and experiment data, and the accuracy of the coupled method is verified. This method is then applied to the cavity backed by a composite plate.

Taking advantage of the dual reciprocity boundary element method, the coupled finite element and boundary element scheme is used to calculate the eigenvalues and eigenvectors of the coupled structural-acoustic system. Those eigenvalues are the natural frequencies of the coupled system. The eigenvectors are employed to form the transformation matrix to transform the coupled equations into modal formulation which has a very small number of equations compared to the original one. The responses of the coupled acoustic-structure system under various external excitations are investigated using the modal formulation to demonstrate its accuracy and capability.

The results show that it is necessary to consider the interaction between the acoustic domain and the structure, and also to consider the mass and stiffness of the piezoelectric patches. The interaction between structure and acoustic cavity significantly influences the overall system natural frequencies, and the full coupling between composite laminate and piezoelectric patches also modifies the natural frequencies of the system.

Based on the modal formulation, two different control designs are applied to reduce the transmitted acoustic pressure inside the cavity with embedded piezoelectric patches as actuators. The linear quadratic regulator gives the best control performance under certain information of the system and external load. The feedforward controller is based on the attempt to neutralize the external excitation in the weighted least mean square sense. For the two controllers, they both can reduce the acoustic pressure field inside the cavity and the deflection of the plate effectively. The higher the transmitted pressure is, the better the control performs. Specifically, for the resonant excitation, the LQR can increases the transmission loss up to 34.4 dB, and feedforward, up to 42.1 dB, at the same time, the maximum deflection of the plate is reduced 98.6% using LQR, and 97.4% for feedforward controller.

The optimal locations of the piezoelectric actuators are investigated for those two controllers. Comparison to the case where piezoelectric patches cover the entire external and internal surfaces of the plate, the optimal located piezoelectric actuators perform rather efficiently.

Currently, industry is striving to reduce the interior noise in aerospace and automobile systems. These goals require more efficient approaches to model the interaction between acoustic and structures, and also the design of suitable controllers. This study is only an attempt to enhance our understanding in that direction.

5.2 Future Work

Many areas of research still need to be considered in order to more accurately model the real world systems. Present finite element/boundary element model could be improved in at least three areas. First, the nonlinear large displacement-strain relation

of the composite laminate needs to be included when external acoustic pressure is high or the exciting frequency is around the natural frequencies of the system. For aerospace engineering, the acoustic pressure level for new supersonic aircraft will be of 190 dB, the thin composite plate will then be into large deflection range. Second, the thermal effect on composite material and piezoelectric material should be considered. For supersonic aircraft, the surface temperature of the fuselage will easily reach few hundreds degree. Third, other elements, such as linear or other higher order boundary elements, or three dimensional elements, like shell elements, should be included to model real system as aircraft fuselage or automobile bodies.

For control, other controllers should be considered. In this study, piezoelectric patches are used only as actuators, the use of piezoelectric patches as sensor and actuator becomes naturally the next step.

REFERENCES

1. J. R. Edson: "Review of testing and information on sonic fatigue," Doc. No. D-17130, Boeing Co., 1957.
2. C. A. Powell and T. L. Parrott: "A summary of acoustic loads and response studies," 10th National Aero-Space Plane Technology Symposium, Paper No. 106, April, 1991.
3. J. W. Strutt Lord Rayleigh: "The theory of sound," Dover, New York, 1945 (2nd ed.).
4. M. C. Junger and D. Feit: "Sound, structures and their interaction," 1986, M.I.T. Press.
5. R. H. Lyon: "Noise reduction of rectangular enclosure with one flexible wall," The Journal of Acoustical Society of America, Vol. 35, No. 11, 1963, pp. 1791–1797.
6. E. H. Dowell and H. M. Voss: "The effect of a cavity on panel vibration," AIAA Journal, Vol. 1, No. 2, 1963, pp. 476–477.
7. M. C. Bhattacharya and M. J. Crocker: "Forced vibration of a panel and radiation of sound into a room," Acustica, Vol. 22, 1969/1970, pp. 275–294.
8. R. W. Guy and M. C. Bhattacharya: "The transmission of sound through a cavity-backed finite plate," Journal of Sound and Vibration, Vol. 27, No. 2, 1973, pp. 207–223.
9. R. W. Guy: "The response of a cavity-backed panel to external airborne excitation: A general analysis," The Journal of Acoustical Society of America, Vol. 65, 1979, pp. 719–731.
10. B. W. McDonald, R. Vaicaitis, and M. K. Myers: "Noise transmission through plates into an enclosure," NASA No. TP-1173, 1987.
11. E. H. Dowell, G. F. Gorman III, and D. A. Smith: "Acoustoelasticity: General theory, acoustic natural modes and forced response to sinusoidal excitation, including comparison with the experiments," Journal of Sound and Vibration, Vol. 52, No. 4, 1977, pp. 519–542.

12. S. Yarayanan and R. L. Shanbhag: "Acoustoelasticity of a clamped sandwich panel backed by a cavity," Journal of Sound and Vibration, Vol. 74, No. 4, 1981, pp. 453–473.

13. S. Yarayanan and R. L. Shanbhag: "Sound transmission through elastically supported sandwich panels into a rectangular enclosure," Journal of Sound and Vibration, Vol. 77, No. 4, 1981, pp. 251–270.

14. L. Cheng and J. Nicolas: "Radiation of sound into a cylindrical enclosure from a point-driven end plate with general boundary conditions," The Journal of Acoustical Society of America, Vol. 91, No. 3, 1992, pp. 1504–1513.

15. J. Pan and D. A. Bies: "The effect of the fluid-structural coupling on sound waves in an enclosure—Theoretical part," The Journal of Acoustical Society of America, Vol. 87, No. 11, 1990, pp. 691–707.

16. J. Pan and D. A. Bies: "The effect of the fluid-structural coupling on sound waves in an enclosure—Experimental part," The Journal of Acoustical Society of America, Vol. 87, No. 11, 1990, pp. 708–717.

17. V. B. Bokil: "Modal analysis of gyroscopically coupled sound-structure interaction problems," Master's Thesis, Old Dominion University, 1992.

18. G. M. L. Gladwell and G. Zimmermann: "On energy and complementary energy formulations of acoustic and structural vibration problems," Journal of Sound and Vibration, Vol. 3, 1966, pp. 233–241.

19. O. C. Zienkiewicz and P. Bettess: "Fluid—structure dynamic interaction and wave forces: an introduction to numerical treatment," International Journal for Numerical Method in Engineering, Vol. 13, 1978, pp. 1–16.

20. O. C. Zienkiewicz and R. E. Newton: "Coupled vibrations of a structure submerged in a compressible fluid," Proceedings of International Symposium on Finite Element Techniques, Stuttgart, 1969.

21. A. Craggs: "The transient response of a coupled plate—acoustic system using plate and acoustic finite elements," Journal of Sound and Vibration, Vol. 15, 1975, pp. 509–528.

22. G. C. Everstine, E. A. Schroeder, and M. S. Marcus: "The dynamic analysis of submerged structures," NASA TM X-3278, 1975.

23. G. C. Everstine: "A NASTRAN implementation of the doubly asymptotic approximation for underwater shock response," NASA TM X-3428, NASTRAN: Users' Experiences, 1976, pp. 207–228.

24. A. J. Kalinowski: "Fluid/structure interaction," in Shock and Vibration Computer programs, Reviews and Summaries, SVM-10, U.S. Naval Research Laboratory, Washington, D.C., 1975

25. L. Kiefling and G. C. Feng: "Fluid-structure finite element vibration analysis," The Journal of Acoustical Society of America, Vol. 14, 1976, pp. 199–203.

26. A. J. Kalinowski: "Transmission of shock wave into submerged fluid filled vessels," in Fluid Structure Interaction Phenomena in Pressure Vessel and Piping Systems, ASME PVP-PB-026, 1977.

27. M. A. Hamdi and Y. Ousset: "A displacement method for the analysis of vibrations of coupled fluid-structure systems," International Journal for Numerical Method in Engineering, Vol. 13, 1978, pp. 139–150.

28. G. C. Everstine: "A symmetric potential formulation for fluid—structure interaction," Journal of Sound and Vibration, Vol. 79, No. 1, 1981, pp. 157–160.

29. R. H. MacNeal (editor): "The NASTRAN theoretical manual," NASA Special Publication 221(01), 1972.

30. C. W. McCormick (editor): "The NASTRAN user's manual," NASA Special Publication 222(01), 1973.

31. D. J. Neffske, J. A. Wolf, Jr, and L. J. Howell: "Structural—acoustic finite element analysis of the automobile passenger compartment: A review of current practice," Journal of Sound and Vibration, Vol. 80, No. 2, 1982, pp. 247–266.

32. D. C. Crskowski and C. A. Brebbia (editors): "Boundary element methods in acoustics," 1991, Computational Mechanics Publications, Southampton.

33. L. H. Chen and D. G. Schweikert: "Sound radiation from an arbitrary body," The Journal of Acoustical Society of America, Vol. 35, 1963, pp. 1626–1632.

34. G. Chertock: "Sound radiation from vibration surfaces," The Journal of Acoustical Society of America, Vol. 36, 1964, pp. 1305–1313.

35. G. B. Brundit: "A solution to the problem of scalar scattering from a smooth bounded obstacle using integral equations," Quarterly Journal of Mechanics and Applied Mathematics, Vol. 18, 1965, pp. 473–489.

36. L. H. Chen: "Acoustic emission from submerged structures, " in Developments in Boundary Element Method II (edited by C.A. Brebbia), Applied Science Publishers, 1980, pp. 245–281.

37. A. F. Seybert, B. Soenarko, F. J. Rizzo, and D. J. Shippy: "An advanced computational method for radiation and scattering of acoustic waves in three dimensions," The Journal of Acoustical Society of America, Vol. 44, 1968, pp. 41–58.

38. H. A. Schenck: " Improved integral formulation for acoustic radiation problems," The Journal of Acoustical Society of America, Vol. 36, 1964, pp. 1305–1313.

39. G. C. Everstine, F. M. Henderson, and L. S. Schuetz: "Coupled NASTRAN/boundary element formulation for acoustic scattering," 15th NASTRAN Users' Colloquium, 1987, pp. 250–265.

40. S. Amini and P. J. Harris: "Boundary element and finite element methods for the coupled fluid—structure interaction problems," in Boundary Elements X (editor: C. A. Brebbia), McGraw–Hill, New York, 1988, pp. 509–520.

41. D. Greenspan and P. Werner: "A numerical method for the exterior Dirichlet problem for the reduced wave equation," Archives of Rational Mechanics and Analysis, Vol. 23, 1966, pp. 288–316.

42. H. Yuying: "A mixed FE-BE method for coupled vibration of floating plates with complicated shape," in Theory and Applications of the Boundary Element Method (edited by Quighua Du and M. Tanaka), McGraw–Hill, New York, 1990, pp. 321–328.

43. G. Koopmann and H. Benner: "Method for computing the second power of machines based on the Helmholtz integral," The Journal of Acoustical Society of America, Vol. 71, 1982, pp. 78–89.

44. S. Suzuki, M. Imai, and S. Ishiyama: "Boundary element analysis of structural—acoustic problems," in Boundary Elements VI (editor: C. A. Brebbia), McGraw–Hill, New York, 1984, pp. 27–35.

45. M. Tanaka and Y. Masuda: "Boundary Integral Equation approach to structural—acoustic coupling problems," in Boundary Elements IX, Vol. 3—Fluid Flow and Potential Applications, McGraw—Hill, New York, 1987, pp. 19–33.

46. M. Tanaka and Y. Masuda: "Boundary element method applied to certain structural—acoustic coupling problems," Computer Methods in Applied Mechanics and Engineering, Vol. 71, 1988, pp. 225–234.

47. J. B. Mariem and M. A. Hamdi: "A new boundary finite element method for fluid—structure interaction problems," International Journal for Numerical Method in Engineering, Vol. 24, 1987, pp. 1251–1267.

48. C. S. Pates, III: "Analysis of random structure—acoustic interaction problems using coupled boundary element and finite element methods," Ph. D. dissertation, Old Dominion University, 1994.

49. C. A. Brebbia and J. Dominguez: "Boundary elements: An introductory course," Computational Mechanics Publications, Southampton and McGraw-Hill, New York, 1989.

50. D. J. Danson: "A boundary element solution of the wave equation," in Boundary Element Techniques in Computer—Aided Engineering (edited by C.A. Brebbia), Martinus Nijhoff Publishers, 1984, pp. 191–199.

51. C. A. Brebbia: "The solution of time dependent problems using boundary elements," in The Mathematics of Finite Elements and Applications V (edited by J.R. Whiteman), Academic Press, London, 1985.

52. J. Tian and J. Z. Sha: "A study of spatial active noise attenuations," Journal of Acoustics (in Chinese), Vol. 6, pp. 77–83, 1987.

53. H. C. Lester and C. R. Fuller: "Active control of propeller induced noise fields inside a flexible cylinder," AIAA conference paper, AIAA-86–1957, 1986.

54. A. J. Nullmore, P. A. Nelson, and S. J. Elliott: "Active minimization of acoustic potential energy in harmonically excited cylindrical enclosed sound fields," AIAA conference paper, AIAA-86–1958, 1986.

55. J, Pan: "A study of the active control of sound transmission through a panel into a cavity," The Journal of Acoustical Society of America, Vol. 84, S182, 1988.

56. S. D. Snyder and C. H. Hansen: "Active noise control in duct: Some physical insights," The Journal of Acoustical Society of America, Vol. 86, 1989, pp. 184–194.

57. A. I. Vyalyshev, A. I. Dubinin, and B. D. Tartakovskii: "Active acoustic reduction of a plate," Sov. Phys. Acoust. Vol. 32, No.2, 1986, pp. 96–98.

58. C. R. Fuller: "Active control of sound transmission/radiation from elastic plates by vibrations inputs: I. Analysis," Journal of Sound and Vibration, Vol. 136, No. 1, 1990, pp. 1–15.

59. J. Pan, C. H. Hansen, and D. Bies: "Active control of noise transmission through a panel into a cavity: I. Analytical study," The Journal of Acoustical Society of America, Vol. 87, No. 5, 1990, pp. 2098–2108.

60. D. R. Thomas, P. A. Nelson, and S. J. Slliott: "Active control of the transmission of sound through a thin cylindrical shell, Part I: The minimization of vibrational energy," Journal of Sound and Vibration, Vol. 167, No. 1, 1993, pp. 91–111.

61. D. R. Thomas, P. A. Nelson, and S. J. Slliott: "Active control of the transmission of sound through a thin cylindrical shell, Part II: The minimization of acoustic potential energy," Journal of Sound and Vibration, Vol. 167, No. 1, 1993, pp. 113–128.

62. S. D. Snyder and C. H. Hansen: "The design of systems to control actively periodic sound transmission into enclosed spaces, Part I: Analytical models," Journal of Sound and Vibration, Vol. 170, No. 4, 1994, pp. 433–449.

63. S. D. Snyder and C. H. Hansen: "The design of systems to control actively periodic sound transmission into enclosed spaces, Part II: Mechanisms and trends," Journal of Sound and Vibration, Vol. 170, No. 4, 1994, pp. 451–472.

64. C. R. Fuller, C. H. Hansen, and S. D. Snyder: "Active control of structurally radiated noise using piezoceramtic actuators," Proceedings of Inter-Noise 89, Newport Beach, CA, 1989, pp. 509–512.

65. H. C. Lester and S. Leefbvre: "Piezoelectric actuator models for active sound and vibration control of cylinders," Journal of Intelligent Material Systems and Structures, Vol. 4, 1993, pp. 295–306.

66. H. T. Banks, W. Fang, R. J. Silcox, and R. C. Smith: "Approximation methods for control of structural acoustic models with piezoceramtic actuators," Journal of Intelligent Material Systems and Structures, Vol. 4, 1993, pp. 98–116.

67. H. T. Banks, R. J. Silcox, and R. C. Smith: "Modeling and control of acoustic structure interaction problems via piezoceramic actuators: 2D numerical examples," Journal of Vibration and Acoustics, Vol. 116, 1994, pp. 386–396.

68. E. K. Dimitriadis and C. R. Fuller: "Active control of sound transmission through elastic plates using piezoelectric actuators," AIAA 12th Aeroacoustics Conference, San Antonio, April 10–12, 1989, Paper 89–1062.

69. L. C. Wrobel and C. A. Brebbia: "The dual reciprocity boundary element formulation for nonlinear diffusion problems," Computer Methods in Applied Mechanics and Engineering, Vol. 65, No. 2, 1987, pp. 147–164.

70. P. W. Partridge, C. A. Brebbia, and L. C. Wrobel: "The dual reciprocity boundary element method," Computational Mechanics Publications, Southampton, Boston, 1992.

71. R. Zhou: "Finite element analysis for nonlinear flutter suppression of composite panels at elevated temperatures using piezoelectric materials," Ph. D. Dissertation, Old Dominion University, 1994.

72. H. F. Tiersten: "Linear piezoelectric plate vibrations," Plenum Press, New York, 1969.

73. IEEE Standard 176: "Piezoelectricity," IEEE, New York, 1978.

74. C. K. Lee, "Theory of laminated piezoelectric plates for the design of distributed sensors/actuators: Part 1. governing equations and reciprocal relationships," Research Report RJ 6332(62001), Engineering Technology, IBM Research Division, San Jose, CA, July, 1988.

75. H. Allik and T. J. R. Hughes, "Finite element method for piezoelectric vibration", International Journal for Numerical Method in Engineering Vol. 2, pp. 51–157, 1970.

76. C. K. Chiang: "A finite element large deflection multiple—mode random response analysis of complex panels with initial stresses subjected to acoustic loading," Ph.D. Dissertation, Old Dominion University, 1988.

77. C. Hirsch: "Numerical computation of internal and external flows," John Wiley & Sons, 1988.

78. D. Nardini and C. A. Brebbia: "A new approach to free vibration analysis using boundary elements," in Boundary Element Methods in Engineering (edited by C.A. Brebbia), Computational Mechanics Publications, Southampton, 1982.

79. D. Nardini and C. A. Brebbia: " Boundary integral formulation of mass matrices for dynamic analysis," in Topics in Boundary Element Research, Vol. 2, Springer-Verlag, Berlin, 1985.

80. H. F. Olson: "Acoustic Engineering ," D. Van Nostrand Company, Inc., 1947.

81. L. Meirovitch: "Dynamic and Control of Structures," John Wiley & Sons, New York, 1990

82. T. E. Fortmann and K. L. Hitz: "An Introduction to Linear Control System," Marcel Dekker, Inc, New York and Basel, 1977.

83. Z. Lai, J-K. Haung, and C. Mei: "Shape and placement of piezoelectric sensor for panel flutter limit—cycle suppression," AIAA Journal, Vol. 34, No. 5, 1996.

APPENDIX A
Derivation of Finite Element Equation

The finite element equation of motion for the laminated composite plate with piezoceramic layers can be obtained from the generalized Harmilton's principle. When the plate is discretized by certain type of elements, this principle is valid for each element. Considering a certain element, substituting equations (2.18) to (2.21) into equation (2.17), we have

$$\int_{V_e} \left[\rho\delta\dot{\vec{w}}\ddot{\vec{w}} + \{\delta E\}^T\{D\} - \{\delta\epsilon\}^T\{\sigma\} + \delta\vec{w}\vec{F}_b\right]dV + \int_{s_{e1}} \delta\vec{w}\vec{F}_s dS + \int_{s_{e2}} \vec{w}\delta\vec{F}_s dS - \int_{s_{e3}} \delta\phi q dS + \delta\vec{w}\vec{F}_c = 0 \tag{A.1}$$

where V_e is the volume of the element, s_{e1} is the element boundary with prescribed forces, s_{e2} is the element boundary with given displacement, and s_{e3} is the surface of piezoelectric material. For thin composite panel, equation (A.1) becomes

$$\int_{-h/2}^{h/2}\int_{A_e} \left[\rho\delta\dot{\vec{w}}\ddot{\vec{w}} + \{\delta E\}^T\{D\} - \{\delta\epsilon\}^T\{\sigma\}\right]dAdz + \int_{A_e} \delta\vec{w}\vec{p}dA - \int_{A_{e3}} \delta\phi q dS = 0 \tag{A.2}$$

where h is the plate thickness and $\vec{p}$ is the external loading on the plate surface A_e.

The displacement vector in the element can be expressed as the displacements at element nodes as (see Appendix B)

$$\vec{w} = \begin{Bmatrix} w \\ u \\ v \end{Bmatrix} = \begin{Bmatrix} [H_w]\{a\} \\ [H_u]\{b\} \\ [H_v]\{b\} \end{Bmatrix} = \begin{Bmatrix} [H_w][T_b]\{w_b\} \\ [H_u][T_m]\{w_m\} \\ [H_v][T_m]\{w_m\} \end{Bmatrix} \tag{A.3}$$

and the strain—displacement relation in equation (2.22) yields the strain vector as

$$\{\epsilon\} = [C_m]\{b\} + z[C_b]\{a\} \tag{A.4}$$

then the constitutive equation (2.14) gives the stress vector for k-th layer as

$$\{\sigma\}_k = \left[\bar{Q}\right]_k([C_m]\{b\} + z[C_b]\{a\} - \left[\bar{d}\right]\{E_3\}) \tag{A.5}$$

where

$$[\bar{d}]_k = \begin{bmatrix} d_{xk}\delta_{ik} & \cdots & d_{xk}\delta_{jk} \\ d_{yk}\delta_{ik} & \cdots & d_{yk}\delta_{jk} \\ d_{xyk}\delta_{ik} & \cdots & d_{xyk}\delta_{jk} \end{bmatrix} \tag{A.6}$$

and $\{E_3\} = \left[(E_3)_{n1}, (E_3)_{n2}, ..., (E_3)_{nn\phi}\right]^T$, we assume the layers $n1,\ n2, ..., nn\phi$ are the location of piezoceramic.

Substitute equations (A.4) to (A.6) into equation (A.2), we have the governing equation in element level as[71]

$$\begin{bmatrix} m_b & 0 & 0 \\ 0 & m_m & 0 \\ 0 & 0 & 0 \end{bmatrix} \begin{Bmatrix} \ddot{w}_b \\ \ddot{w}_m \\ 0 \end{Bmatrix} + \begin{bmatrix} k_b & k_{bm} & k_{b\phi} \\ k_{mb} & k_m & k_{m\phi} \\ k_{\phi b} & k_{\phi m} & k_\phi \end{bmatrix} \begin{Bmatrix} \dot{w}_b \\ \dot{w}_m \\ \dot{w}_\phi \end{Bmatrix} = \begin{Bmatrix} f_b \\ f_m \\ f_\phi \end{Bmatrix} \tag{A.7}$$

where the element matrices are defined as

$$[m_b] = (\rho_\phi h_\phi + \rho_c h_c)[T_b]^T \int_{A_e} \{H_w\}\{H_w\}^T dA[T_b] \tag{A.8}$$

$$[m_m] = (\rho_\phi h_\phi + \rho_c h_c)[T_m]^T \int_{A_e} [H_u, H_v][H_u, H_v]^T dA[T_m] \tag{A.9}$$

$$[k_b] = [T_b]^T \int_{A_e} [C_b]^T \Big([D]_c + [D]_\phi\Big)[C_b] dA[T_b] \tag{A.10}$$

$$[k_m] = [T_m]^T \int_{A_e} [C_m]^T \Big([A]_c + [A]_\phi\Big)[C_m] dA[T_m] \tag{A.11}$$

$$[k_{mb}] = [k_{bm}]^T = [T_m]^T \int_{A_e} [C_m]^T \Big([B]_c + [B]_\phi\Big)[C_b] dA[T_b] \tag{A.12}$$

$$[k_{\phi b}] = [B_h]^T [G_\phi]^T \int_{A_e} [C_b] dA[T_b] \tag{A.13}$$

$$[k_{\phi m}] = [B_h]^T [F_\phi]^T \int_{A_e} [C_m] dA[T_m] \tag{A.14}$$

$$[k_\phi] = -h_p A_e \epsilon_{33} [B_h]^T [B_h] \tag{A.15}$$

$$\{f_b\} = [T_b]^T \int_{A_e} p_z [H_w]^T dA \tag{A.16}$$

$$\{f_m\} = [T_m]^T \int_{A_e} \left(p_x [H_u]^T + p_y [H_v]^T \right) dA \tag{A.17}$$

$$\{f_\phi\} = \int_{A_e} q dA \tag{A.18}$$

where

$$([F_\phi], [G_\phi]) = \int_{-h/2}^{h/2} [\bar{Q}]_k [\bar{d}]_k (1, z) dz \tag{A.19}$$

where $[B_h]$ has been defined in equation (2.24).

It is noticed that, in the element mass matrices (A.8 and A.9) and stiffness matrices (A.10 and A.11), the modification of piezoceramic layers is included. ρ_ϕ and ρ_c are the mass density of piezoelectric material and composite material, respectively, h_ϕ and h_c are the thickness of piezoceramic layers and composite layers, respectively. $[A]$, $[B]$ and $[D]$ matrices for composite and piezoelectric lamina are defined as

$$([A]_c, [B]_c, [D]_c) = \int [\bar{Q}_c]_k (1, z, z^2) dz \tag{A.20}$$

where the integrals are through the thickness of composite layers, and

$$\left([A]_\phi, [B]_\phi, [D]_\phi \right) = \int [\bar{Q}_\phi]_k (1, z, z^2) dz \tag{A.21}$$

where the integrals are through the thickness of piezoelectric layers.

APPENDIX B
Finite Element Characteristics

The rectangular element under consideration is with 24 structural degrees of freedom (DOF) for bending and membrane plus one extra electrical DOF for each piezoceramic layer. The unknown displacements, w, w_x, w_y, w_{xy}, u, and v are defined at each element node, while the electric potential ϕ (electrical DOF) is defined for each piezoelectric layer (see Figure 2.2).

B.1 Transformation between nodal displacements and generalized coordinates

The transformation matrices between nodal displacements and generalized coordinates can be derived by considering an element in its local coordinates. For the bending deflection, the C^1 conforming element assumes the bending deflection in the element is distributed as:

$$\begin{aligned} w(x,y,t) &= a_1 + a_2x + a_3y + a_4x^2 + a_5xy + a_6y^2 + a_7x^3 \\ &\quad + a_8x^2y + a_9xy^2 + a_{10}y^3 + a_{11}x^3y + a_{12}xy^3 \\ &\quad + a_{13}x^2y^2 + a_{14}x^3y^2 + a_{15}x^2y^3 + a_{16}x^3y^3 \\ &= [H_w(x,y)]\{a(t)\} \end{aligned} \tag{B.1}$$

where $[H_w(x,y)]$ is the transverse shape function

$$\begin{aligned} [H_w(x,y)] = [1, x, y, x^2, xy, y^2, x^3, x^2y, xy^2, y^2, \\ x^3y, x^2y^2, xy^3, x^3y^2, x^2y^3, x^3y^3], \end{aligned} \tag{B.2}$$

and $\{a(t)\}$ is the generalized bending coordinates

$$\begin{aligned} \{a\}^T = [a_1, a_2, a_3, a_4, a_5, a_6, a_7, a_8, a_9, a_{10}, \\ a_{11}, a_{12}, a_{13}, a_{14}, a_{15}, a_{16}] \end{aligned} \tag{B.3}$$

If the vector of the 16 bending nodal displacements is given as

$$\begin{aligned} \{w_b\}^T = [w_1, w_{x1}, w_{y1}, w_{xy1}, w_2, w_{x2}, w_{y2}, w_{xy2}, \\ w_3, w_{x3}, w_{y3}, w_{xy3}, w_4, w_{x4}, w_{y4}, w_{xy4}] \end{aligned} \tag{B.4}$$

then equation (B.1) and its derivatives at the four element nodes yield a set of 16 linear equations,

$$\{w_b\} = [T_b]^{-1}\{a\} \tag{B.5}$$

which gives the generalized coordinates from the nodal bending displacements, so does the bending deflection distribution in the element, as

$$\{a\} = [T_b]\{w_b\} \tag{B.6}$$

where the transformation matrix between transverse displacements and generalized bending coordinates, $[T_b]$, is only a function of the coordinates of the four element nodes.

The transformation matrix between inplane displacements and generalized inplane coordinates can be determined in a similar way. The inplane displacements are assumed to be bilinear, that is

$$\begin{aligned} u(x,y,t) &= b_1 + b_2 x + b_3 y + b_4 xy = [H_u(x,y)]\{b(t)\} \\ v(x,y,t) &= b_5 + b_6 x + b_7 y + b_8 xy = [H_v(x,y)]\{b(t)\} \end{aligned} \tag{B.7}$$

where $[H_u(x,y)]$ and $[H_v(x,y)]$ are the inplane shape functions

$$\begin{aligned} [H_u(x,y)] &= [1, x, y, xy, 0, 0, 0, 0] \\ [H_v(x,y)] &= [0, 0, 0, 0, 1, x, y, xy] \end{aligned} \tag{B.8}$$

and $\{b(t)\}$ is the generalized inplane coordinates

$$\{b\}^T = [b_1, b_2, b_3, b_4, b_5, b_6, b_7, b_8] \tag{B.9}$$

If the 8 inplane displacements at four element nodes are given as

$$\{w_m\}^T = [u_1, v_1, u_2, v_2, u_3, v_3, u_4, v_4] \tag{B.10}$$

Then equation (B.7) at the four element nodes yield a set of 8 linear equations,

$$\{w_m\} = [T_m]^{-1}\{b\} \tag{B.11}$$

which gives the generalized coordinates from the nodal inplane displacements, so does the inplane displacements distribution in the element, as

$$\{b\} = [T_m]\{w_m\} \tag{B.12}$$

where the transformation matrix between inplane displacements and generalized inplane coordinates, $[T_m]$, is also only a function of the coordinates of the four element nodes.

B.2 Transformation between Nodal Displacements and Strains

The transformation between the nodal displacements and strains can be determined directly from the strain—displacement relation. Substitute equations (B.1) and (B.7) into equation (2.22), we obtain the matrix in equation (A.4) as

$$[C_b] = \begin{bmatrix} -\partial^2 H_w/\partial x^2 \\ -\partial^2 H_w/\partial y^2 \\ -2\partial^2 H_w/\partial x \partial y \end{bmatrix} \tag{B.13}$$

and

$$[C_m] = \begin{bmatrix} \partial H_u/\partial x \\ \partial H_v/\partial y \\ \partial H_u/\partial y + \partial H_v/\partial x \end{bmatrix} \tag{B.14}$$

APPENDIX C
Coupling between FEM and BEM

The velocity vector of each element in a constant rectangular BEM model is the displacement at the center of the element

$$\{u_n\} = [u_{on}]^T \tag{C.1}$$

while in FEM, the displacement vector is

$$\begin{aligned} \{w\}_i &= [w_i, w_{ix}, w_{iy}, w_{ixy}, u_i, v_i] \\ \{w\} &= [\{w\}_1, \{w\}_2, \{w\}_3, \{w\}_4]^T \end{aligned} \tag{C.2}$$

If the mesh of FEM model and BEM model on the internal surface of the plate are identical, then from the displacement shape functions, we have,

$$[T_e] = \begin{bmatrix} H_w(x_o, y_o) & 0 \\ 0 & H_u(x_o, y_o) \\ 0 & H_v(x_o, y_o) \end{bmatrix} \begin{Bmatrix} [T_b] \\ [T_m] \end{Bmatrix} \tag{C.3}$$

where

$$\begin{aligned} x_o &= \frac{x_1 + x_2 + x_3 + x_4}{4} \\ y_o &= \frac{y_1 + y_2 + y_3 + y_4}{4} \end{aligned} \tag{C.4}$$

with x_i and y_i are the coordinates of element nodes.

Due to the compatibility of the velocity at the inner surface of the plate, we have the element in vector $\{u_n\}$ as

$$u_{ne} = \{\beta_e\}^T [T_e] \{\dot{w}\} \tag{C.5}$$

and

$$\{\beta_e\} = [n_x, n_y, n_z]^T \tag{C.6}$$

where n_x, n_y, and n_z are the components of the unit normal vector of the element plane.